Damage Detection of Defects Using Linear and Nonlinear Guided Waves

Thesis submitted

in fulfilment of the requirements for the degree of

Doctor of Philosophy

by Reza Soleimanpour

Faculty of Engineering, Computer and Mathematical Sciences

School of Civil, Environmental and Mining Engineering

The University of Adelaide, North Terrace Campus

South Australia

September 2016

Damage Detection of Defects Using Linear and Nonlinear Guided Waves

By: Reza Soleimanpour

BSc, M.Sc (Civil Engineering)

Thesis submitted in fulfilment of the requirements for the degree of

Doctor of Philosophy

LIBRARY COPY after examination

Faculty of Engineering, Computer and Mathematical Sciences

School of Civil, Environmental and Mining Engineering

Table of contents

List of Tables

List of Figures

List of symbols

A_0	Signal amplitudes at reference point
$A(\Delta x)$	Signal amplitudes at distance Δx away from the reference point
A_n	Amplitude of the *n*-th harmonic
c_L	Longitudinal wave speed
c_g	Group velocity of the wave packet
$c_g(f_c)$	Group velocity of the incident A_0 guided wave at the excitation frequency f_c
$c_g(2f_c)$	Group velocity of the second harmonic guided wave
c_p	Phase velocity of the wave packet
d	delamination size
d_{a-r}	Distance between the actuator and receiver
d_{d-r}	Distance between the delamination and the receiver
d_{a-d}	Distance between the actuator and delamination
$D_s^{(r,\theta)}$	Out-of-plane displacement of the scattered wave
$D_d^{(r,\theta)}$	Out-of-plane displacement in the damaged model
$D_i^{(r,\theta)}$	Out-of-plane displacement in the intact model
E	Young's modulus
E^{II}	Intact material second-order linear elasticity
f_c, f	Excitation frequency
h	Overclosure

$H(\varepsilon)$	Heaviside unit
k	Wavenumber
k_i	Attenuation coefficient
L_{min}	Smallest mesh size
l_e	Maximum mesh size
p	Contact pressure
p^*, q	Wavelet transform factors
t_{f_c}	Incident wave packet arrival time
t_{2f_c}	Second harmonic wave packet arrival time
$u(t)$	Out-of-plane displacement of the guided wave signal
$w_s(t)$	Scattered wave data
$w_b(t)$	Baseline wave packet data
$w_t(t)$	Total wave packet data
$\widehat{w_s}(f_c)$	Scattered wave packet data in frequency domain
$\widehat{w_t}(f_c)$	Total wave packet data in frequency domain
$\widehat{w_s}(2f_c)$	Second harmonics scattered wave packet data in frequency domain
α_ω	Mass proportional Rayleigh damping constant
β_ω	Stiffness proportional Rayleigh damping constant
Δt	Time increment
Δx	Distance between two measurement points

$\Delta\phi$	Phase change
$\Delta\tau$	Normalized modulation pulse length
ε	strain
ε^0	Initial static contact strain
λ_{min}	Minimum wavelength size
υ	Poison's ratio
$\delta\prod^c$	Contact virtual work contribution
ρ	Density
σ	Stress
$\chi(t)$	Mother wavelet
ω	Angular central frequency

Statement

I certify that this work contains no material which has been accepted for the award of any other degree or diploma in any university or other tertiary institution and, to the best of my knowledge and belief, contains no material previously published or written by another person, except where due The University of Adelaide - 2013 Program Rules Adelaide Graduate Centre 41 reference has been made in the text. In addition, I certify that no part of this work will, in the future, be used in a submission for any other degree or diploma in any university or other tertiary institution without the prior approval of the University of Adelaide and where applicable, any partner institution responsible for the joint-award of this degree. I give consent to this copy of my thesis when deposited in the University Library, being made available for loan and photocopying, subject to the provisions of the Copyright Act 1968. The author acknowledges that copyright of published works contained within this thesis resides with the copyright holder(s) of those works. I also give permission for the digital version of my thesis to be made available on the web, via the University's digital research repository, the Library catalogue and also through web search engines, unless permission has been granted by the University to restrict access for a period of time.

Acknowledgements

I dedicate my dissertation work to my wife Zahra for standing beside me throughout my PhD study and writing this thesis. She has been my inspiration and motivation for continuing to improve my knowledge forward. I dedicate this dissertation to my son Amirali who is just about the best child a dad could hope for: happy, loving, and fun to be. A special feeling of gratitude to my loving parents Mohammadreza and Ashraf Soleimanpour whose words of encouragement and push for tenacity ring in my ears. My brother Mohammad and my sister Mojgan have never left my side and are very special.

I gratefully acknowledge my supervisor, Dr. Alex Ching-Tai Ng, for his invaluable guidance, encouragement and supports during my candidature at The University of Adelaide. Without his great contribution, completion of this study would not be possible.

Thanks to all my friends for sharing my happiness when starting this study and following with encouragement when it seemed too difficult to be completed. I would have probably give up without their support and example on what to do when you really want something.

I would like to thank Professor Chun Wang for his contribution in the third journal paper which is composed of this thesis.

Many thanks to all the staff of Adelaide University graduate centre, especially Miss. Antoinette Brincat for her support.

Many thanks go to all the staff of the School of Civil, Environmental and Mining Engineering for their individual help and support.

Abstract

In the past few years, application of guided waves for damage detection has been a topic of significant interest for many studies. Conventional guided wave techniques have been widely used in industry and technology for material characterisation and quality assessment by making use of so called linear acoustic response of material. It generally results in modification of linear parameters of guided waves such as wave amplitude, wave velocity, wave mode, and wave reflection and transmission. However, conventional guided wave techniques rely on baseline data known as the major linear guided wave techniques culprit. Among all guided wave techniques, nonlinear guided wave has been known as a promising baseline free approach, which offers enhanced reliability and practicability for damage detection. However, understanding of nonlinear guided waves is of essential importance for detecting and localising defects in structures. The nonlinear approach to acoustic non-destructive testing (NDT) is concerned with nonlinear responses of the guided waves, which is inherently related to the frequency changes of the input signal.

Nowadays, composite materials are widely used in structures due to their attractive properties such as higher stiffness to mass ratio and better corrosion resistance compared to metals. So far, most of studies on application of nonlinear guided waves have been dedicated to isotropic materials, such as aluminium and steel, whereas only a limited number of works have been carried out on application of nonlinear guided waves in anisotropic materials. Moreover, most of works in this area have focussed on classical nonlinearity raised from material nonlinearity whereas a limited number of researches have focused on non-classical nonlinearity raised from contact acoustic nonlinearity (CAN).

This research deals with linear and non-classical nonlinear interaction of guided waves with defects in structures from both numerical and experimental prospective. The aim of this research is to investigate guided waves for damage detection and damage localisation by developing an advanced 3D explicit finite element model for predicting the interaction of

guided waves with defects in isotropic and anisotropic material. The study first focuses on linear guided waves for damage detection and is expanded to nonlinear guided waves. Chapters 3 and 4 focus on linear guided waves whereas Chapters 5 and 6 focus on nonlinear guided waves. The numerical work has been carried by an advanced 3D explicit finite element code in ABAQUS v6.14. Verification of finite element models has been carried out by comprehensive experimental studies. The linear guided wave measurement has been carried out using high precision scanning laser Doppler vibrometer (Polytec PSV-400-3D-M) and nonlinear guided waves measurement has been captured using a computer controlled arbitrary waveform generator (NI PXI-5412) and a NI PXI-5105 digitizer. The data has been processed in time domain and frequency domain and time-frequency domain using Matlab.

The results of this study provide an improved physical insight into linear and nonlinear guided waves techniques. The results show that guided waves can be used for detecting and locating damages in beams and plates. However, nonlinear guided wave technique is a better option as it does not rely on baseline data and is more sensitive to small damages than the linear guided waves. A nonlinear guided wave damage localisation technique is introduced in this study which can accurately detect and locate damages without relying on baseline data.

Introduction

1. Aim and objectives

Guided wave techniques have shown potential in various studies as a solution to structural health monitoring (SHM) for damage prognosis. However, application of guided waves in SHM is a new field and there is still much work to be done in order to integrate this technique to the industry. On the other hand, there are remarkable gaps in previous studies which need to be addressed. Therefore, an in-depth understanding and investigation of interaction of guided waves with structural defects are essential for utilisation of guided waves.

This research will examine some of the fundamental issues in guided waves technique and aims at investigating the application of guided waves for damage detection in isotropic and anisotropic materials. In this research a comprehensive investigation will be carried out using numerical and experimental approaches. In summary, the overall objective of this research is to investigate the feasibility of using guided waves for detecting and locating defects in isotropic and anisotropic materials. To achieve this objective, the aims are

1. To gain fundamental understanding of guided waves propagation and scattering characteristics at defects, which are essential for developing practical and reliable guided waves-based damage detection techniques. In this aim, the scattering characteristics of fundamental asymmetric guided waves with defects will be thoroughly investigated.
2. To gain new insight into the generation mechanisms of nonlinear higher order harmonics in composite materials which can enhance the detection and monitoring of damage in composite structures.
3. To develop a reliable, accurate and realistic 3D numerical approach for prediction of propagation of guided waves in isotropic and anisotropic material.

4. To investigate the effects of various factors such as defect size, location and orientation, material damping and incident wave parameters on propagation and scattering characteristics of guided waves in isotropic and anisotropic material.
5. To introduce a reliable and sustainable damage detection and damage localisation technique for detecting and locating defects.

2. Significance and expected outcomes from the research

The outcome of this study can be summarised as follows;

1. The outcome of this research, will contribute in fundamental understanding of propagation and scattering characteristics of guided waves in isotropic and isotropic material. This will help potential researchers to extend this technique in other fields as well.
2. The outcome of this research will contribute in better understanding of CAN due to clapping in delaminated composite beams. This will extend the application of nonlinear guided waves approach to more geometric complex structures and will recover existing gaps in the literature.
3. In this study a 3D FE simulation techniques is introduced for predicting propagation and scattering of guided waves in isotropic and anisotropic material.
4. This study provides a detailed study on effect of several parameters on scattering and propagation characteristics of guided waves.
5. The common NDT guided waves based techniques often require a baseline data and are sometimes insensitive to small damages while the proposed approach in this study offers more reliability and accuracy in damage detection and damage localisation without relying on baseline data.

3. Background knowledge

3.1. Structural health monitoring

SHM is defined as the process of implementing damage detection and characterization strategy for engineering structures to ensure the structural safety and functionality (Dawson 1976). SHM aims at assessing the working condition of a structure in order to in advance detect any incipient damage that may exist, which otherwise may lead to a catastrophic failure. SHM systems have increased their popularity by providing valuable solutions for structural maintenance in order to prevent catastrophic events and reduce the cost. In SHM:

1– Allows an optimal use of the structure by minimising downtime and preventing catastrophic failures.

2– Provides the constructor with an improvement in the products.

3– Drastically changes the work organization of maintenance services by replacing periodic or scheduled maintenance with long-term performance-based maintenance.

4- Reduces present labour cost by avoiding dismounting parts where there is no hidden defects or by drastically reducing human involvement and human error and thus increasing structural safety and integrity.

5- Increases structural safety and sustainability by non-stop monitoring performance of the structure. This point seems to be a strong motivation for SHM application especially after aforementioned reported disasters due to structural failure, which could be prevented by using proper structural health monitoring system.

3.2. Background of Structural Health Monitoring

SHM plays an important role in structural safety and increasing life span of existing structures. Structural failures impose dramatic economic loss and human casualties that often happen due to structural damages, which can be prevented by utilisation of proper damage detection techniques. Although, many damage detection techniques have been introduced to address this

issue, many structural failures could still not be avoided. Below are some examples of collapses due to structural failure in the past 20 years which claimed many lives and injured several people. Collapse of a highway bridge carrying Interstate 95 over the Mianus River in Connecticut USA (1993) killed and injured several motorists, caused by failure of two pin and hanger assemblies that held the deck in place on the outer side of the bridge (USA National Transportation Safety Board 1985) (Figure 1).

Figure 1. Collapse of Interstate 95 Mianus Bridge in Connecticut - USA (Kirk & Mallett 2007)

Collapse of Interstate I- 35W Mississippi River Bridge in USA (2007) killed 13 and injured 145 people, was a result of improper design and excess weight (Kirk and Mallett 2007). Collapse of Sultan Mizan Zainal Abidin Stadium in Malaysia (2009) was identified to be due to the design faults and inappropriate materials.

In the recent years, SHM has been successfully tested and integrated to various types of structures such as damns, bridges, buildings, and aircrafts. Below are a few successful examples of SHM utilisation in structures.

In 1998, a crack monitoring system using optical fibre sensors was implemented in a temporary ship milldam and concrete face rock fill dam of the Three Gorges Project located in Xingshan county of Hubei province in China. In June 16 and July 30, 1998, the SHM system reported a crack with 0.2mm length on the concrete face of dam which was verified by a person checking in the field (Jinping Ou 2003). A health monitoring system was developed for a steel jacket platform in Bohai Ocean under the project supported by the National Hi-tech Research and Development Program of China. The system includes more than 200 OFBG sensors, 177

PVDF sensors, 56 fatigue life meters, 16 acceleration sensors, a set of environmental condition monitoring system and also the transmission wire (Jinping Ou 2003).

3.3. Non-destructive testing

In the last two decades, there has been an increasing awareness in importance of Non-destructive testing (NDT). As such, many studies have been dedicated to develop non-destructive damage detection techniques. NDT is defined as the process of inspecting, testing, or evaluating materials, components or assemblies for discontinuities, or differences in characteristics without destroying the serviceability of the part or system. In other words, when the inspection or test is completed the part can still be used. In contrast to NDT, common damage detection techniques are often destructive in nature and are usually done on a few and limited number of samples or on a certain part instead of whole structure. Although NDT is used as a tool in SHM but there are major differences between SHM and NDT in term of operation principles. NDT techniques are usually done offline and are applied in the region where damage are expected to be (Stepinski & Staszewski 2003), while a typical SHM system is often associated with an online global damage identification in the structure which makes it more complicated (Farrar & Worden 2007). Figure shows the SHM components and its link with NDT

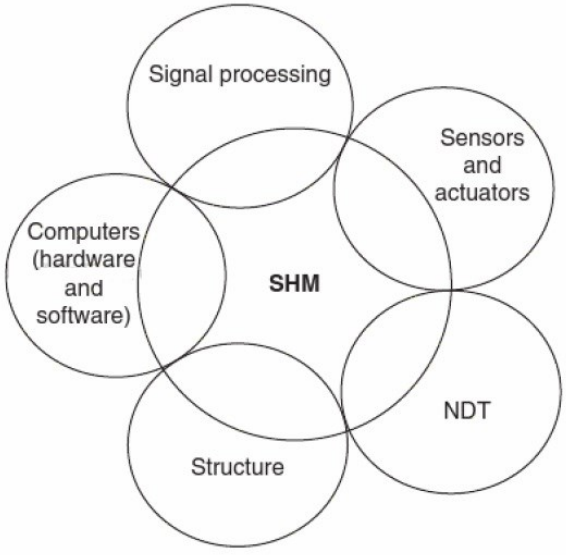

Figure 2. SHM components and its relation with NDT (Stepinski & Staszewski 2003)

Today, different NDT techniques are used in manufacturing, fabrication and in-service inspection of structures to ensure the integrity and reliability. During the construction, NDT is used to ensure the quality of the materials and joining process in fabrication and during erection. In-service NDT techniques are used to ensure that the elements in use continue to provide service in order to ensure the quality and safety of the structure. NDT applications are commonly used in aerospace engineering and civil structures, automotive, power generation, railway and pipeline.

Below, are some of the major NDT techniques;

1. Radiography - X and Gamma
2. Eddy current technique
3. Visual inspection
4. Acoustic emission
5. Magnetic particle inspection
6. Traditional ultrasonic
7. Guided wave technique

However, some techniques are inefficient during implementation and are costly, and some techniques are unreliable due to uncertainty in accuracy and reliability of the results. For example, Radiography-X and Gamma techniques are unsuitable for thick media, eddy current techniques is only applicable for electrically conductive materials and the visual inspection technique encounters structural components removal, which can be costly and may involve human errors as well. Similarly in acoustic emission technique, it is possible for flaws to be undetected if the loading is not high enough to cause an acoustic event. Magnetic particle inspection is time consuming and inapplicable for non-ferrous materials and non-magnetic ferrous materials, such as stainless steel. Therefore, only a few techniques have been successful in damage detection. The conventional non-destructive structural tests usually consume a significant amount of time and energy and also involve heavy workload for inspection.

Moreover, during the implementation of these techniques, they cause interruptions to the service of the structure. These techniques have been comprehensively reviewed and evaluated by researchers such as Rose (2002), Sohn (2003), Van Der Auweraer (2003), Su et al. (2006) and Raghavan (2007).

Among aforementioned damage detection techniques, guided waves technique has been recognized as a very prominent option. Guided waves due to their attractive mechanisms, can offer an efficient method for damage detection, localisation and also quantification and characterisation. Since the characteristics of guided waves are directly related to the properties of the material, they are known as one of the powerful and well-established NDT and SHM techniques in the industry.

4. Thesis structure

The research starts with investigation of linear interaction of guided waves with structural flaws in isotropic and anisotropic material and is eventually expanded to nonlinear interaction of guided waves with delamination in anisotropic material. With the aim of better understanding of the guided waves propagation in structures, two chapters of this thesis focus on linear guided waves. The linear guided waves study provides some insight into propagation of guided waves in beams and plates. Moreover, the numerical and experimental methods used in the first part are then used for initial verification of approaches used in nonlinear guided wave studies. Chapters 5 and 6 of the thesis, are focussed on propagation of nonlinear guided waves in composite beams in form of nonlinear guided waves scattering study and investigating the effects of various parameters on nonlinear guided waves propagation. Results of Chapter 5 are used for introducing a nonlinear guided waves technique for damage detection and damage localisation in composite beams. Conclusions and recommendations for future works are presented in Chapter 7.

The major research contribution and outcomes of the overall researches are presented in four journal publications, which form the thesis. The titles of Chapters 3 through Chapter 6 reflect the title of the journal papers.

4.1. Chapter 2

This chapter provides a brief discussion about guided wave technique, nonlinear guided wavesand contact acoustic nonlinearity (CAN).

4.2. Chapter 3

In this chapter, scattering analysis of the asymmetric Lamb wave (A_0) in aluminium plate with notches is investigated. The study involved both analytical and numerical approaches. Initially, a finite element based modelling approach is proposed for simulation of propagation of asymmetric Lamb waves in aluminium plates with notches. The model is verified using an analytical method and is then used for scattering analysis of propagation of asymmetric Lamb waves in aluminium plates with several notches of different sizes and orientations. The study shows that the amplitude of the scattered A_0 Lamb wave is very sensitive to the incident wave propagation and measurement direction. Moreover, it is shown that the FE simulation can be used for prediction of propagation of A_0 Lamb wave in Aluminium plates with notches.

4.3. Chapter 4

In this chapter, mode conversion of asymmetric guided waves due to delamination in composite beams is investigated. The study involves both experimental and numerical approaches. Several composite beams with different delamination to wavelength ratios and delamination through thickness locations are studies. It is shown that several guide waves modes are generated when asymmetric guide waves pass through delamination. The results of this chapter, provide some insights into damage detection using guided waves. Moreover, a special finite element modelling approach for modelling the propagation of guided waves in delaminated composite beams is proposed which is successfully verified using experimental data.

4.4. Chapter 5

In this chapter, nonlinear response of guided waves particularly CAN is studied. The linear parameters of the guided waves are initially verified using the method described in previous chapters and then nonlinear interactions of the guided waves in delaminated composite beams are investigated in detail. Numerical and experimental approaches are used in this chapter. Several delaminated composite beams are studied numerically and experimentally. The data is processed in time, frequency and time and frequency domain. It is shown that FE simulation can predict the acoustical nonlinearity due to interaction of the guided waves with delamination. Moreover, it is shown that CAN generates higher harmonic which is a good indicator of delamination in composite beams. The effects of other parameters such as material damping, the incident wave amplitude and number of cycles and through thickness location and the size of delamination on second harmonic of the guided waves is investigated.

4.5. Chapter 6

Chapter 6 is focussed on using nonlinear parameters of the guided waves for damage detection and damage localisation of the delamination in composite beams. In this chapter, a damage localisation approach for locating delamination in composite beams is proposed and verified using experimental case studies. Numerical and experimental approaches are used in this chapter. The study shows that the proposed damage detection and localisation techniques can be successfully used for detecting and locating delamination in composite beams.

4.6. Chapter 7

Chapter 7 provided a summary of the thesis.

5. List of publications

During the study, one conference paper and four journal papers have been produced which are listed as follows:

5.1. List of journal papers

1. Soleimanpour, R, Ng, C.T. Scattering of the fundamental anti-symmetric Lamb wave at through-thickness rectangular notches in isotropic plates. Civil Structural Health Monitoring, 2016; 6(3), 447-459.
2. Soleimanpour, R, Ng, C.T. Mode conversion and scattering analysis of guided waves at delaminations in laminated composite beams. Structural Monitoring and Maintenance, 2015; 2(3), 213-236.
3. Soleimanpour, R, Ng, C.T., Wang, C. Higher harmonic generation of guided waves at delaminations in laminated composite beams. Structural health monitoring, 2016 (In-print).
4. Soleimanpour, R, Ng, C.T. Locating delaminations in laminated composite beams using nonlinear guided waves. Engineering Structures, 2016 (Under peer review).

5.2. List of conference paper

1. Soleimanpour, R, Ng, C.T. Numerical study of nonlinear guided waves in laminated composite beams with delaminations, 8th Australasian Congress on Applied Mechanics, 2014;379-388.

6. References

1) Dawson B (1976). "Vibration condition monitoring techniques for rotating machinery". The Shock and Vibration Digest. Vol. 8, Iss:12,pp 3-15.
2) Robert S., K and Mallett, W.J (2007). 'Highway Bridges: Conditions and the Federal/State Role'. Transportation Policy Resources Science and Industry Division.
3) Esslinger, V., Kieselbach, R., Koller, R. (2004), 'The railway accident of Eschede - technical background'. Engineering Failure Analysis, Vol. 11, no. 4, pp.515-534
4) Apostolopoulos, Ch. Alk. (2010). 'Coastal bridges and the 120 Life Span – the Rio-Antirio case study'. International Journal of Structural Integrity, Vol. 1, Iss: 2, pp.173 – 183.

5) Kleinhans, D. D. (2009). ‘Structural Monitoring for the Huey P. Long Bridge Widening Project’. AREMA 2009 Annual Conference, Chicago, IL, September 20-23.

6) Celebi, M., Sanli, A., Sinclair, M., Gallant, S., Radulescu, D., (2004). ‘Real-time seismic monitoring needs of a building owner and the solution: A cooperative effort’. Earthquake Spectra, Vol. 20, Iss: 2, pp.333-346.

7) Ou, J. P., (2003). ‘Some recent advance of intelligent monitoring system for civil infrastructures in mainland China’. Proceeding of the first international conference on structural health monitoring and intelligent Infrastructures, November, Tokyo, Japan: pp.131-144.

8) Rose, J.L., (2002). ‘A baseline and vision of ultrasonic guided wave inspection potential’. Journal of Pressure Vessel Technology, vol.124, Iss: 3, pp. 273–282.

9) Sohn, H., Farrar, C.R., Hemez, F.M., Shunk, D.D., Stinemates, D.W., Nadler, B.R. (2003). ‘A review of structural health monitoring literature: 1996-2001, report number LA-13976-MS’. Technical report, Los Alamos National Laboratory, Los Alamos, NM.

10) Van der Auweraer, H. and Peeters, B. (2003). ‘International research projects on structural health monitoring: An overview’. Structural Health Monitoring, Vol.2, Iss: 4, pp. 341–358.

11) Su, Z., Ye, L. and Lu, Y. (2006). ‘Guided Lamb waves for identification of damage in composite structures: A review’. Journal of Sound and Vibration, Vol.295, Iss:3-5, pp.753–780.

Chapter 2: Linear and Nonlinear Guided Waves

1. Guided waves technique

Guided wave testing is one of latest techniques in NDT. The method employs mechanical stress waves that propagate in the structure which are guided by structure's boundaries. This allows the waves to travel a long distance with a very little loss in energy. Nowadays, guided waves technique is widely used for damage detection in a wide range of engineering structures, such as pipelines, aircrafts, railways and bridges. In this technique, large structures and big areas can be inspected from a single location. Guided waves can propagate in various structures such as bar, beam, plates and pipes. Early studies of guided waves were carried out by Rayleigh (1889), Lamb (1917), Stoneley (1924) and Love (1926). Comprehensive analyses of guided waves were performed by Viktorov (1967), Achenbach (1973), Graff (1975) and Rose (1999). Guided waves have many advantages over other techniques such as cost effectiveness, large area monitoring, sensitive to small damage, feasibility of in-situ monitoring and inaccessible area inspection. Since this technique can be applied for in-situ monitoring of the structure, maintenance of the structures can be performed without any interruption in the service. This is why there is an increasing interest in utilisation of guided waves for damage detection and maintenance of the structures. The guided wave techniques are generally categorized into linear techniques and non-linear techniques. The linear techniques include phased array and sparse array time-reversal imaging method, pitch-catch and pulse-echo methods (Su et al. 2006). The linear techniques reply on linear parameters of the guided waves such as wave reflection, wave transmission, wave attenuation, wave speed and wave amplitude whereas the prevalent nonlinear techniques are higher harmonic generation, subharmonic generation, and mixed frequency response (nonlinear modulation).

2. Propagation of guided waves in solids

Guided waves are a general term that refers to waves whose propagation characteristics depend on structural boundaries. Bulk waves propagate in infinite media without any restriction and

the wave type differs depending on restriction imposed on media. Longitudinal waves and shear waves are two wave components of bulk waves. The particle motion in which the longitudinal waves propagate is compressing or stretching and the direction of medium point motion is parallel to the direction of wave propagation. In case of shear waves, transverse particle motion in alternating direction is observed and the direction of medium point motion is perpendicular to the direction of wave propagation. Shear waves can be horizontal (SH) or vertical (SV) depending on particles motion direction. The following sections describe different types of guided waves and the boundary conditions by which they are generated in a media.

3. Rayleigh waves

Rayleigh wave propagate in a 3D solid bounded by one surface. Rayleigh waves are surface guided waves that travel near the surface of the media and are names after the famous English physicist Lord Rayleigh (1885). Rayleigh waves include both longitudinal and transverse motions. The particle motion consists of elliptical movement in the *x*-*y* vertical plane and of motion parallel to the wave propagation direction that decreases exponentially in amplitude as distance from the surface increases. There is a phase difference between these component motions (Figure 1a) (Ostachowicz 2011, Telford 1990).

4. Love Waves

Love waves are names after A. E. H. Love, the famous mathematician (1911) and they propagate in 3D solids when a surface in bounded. Love waves are horizontally polarized surface waves and are characterised by particles oscillation in alternating transverse movement. Similar to Rayleigh waves the particle motion amplitude decreases with depth. The direction of medium particle oscillation is horizontal and is perpendicular to the wave propagation direction (Ostachowicz 2011) (Figure 1b).

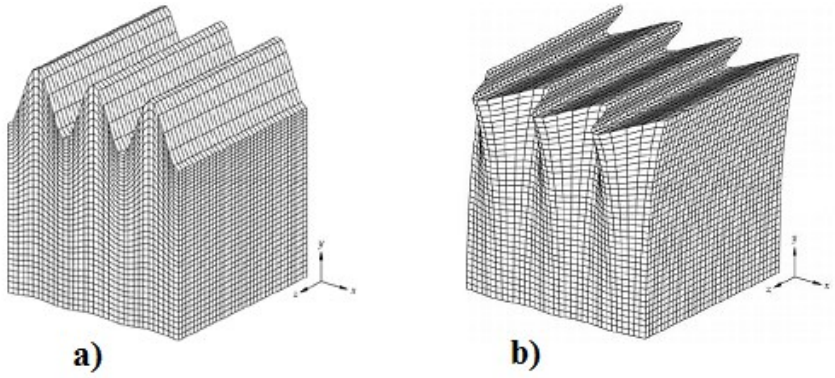

Figure 1. a) Rayleigh Wave b) Love Wave displacement in a solid

5. Lamb waves

Lamb waves were discovered by the famous British mathematician Horace Lamb who developed the theory of propagation of Lamb waves in solids in 1917. However, Lamb waves did not attract researchers due to complexity of understanding and generating of them. A comprehensive solution to Lamb waves was completed by Mindlin in 1950, followed by considerable detail provided by Gazis in 1958. Lamb waves were not generated physically until 1961 when Worlton managed to generate and use them in damage detection. Later Fredrick and Worlton carried out experiments on Lamb waves. Viktorov in 1967 first evaluated the dispersive properties of Lamb waves.

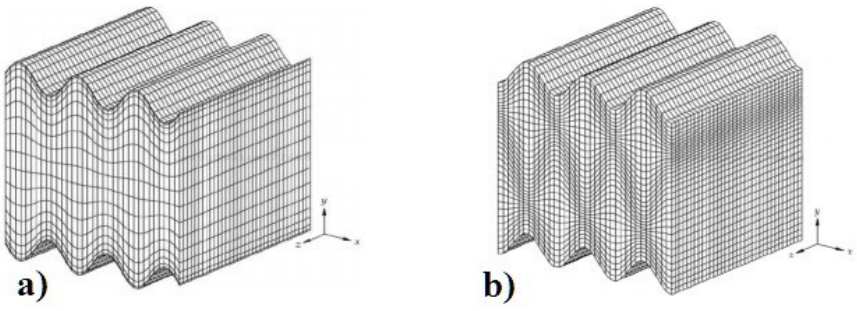

Figure 2. Lamb wave mode shapes in a solid: a) symmetric b) asymmetric mode Lamb wave

Comprehensive studies of Lamb wave were done by Achenbach (1973), Graff (1975) and Rose (1999). During the Second World War Lamb waves were used in medical industry. It was only in 1990 that the importance and efficiency of Lamb waves in detecting structural damages was discovered and since then their usage in NDT has increased significantly. Lamb waves are

mechanical waves which propagate in infinite media bounded by two surfaces and are generated as a result of superstition of multiple reflection of longitudinal P waves and shear SV waves. When Lamb waves propagate, medium particle oscillation becomes very complex. Lamb waves are dispersive; meaning the value of wave velocity is dependent on the value of wave frequency. Three forms of Lamb wave propagate in a media depending on the distribution of stress and forces on the top and bottom surfaces; 1) symmetric mode (S_0, S_1, S_2,…) (Figure 2a) 2) asymmetric mode (A_0, A_1, A_2,…) (Figure 2b) 3) shear horizontal mode (SH_0, SH_1, SH_2,…) of which symmetric and asymmetric modes have attracted researchers due to their abilities in damage detection. It should be noted that the number of Lamb wave modes are infinite contrary to bulk waves.

5.1. Lamb waves dispersion curve

Dispersion curve which is the fundamental way to describe the Lamb wave propagation in a solid medium for example an aluminium plate (Figure 3). In 1877, Lord Rayleigh observed that the velocity of a group of waves can be different to the value of each individual wave and described two definitions of wave velocity as group velocity and phase velocity. The group velocity is the velocity at which a guided wave packet will travel at a given frequency while the phase velocity is the speed at which the individual peaks within that packet travels.

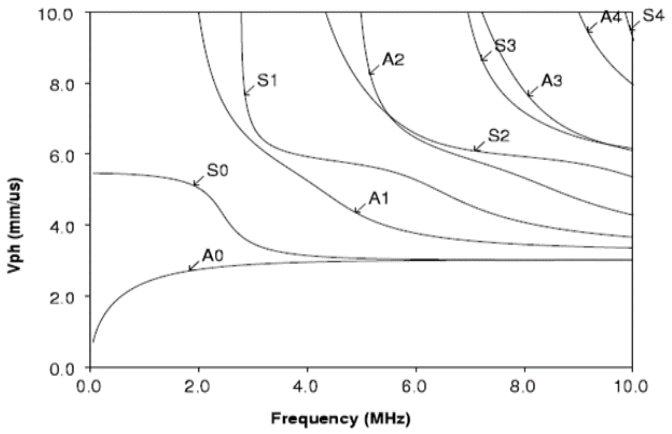

Figure 3. Phase velocity dispersion curve (Pavlakovic and Lowe)

In general, the computation of dispersion relations of the frequency and the wavenumber requires finding the roots of a complicated determinant which can be solved numerically. DISPERSE v2.0.16b is a powerful software which has been created to generate dispersion curve for various systems as well as composite materials through Global Matrix method in imperial college of London (Pavlakovic and Lowe 2003). Calculation of phase velocity, group velocity, mode shapes and other characteristics of waves in various systems such as flat plate or cylindrical geometries, with arbitrary numbers of layers can be done by DISPERSE. This software uses robust root finding and mode tracing procedures, which have evolved through extensive modelling experience and has been verified by wide use, comparison with published materials and experiments.

6. Nonlinear guided waves

Linear guided waves are generally sensitive to gross defects such as open cracks, holes, notches and large scale corrosion. However, it is highly desirable to detect damage at the smallest scale possible to maintain the best achievable structural integrity. Nonlinear ultrasonics has been shown to have the capability to provide sensitivity to micro-structural defects and closed cracks. To tackle the limitation of linear guided wave techniques, a body of research has gone into the development of nonlinear guided waves techniques, which focusses on nonlinear characteristics such as harmonics and modulations (spectral sidebands) created by defects. Nonlinear Lamb wave focuses on nonlinear acoustical phenomena which can be related to various imperfections of materials microstructure or non-symmetric thermoelastic behaviour of interfaces such as crack, contact and rubbing or clapping surfaces. Some of nonlinear acoustical phenomena are 1) higher harmonic generation, 2) sub-harmonic generation, 3) nonlinear resonance and a 4) mix frequency response, of which the first and last phenomena are very common in evaluating acoustic nonlinearities of the mediums. Nonlinear methods involving intrinsic or materials global nonlinearity are referred as nonlinear elasticity that have been used for detecting materials imperfections such as micro cracks. Nonlinear methods, which focus on thermoslastic

behaviour of interfaces referred as local nonlinearities, have received a lot of interest in theoretical and applied research in the past few years. Nonlinear ultrasonic technique is an efficient type of guided wave technique which uses distinctive side bands and higher harmonics and has proven itself as a promising technique for detecting inherent structural flaws due to higher sensitivity to structural damages and large inspection range.

Generally, the nonlinear acoustic phenomena is divided into classical and non-classic nonlinear responses. The classical non-linear response is concerned with material imperfections such as intrinsic nonlinearities due to imperfections in atomic lattices leading to higher harmonic generation whereas the latter is usually concerned with contact acoustic nonlinearity (CAN). As such, non-classical nonlinear response, mostly deals with contact type defects in material. Fatigue cracks, micro-cracks, material nonlinearity or other material imperfections are some sources of classical non-linear response while delamination-wave interactions that exhibit vibro-acoustic modulations, sub-harmonic generation or stress-strain hysteresis are some sources of non-classical nonlinear responses. Research work in classical nonlinear response mostly relies on higher harmonic generation of guided waves due to its interaction with the material imperfections whereas the non-classical responses replies on interaction of guided waves with interfaces. Non-classical nonlinear responses are sensitive feature in detecting contact type damages in medium. Specially, when the contact region (i.e. crack or delamination) is closed there will not be any reflection from damage, meaning that it will remain undetected by linear guided waves, while nonlinear guided waves will detect the existence of the damage by generating higher harmonics.

6.1. Contact Acoustic Nonlinearity (CAN)

Contact acoustic nonlinearity (CAN) is a nonlinear effect resulting from mechanical interaction between damage interfaces appearing as generation of higher harmonics. Consider a propagating sinusoidal wave passing through a closed crack perpendicularly (Figure 4a-c). In this case, the compressional part of the wave penetrates into the contact region (Figure 4a) while

the tensile part does not (Figure 4c). Thus, after hitting the interface region, the waves shape becomes nearly half-wave rectification, which causes obvious nonlinearity in form of higher harmonics.

Two mechanisms are possible due to interaction of interfaces with propagating incident wave. The first one is referred as clapping which is generated due to asymmetry in stress-strain characteristics for damaged interfaces and causes the stiffness of the materials to be higher for compression than for tension. It is observed as several harmonics of the fundamental wave. The other mechanism, which cause change in materials stiffness is due to interaction of a shear acoustic wave in damage area and is refereed as symmetrical nonlinearity which results in generation of odd harmonics.

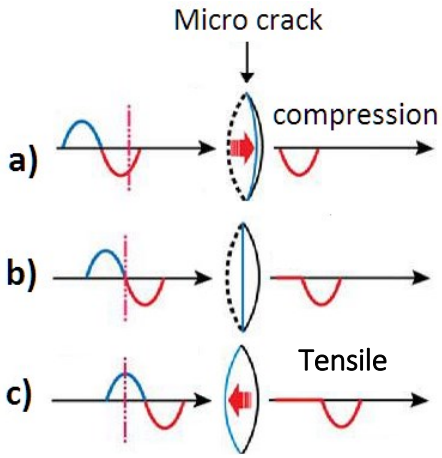

Figure 4. Interaction of incident wave with interface (Pecorari and Solodov 2006)

This mechanism is often caused by the friction forces between damage interfaces when they slip. The clapping behaviour, which is caused by asymmetrical dynamics of the interface stiffness, can be approximated by a stress-strain relation as (Solodov 2002)

$$\sigma = E^{II}[1 - H(\varepsilon - \varepsilon^0)\left(\frac{\Delta E}{E^{II}}\right)]\varepsilon \quad (1)$$

$$\Delta E = [E^{II} - \frac{d\sigma}{d\varepsilon}] \text{ for } \varepsilon>0 \quad (2)$$

where ε is strain and σ is stress, $H(\varepsilon)$ is the Heaviside unit step function and E^{II} is the intact material second-order linear elasticity. ε^0 is the initial static contact strain.

In the recent years, CAN has been investigated by a number of researchers. Kim *et al*. (2011) developed a nonlinear model for CAN of a closed crack in aluminum plate in order to analyze the nonlinear characteristics of the transmitted waves. It was shown that the interfacial stiffness has a significant effect on the amplitude of the resultant second order harmonic. Solodov *et al*. (2014) investigated the acoustic wave interaction with crack in solids using numerical and experimental approaches. It was shown that changes in the interface stiffness characteristics are the major cause of CAN. The stiffness parametric modulation and instability of oscillations are due to the asymmetry in the contact restoring forces, which results in the generation of sub-harmonics. Hong *et al*. (2012) investigated the phenomenon of CAN due to breathing fatigue cracks and the material nonlinearity using a piezoelectric sensor network. It was shown that the relative acoustic nonlinearity parameter increases proportionally with the wave propagation distance. Kishiwada *et al*. (2009) used fundamental antisymmetric mode (A_0) Lamb wave for detecting clapping between two thin aluminum plates under different loads at the contact interface. It was shown that higher or odd harmonics of Lamb wave are generated due to clapping between two aluminum plates. Moreover, the applied load affects the dispersive behavior of asymmetric Lamb waves. It was shown that the phenomena of generation of odd harmonics due to clapping effect could be used for damage detection and imaging. More advanced non-classical nonlinear response techniques such as modulation methods were invented by Korotkov *et al*. (2014) and Donskoy *et al*. (2001) which involved both classical and non-classical nonlinear responses and exploited the effects of the nonlinear interaction between ultrasonic probing signal and a low frequency vibration for damage detection.

7. References

1) Pecorari C and Solodov I (2006). Non-classical Nonlinear Dynamics of Solid Interfaces in Partial Contact for NDE Applications. Springer Journals; 307-324.
2) Raghavan A. and Cesnik C.E.S. (2007). 'Review of guided-wave structural health monitoring'. The Shock and Vibration Digest, Vol. 39 (2), pp. 91–114.
3) Rayleigh, J.W.S., (1889). 'On waves propagated along the plane surface of an elastic solid'. Proceedings of the London Mathematical Society, Vol.17, pp. 4–11.
4) Lamb, H. (1917). 'On waves in an elastic plate. Proceedings of the Royal Society of London'. Seriers A, Containing Papers of a Mathematical and Physical Character, Vol. 93 (648), pp. 114–128.
5) Stoneley, R. (1924). 'Elastic waves at the surface of separation of two solids'. Proceedings of the Royal Society of London. Series A, Containing Papers of a Mathematical and Physical Character 106, pp. 416–428.
6) Love, A.E.H. (1926). Some Problems of Goedynamics. Cambridge University Press.
7) Viktorov, I.A. (1967). 'Rayleigh and Lamb Waves Physical Theory and Applications'. New York: Plenum Press.
8) Achenbach, J.D., (1973). 'Wave Propagation in Elastic Solids'. Elsevier.
9) Graff, K.F., (1975). 'Wave Motion in Elastic Solids. Mineola', New York: Oxford University Press.
10) Rose, J.L., (1999). 'Ultrasonic Waves in Solid Media'. New York: Cambridge University Press.
11) Ostachowicz, W., Kudela, P., Zak, M.K.A., (2011).' Guided Waves in Structures for SHM: The Time - domain Spectral Element Method',Wiley.
12) Pavlakovic, B. and Lowe, M.J.S. (2003). 'Disperse Software Manual Version 2.0.16B'. Imperial College London, UK.
13) Farrar, C.R., Worden, K. (2007). 'An introduction to structural health monitoring'. Phil. Trans. R. Soc. A. 365, 303-315

14) Kim N, Lee TH, Jhang KY and Park IK. (2011). Nonlinear Behaviour of Ultrasonic Wave at Crack. AIP Conf . 1211, 73.

15) Hong M, Su Z, Wang Q, Cheng L and Qing X (2012). Modelling nonlinearities of ultrasonic waves for fatigue damage characterization. Ultrasonics. 54, 770-778.

16) Solodov I. Wackerl J, Pfleiderer K and Busse G. (2014). Nonlinear self-modulation and subharmonic acoustic spectroscopy for damage detection and location. Appl Phys Lett; 84:N26, 5386-5388.

17) Kishiwada S, Biwa S, Inserra I, Matsumoto E. (2009). Nonlinear Ultrasonic Characterization of Lamb Wave in a Plate with Contacting Interfaces. Proceed ICCAS-SICE. 2368: 1-6.

18) Korotkov AS, Slavinsky MM and Sutin AM. (2014). Variations of acoustic nonlinear parameters with the concentration of defects in steel. J Acoust Phys; 40: 71-74

19) Donskoy A, Sutin A and Ekimov C. (2001). Nonlinear Acoustic Interaction on Contact Interfaces and its use for Nondestructive Testing. NDT & E In. 34: 231-238.

Statement of Authorship of the Journal Paper 1

Statement of Authorship of the Journal Paper Title of Paper	Scattering of the fundamental anti-symmetric Lamb wave at through-thickness rectangular notches in isotropic plates
Publication Status	☑ Published ☐ Accepted for Publication ☐ Submitted for Publication ☐ Unpublished and Unsubmitted w ork w ritten in manuscript style
Publication Details	Journal of Civil Structural Health Monitoring, 2016, Vol.6(3), pp.447-459

Principal Author

Name of Principal Author (Candidate)	Reza Soleimanpour		
Contribution to the Paper	Performed the study and wrote the manuscript		
Overall percentage (%)	60		
Certification:	This paper reports on original research I conducted during the period of my Higher Degree by Research candidature and is not subject to any obligations or contractual agreements with a third party that would constrain its inclusion in this thesis. I am the primary author of this paper.		
Signature		Date	12/09/2016

Co-Author Contributions

By signing the Statement of Authorship, each author certifies that:

i. the candidate's stated contribution to the publication is accurate (as detailed above);

ii. permission is granted for the candidate in include the publication in the thesis; and

iii. the sum of all co-author contributions is equal to 100% less the candidate's stated contribution.

Name of Co-Author	Ching-Tai Ng		
Contribution to the Paper	Supervised development of the work and manuscript evaluation		
Signature		Date	12/09/2016

Please cut and paste additional co-author panels here as required

Chapter 3: Scattering of the fundamental anti-symmetric Lamb wave at through-thickness rectangular notches in isotropic plates

Abstract. Lamb wave based structural health monitoring technique is one of the promising techniques for detecting damages in structures. Among different types of guided waves, the fundamental anti-symmetric Lamb wave (A_0) has attracted considerable attention for damage detection in plates due to its outstanding properties, such as sensitivity to small and different types of defects, which make it a powerful tool for damage detection. Notches are one of the major culprits in metallic structures, which affect their durability and serviceability. Once the notch appears on the structures, it can affect its serviceability. It is important to detect notches at early stage to avoid any catastrophic failure of the structures. This paper presents an study on the capability of using the A_0 Lamb wave in detecting notches in aluminium plates, in which the scattering behaviour of the A_0 Lamb wave at through-thickness notches in aluminium plates is studied in detail. 3D explicit finite element (FE) simulations are used to provide a comprehensive study on the scattering characteristics of the A_0 Lamb wave at notches with different sizes and orientations. This study also considers different incident and scattered wave directions on the scattering characteristics. The results show that scattering characteristics of the A_0 Lamb wave are sensitive to the size and orientation of notches. The findings of this study can improve the understanding of the capability of the A_0 Lamb wave in detecting the notches and further advance damage detection techniques.

Keywords: scattering, anti-asymmetric mode, Lamb wave, 3D finite element, through-thickness notch

1. Introduction

The use of Lamb waves in non-destructive evaluation and structural health monitoring has attracted considerable attention in the last few decades [1-4]. Different damage detection techniques using Lamb waves have been developed to detect, locate and identify defects in the variety of engineering structures [5,9]. It has been demonstrated that Lamb waves are 1) able to inspect large areas, 2) sensitive to detect different types of defects and 3) efficient in detecting small defects in thin-walled structures. The use of Lamb waves for damage detection relies on the wave scattering at the defects and it usually requires baseline subtraction to extract the scattered wave signals due to the complexity of the received signals and the structures being inspected [10]. Therefore, the characteristics of the scattered waves, such as scattering magnitude and directivity pattern are important for the damage detection.

In the last decade different research works have focused on investigating the characteristics of Lamb wave propagation and scattering at different types of defects, such as crack [11], hole [12], corrosion [13], delamination [14] and debonding [15,16,17]. The findings of these studies have improved fundamental insights into the scattering phenomena of Lamb waves at the defects, which have supported the developments of the damage detection techniques using Lamb waves. Early researches focused on using analytical models to investigate the scattering characteristics but they are only available for defects with simple geometry, such as circular through hole [18], part-thickness circular defects [19]. Analytical and models also exist for Lamb wave scattering at cracks [20,21] but these have restrictions on the geometry of the crack.

Numerical simulation methods, such as finite difference method [12], finite element (FE) method [22,23], spectral FE method [16,17,24], elastodynamic finite integration method [25] and local simulation method [26] have been employed to investigate the fundamental symmetric (S_0) and anti-symmetric (A_0) Lamb wave scattering at different types of defects. For common structural defects such as cracks and notches, a number of studies have been carried out using the numerical methods in the literature; Wang and Shen [27] employed a T-matrix and the boundary element hybrid method to study the scattering of the S_0 Lamb wave at crack

in a plate. The reflection and transmission coefficient were studied as a function of frequency. Lowe et al. [28] studied the reflection characteristics of the A_0 Lamb wave from surface-breaking rectangular notches in isotropic plates using a two-dimensional (2D) FE method and experimental data. They showed that the reflection coefficient exhibits a consinusoidal periodic shape when it is plotted as a function of the notch width due to the interference between the separate reflections from the start and the end of the notch. Lowe and Diligent [29] investigated the low-frequency reflection characteristics of the S_0 Lamb wave from a rectangular notch in a plate using a 2D FE method. The numerical simulation results were compared with experimental data. An interference phenomenon was identified that explains the periodic nature of the reflection coefficient as a function of notch width. Lu et al. [30] analysed the S_0 Lamb wave interaction at a through-thickness cracks in aluminium plates using three-dimensional (3D) FE method and experiment measurements. They analysed the effect of wavelength of the S_0 Lamb wave and wave diffraction on the properties of the reflection and transmission coefficients. Moreau et al. [13] proposed a FE modelling approach for predicting S_0 and the A_0 Lamb waves scattering at irregular defects. The study showed that significant performance improvement can be achieved by optimising some parameters of the numerical model, such as size of elements and smoothness of the defect geometry. Quek et al. [31] and Salvino et al. [32] used the Hilbert transform to process guided waves in plates with notches. This technique separates the guided waves into an intrinsic mode functions and a residue which is followed by the Hilbert transform to determine the energy time signal of each mode for locating the notch. Sun et al. [33] used continuous wavelet transform methods with a Morlet mother wavelet for characterising notches in pipes.

Compared to the S_0 Lamb wave, the A_0 Lamb wave has a shorter wavelength, and hence, it is potentially more sensitive to small damage. In addition, the A_0 Lamb wave is generally easier activated and has larger signal magnitudes than S_0 Lamb waves at low frequency. Recently Fromme and Rouge [34] investigated directivity pattern of the scattered A_0 Lamb wave at

notches and cracks. Both the 3D FE method and experimental data were used to study the amplitudes of the A_0 Lamb wave scattering at these defects when the incident wave was at two difference directions. They demonstrated that the scattered wave has almost no energy at certain directions from the cracks.

The aim of this research is to provide a comprehensive investigation of the A_0 Lamb wave scattering characteristics at through-thickness notches in isotropic plates. In this study 3D explicit FE simulations were used to study the 3D characteristics of the A_0 Lamb wave at through-thickness notches. The sensitivity of the A_0 Lamb wave at notches with different sizes and orientations was assessed quantitatively. The scattering directivity pattern (SDP) was used to investigate the scattering characteristics of the scattered A_0 Lamb wave at the notches in different directions. The findings of this study provides physical insights into the A_0 Lamb wave scattering phenomena at through-thickness notches, which are important to further advance Lamb wave based damage detection techniques and optimise transducer networks for damage detection.

The paper is organised as follows. Section 2 explains the 3D explicit FE simulation used in this study and describes calculation of group and phase velocity of Lamb waves. In Section 3, the FE models are described and numerical verification of the incident A_0 Lamb wave is carried out using the software DISPERSE [35]. Section 4 presents an analytical verification of damaged models and described series of damage case studies. A comprehensive study of the A_0 Lamb wave scattering at through-thickness notches is presented. A series of parameters, such as notch orientation, scattered wave direction and notch length to wavelength ratio are also studied and discussed in Section 4. Section 5 presents the conclusions of the study.

2. Guided waves propagation in isotropic plates

2.1. Numerical simulation and material properties

In this study, a 3D explicit FE method was used to simulate the A_0 Lamb wave propagation in an aluminium plate. The size of the aluminium plate is 400mm × 200mm × 0.8mm, which is large enough to avoid the wave reflections from the plate boundaries in the scattering study. The FE software ABAQUS was used to model the aluminium plate. The plate was modelled using four-noded 3D doubly curved shell, reduced integration, hourglass control, finite membrane strains element (S4R), which approximates a 3D continuum with a 2D theory. Each of the nodes of this element has six degrees-of-freedom (DOFs). In this study the mesh size for all models is 0.4×0.4 mm^2. Since the S4R element is a reduced integration element, a model with S4 shell elements, which uses the full integration in the simulation, was also used to model the Lamb wave propagation and the results were compared against the results of S4R shell elements. The S4 shell element uses full integration, and hence, it does not have problem of hourglassing but it is computationally more expensive. Therefore, the results of these two types of elements were compared to ensure the accuracy and to investigate the capability of S4R elements in simulating the Lamb wave propagation. The plate's Young's modulus (***E***) is 70*Gpa*, the poison's ratio (***υ***) is 0.33 and the density (***ρ)*** is 1517kg/m^3.

The A_0 Lamb wave was excited by applying out-of-plane displacements to a half circular area with 6 mm diameter as shown in Figure 1. Shell elements with dimensions of 0.4×0.4 mm^2 were used in all plate models. Alleyne and Cawley [1] recommended the following equation for determining the maximum mesh size in simulating the propagation of guided wave:

$$l_e \leq \frac{\lambda_{min}}{10} \tag{1}$$

where l_e is the maximum mesh size and λ_{min} is the minimum wavelength size in the simulations. The small mesh size (0.4×0.4 mm^2) used in this study satisfies the requirement in Equ. (1) and ensures the accuracy of the simulations.

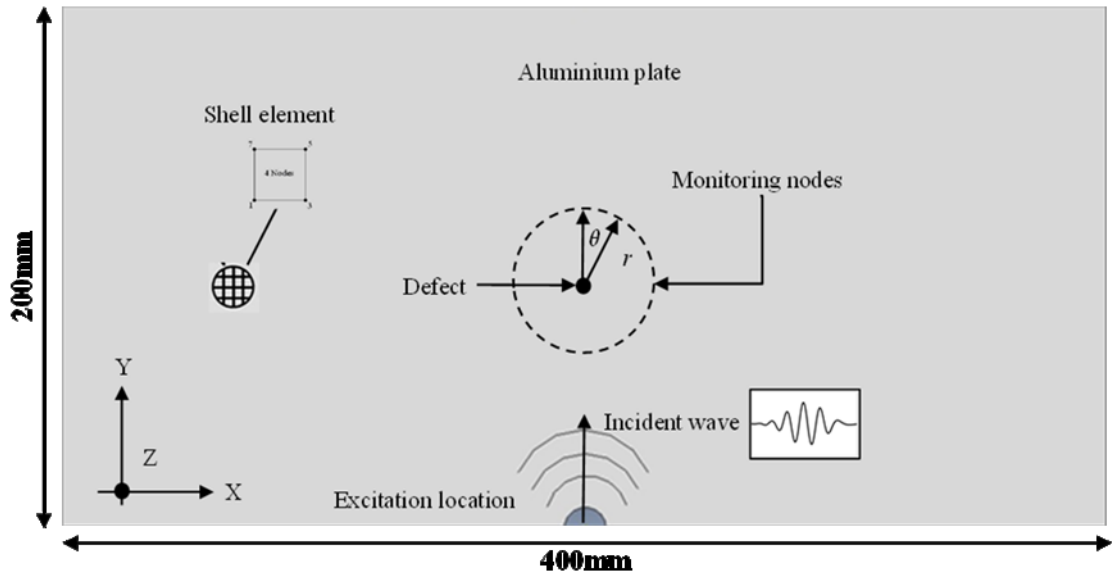

Figure 1. Schematic diagram of the 3D FE model

The dynamic simulation was solved using the explicit FE code in ABAQUS, which uses the central-difference integration. In this scheme, the integration operator matrix is inverted and a set of nonlinear equilibrium equations is solved at each time increment. Since the central different integration scheme is conditionally stable, the increment time step has to be small enough to ensure the stability. Stewart et al. [36] recommended limiting the hourglass energy to less than 2% of the total energy to ensure the accuracy of predicting the guided wave propagation in solids. Bathe [37] recommended the following condition in order to ensure the stability of the explicit analysis:

$$\Delta t \leq \frac{L_{min}}{c_L} \tag{2}$$

where Δt is the time increment, L_{min} is the smallest mesh size and c_L is the longitudinal wave speed. However, the time increment is automatically determined by ABAQUS for all simulations in this study.

2.2. Phase and group velocity calculation

The phase velocity of the Lamb waves (c_p) can be calculated by [11,38]

$$c_p = \frac{2\pi f}{k} = \frac{2\pi f\, \Delta\phi}{\Delta x} \tag{3}$$

where f is the central frequency of the incident Lamb wave, k is the rate of phase change at a certain distance, $\Delta\phi$ is the phase change corresponding to measurement points with a distance of Δx (less than the wavelength).

The group velocity is calculated from the energy density spectrum of the Lamb wave signals. The energy density spectrum can be calculated by continuous wavelet transform (CWT) (Veidt and Ng [14]).

$$WT(p,q) = \int_{-\infty}^{\infty} u(t)\chi^*_{p,q}(t)dt \tag{4}$$

where

$$\chi_{p,q}(t) = \frac{1}{\sqrt{q}}\,\chi\left(\frac{t-p}{q}\right) \tag{5}$$

p and q are wavelet transform factors and $u(t)$ is the out-of-plane displacement of the guided wave signal. The asterisk donates the complex conjugate. $\chi(t)$ is the mother wavelet which is Gabor wavelet and is defined as:

$$\chi(t) = \frac{1}{\sqrt[4]{\pi}}\sqrt{\frac{\omega_0}{\eta}}\exp\left[-\frac{(\frac{\omega_0}{\eta})^2}{2}\,t^2 + i\omega_0 t\right] \tag{6}$$

The time-frequency analysis resolution is affected by the value of ω_0 and η. These values are usually considered as $\omega_0 = 2\pi$ and $\eta = \pi\sqrt{2/ln2} \approx 5.336$. The energy density spectrum is calculated by $|WT(p,q)|^2$, which indicates the energy distribution of the signal around $t = p$, $\omega = \omega_0/q$ and is used to calculate the arrival time of the guided waves. The group velocity is defined as

$$c_g(f_c) = \frac{\Delta x}{\Delta t} \quad (7)$$

where Δt is the difference of the wave packet arrival times between two measurement points.

3. Verification of intact finite element models

3.1. Element type verification in FE simulation

The aim of this section is to verify the element type used in the FE models. The model was the same aluminium plate as described in Sec. 2.1. The dimension of the aluminium plate was 400 mm × 200 mm × 0.8 mm. As discussed in Sec. 2.1, S4R elements were used to simulate the Lamb wave propagation. In this section S4R and S4 elements were used to simulate the same aluminium plate and the results were compared to investigate the accuracy of S4R elements in simulating the A_0 Lamb wave propagation. A sinusoidal tone burst pulse with signal frequency of 140 kHz and 5-cycle modulated by Hanning window was used for generating the A_0 Lamb wave and the centre of the excitation area was located at r = 40mm and θ =180°. Fig. 1 shows the FE setup in this study and the locations of measurement points. The out-of-plane displacement signal at the monitoring point located at r = 40mm and θ =180° is shown in Fig. 2. As shown in Fig. 2 there is a very good agreement between the results from these two FE models. Therefore, the S4R element was used for the rest of the studies in this paper.

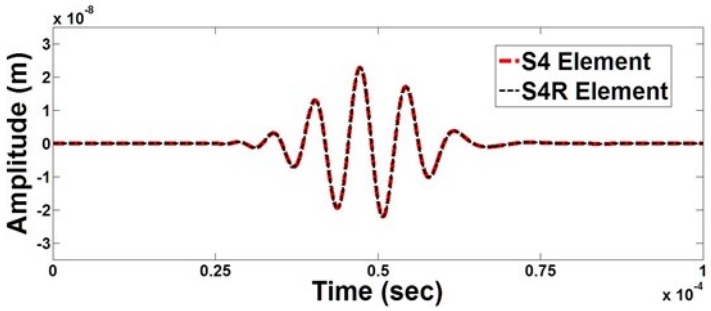

Figure 2. Comparison between the out of-plane displacement results of S4R and S4 models

3.2. Numerical verification of intact FE model

This section presents a study of the A_0 Lamb wave propagation in the aluminium plate described in Secs. 2.1 and 3.1. The FE model was validated by comparing the phase and group velocity of the Lamb wave with results calculated by DISPERSE [35]. In this part of the study, there are no defects in the aluminium plate. This study considered excitation frequencies from 20 kHz to 380 kHz with steps of 20 kHz. In the FE simulation, the out-of-plane displacement of the A_0 Lamb wave was calculated at four measurement points with 2mm distance away from each other, in which the first measurement point is at 6mm from the excitation location. The captured data was used to calculate the group and phase wave velocities at different excitation frequencies.

The group velocity was calculated by dividing the distance between the measurement points (2mm) by the difference of arrival time of the incident wave at two measurement points (Eq. 7). Similarly, the phase velocity was obtained by calculating the phase change of the signals between two measurement points and then substituting them into Eq. (3). The phase and group velocity of the wave at each excitation frequency was calculated by averaging the calculated velocities from these four measurement points. The simulation results are compared with DISPERSE results to ensure that the FE simulations can accurately predict the propagation of the A_0 Lamb wave in the aluminium plate. Figs. 3 and 4 show the phase and group velocity dispersion curves calculated by the FE simulations and DISPERSE.

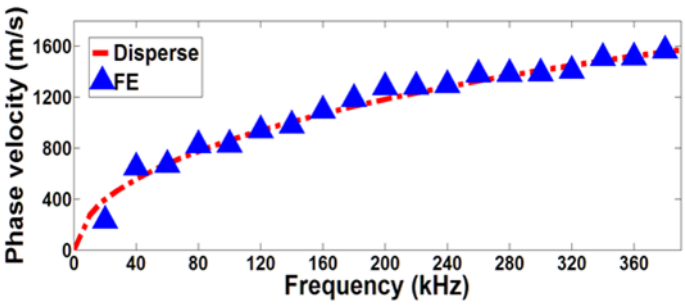

Figure 3. Comparison between phase velocity dispersion curves obtained from FE simulations and DISPERSE

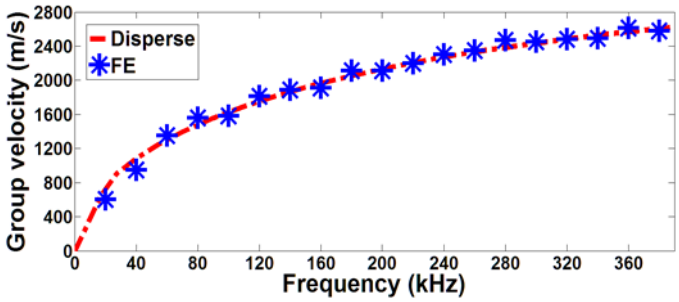

Figure 4. Comparison between group velocity dispersion curves obtained from FE simulation and DISPERSE

As shown in Figs. 3 and 4, the phase and group dispersion curves calculated from FE and DISPERSE have a very good agreement. This shows that, the FE simulations are able to predict the propagation of the A_0 Lamb wave in the aluminium plate.

4. Scattering analysis of the A_0 Lamb wave at defects in the aluminium plate

4.1. Analytical verification of FE model with damage

This section presents a study of the A_0 Lamb wave propagation in an aluminium plate with a damage. The aluminium plate has the same material properties and size as the one described in Secs. 2.1 and 3.1. A 7mm diameter through hole at the centre of the aluminium plate was modelled in the FE simulation. The aim of this section is to investigate the capability of 3D FE simulations in predicting the A_0 Lamb wave scattering at defects. The accuracy of the results was verified using an analytical method, i.e the wave function expansion method [18].

The FE setup is shown in Fig.1. A sinusoidal tune burst pulse with a signal frequency of 140 kHz and 5-cycle modulated by Hanning window was used for generating the Lamb wave. The A_0 Lamb wave was generated by applying an out-of-plane displacement to the nodal points. The wavelength of the incident A_0 Lamb wave at 140 kHz is 7mm, and hence, the diameter of the through hole is the same as the wavelength. The through hole was created by removing the

FE elements as shown in Fig. 5. To extract the scattered wave signals, two simulations were carried out in the study. One is an intact plate and the other one is a plate with a through hole. Baseline subtraction technique was used for extracting the scattered A_0 Lamb wave at the defect. The scattered A_0 Lamb wave was obtained by subtracting data calculated from both FE models using Eq. 8.

$$D_s^{(r,\theta)} = D_d^{(r,\theta)} - D_i^{(r,\theta)} \tag{8}$$

where $D_s^{(r,\theta)}$ is the out-of-plane displacement of the scattered wave obtained from the measurement point located at (r,θ). $D_d^{(r,\theta)}$ is the out-of-plane displacement from the damaged model and $D_i^{(r,\theta)}$ is the out-of-plane displacement of the from the intact model. Based on the polar coordinate as shown in Fig. 1, the data was recorded at 36 measurement points located at $r = 40mm$ and $0 \leq \theta \leq 360$ with θ =10° interval from each other. Since the distance of measurement points from the through whole is much larger than the wavelength, the generated evanescent waves can be ignored.

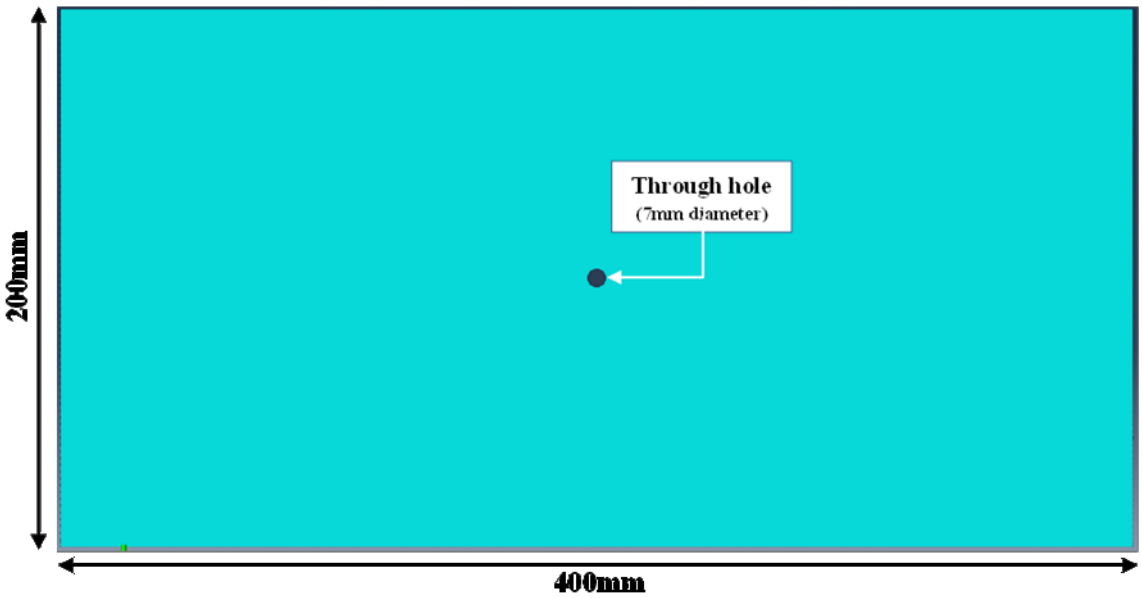

Figure 5. Through hole in the FE model

Fig. 6 shows the scattered A_0 Lamb wave at the through hole. The SDP was used for comparing the results of the analytical method with FE simulation results.

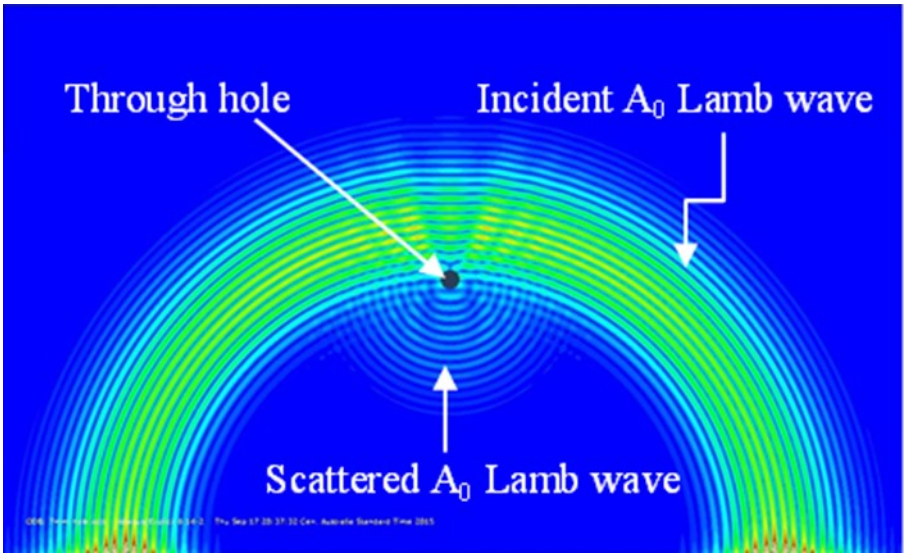

Figure 6. Scattered A_0 Lamb wave at through hole

The SDP was obtained by calculating the maximum absolute amplitude of the scattered A_0 Lamb wave and then normalising them to the maximum absolute amplitude of the incident A_0 Lamb wave at the centre of the through hole in the intact model. Fig. 7 shows a comparison of the SDP obtained from the analytical approach and FE simulation.

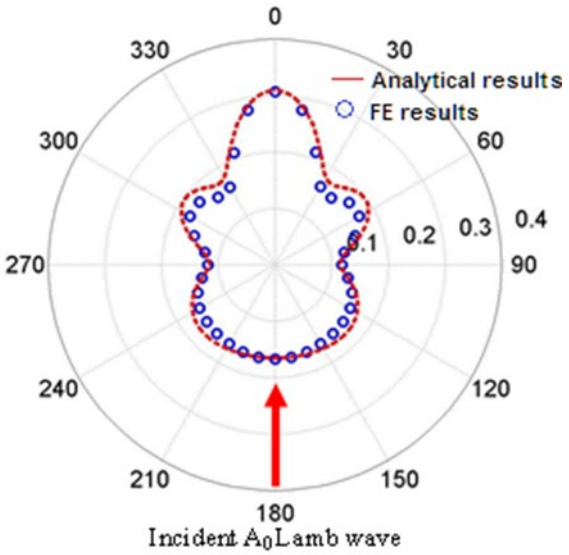

Figure 7. Analytical results and FE results of SDP for 7mm diameter through hole

Fig. 7 shows that the analytical results and FE results are in a very good agreement. Therefore, the FE simulation can accurately predict the Lamb wave propagation and scattering at defects in the aluminium plates.

4.2. Damage case studies with through-thickness notches

This section provides a comprehensive study of scattering characteristics of the A_0 Lamb wave in aluminium plates with through-thickness notches. For this purpose, a number of FE models are considered in this section. The size and material properties of the plate is the same as the FE models described in Secs. 2 & 3. The through-thickness notches were created at the centre of the plate by removing FE elements. Five different notch orientations were considered in the study, i.e. 0°, 30°, 45°, 60° and 90°. For each notch orientation, the notch length to wavelength ratios ($\alpha=d/\lambda$) from 0.2 to 2 with 0.2 steps are considered, where d is the notch length and λ is the wavelength of the incident A_0 Lamb wave. The notch width is 1mm for all damage cases. As explained in Sec.3, the wavelength for 140 kHz is 7mm. Table 1 summarises the notch lengths considered for each notch orientation.

Table 1. Notch lengths considered for each notch orientation

Damage case	1	2	3	4	5	6	7	8	9	10
$\alpha=d/\lambda$	0.2	0.4	0.6	0.8	1.0	1.2	1.4	1.6	1.8	2.0
Crack size (mm)	1.4	2.8	4.2	5.6	7.0	8.4	9.6	11.2	12.6	16

The A_0 scattered Lamb waves at 36 measurement points were calculated at r = 40mm *and* $0° \leq \theta \leq 360°$ with 10° intervals from the centre of the through-thickness notch, which fulfils the far field requirement for ignoring evanescent waves. Since the out-of-plane motion is the dominant displacement for the A_0 Lamb wave, the nodal out-of-plane displacements were used in the study. Fig. 8 shows the through-thickness notch for Damage Case 8 ($\alpha = 1.6$) with notch orientation 90°.

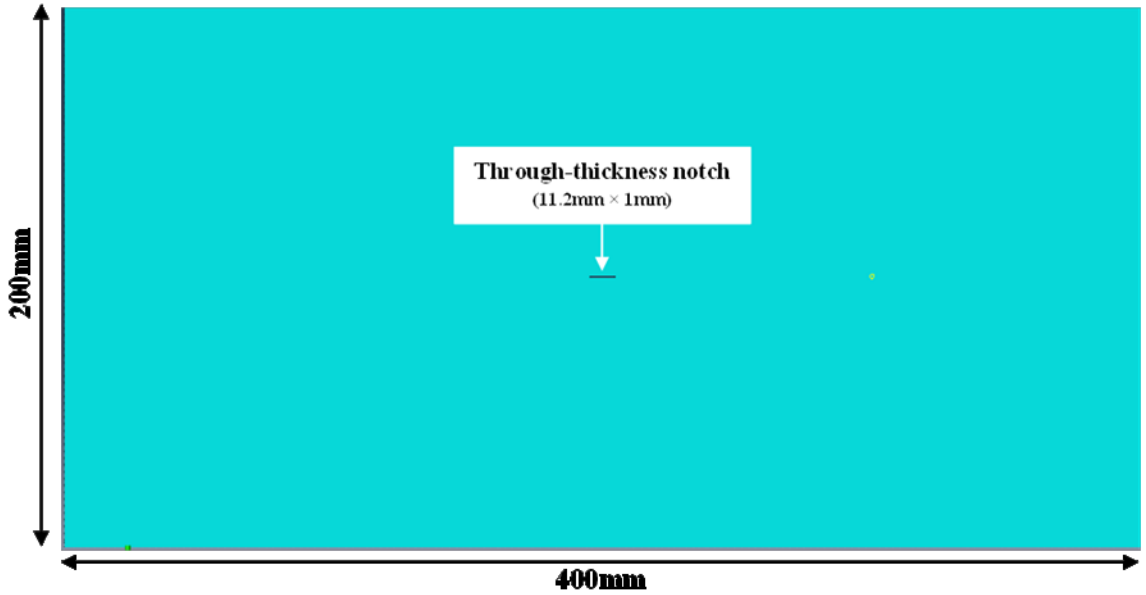

Figure 8. Through-thickness notch with 90° orientation and α =1.6

4.3. Scattering directivity pattern of the scattered A_0 Lamb wave from through-thickness notches

The SPD was calculated using the method described in Sec. 4.1. Here, the scattered wave amplitudes were normalised by the maximum absolute amplitude of the signal at the centre of notch in the intact model. Figs. 9a - 9e show pictures of the incident A_0 Lamb wave interacting and scattering at the through-thickness notches with α=1.4 (Damage Case 7) and different orientations (0°, 30°, 45°, 60°, 90°). The figures show that the energy distribution of scattered wave at each direction varies with notch orientation. Figs. 10a – 10e show the SDP of the scattered A_0 Lamb wave from the notches with α *=2.0* (Damage Case 10) and different orientations. The incident A_0 Lamb wave direction and notch orientations are also shown in Fig. 10.

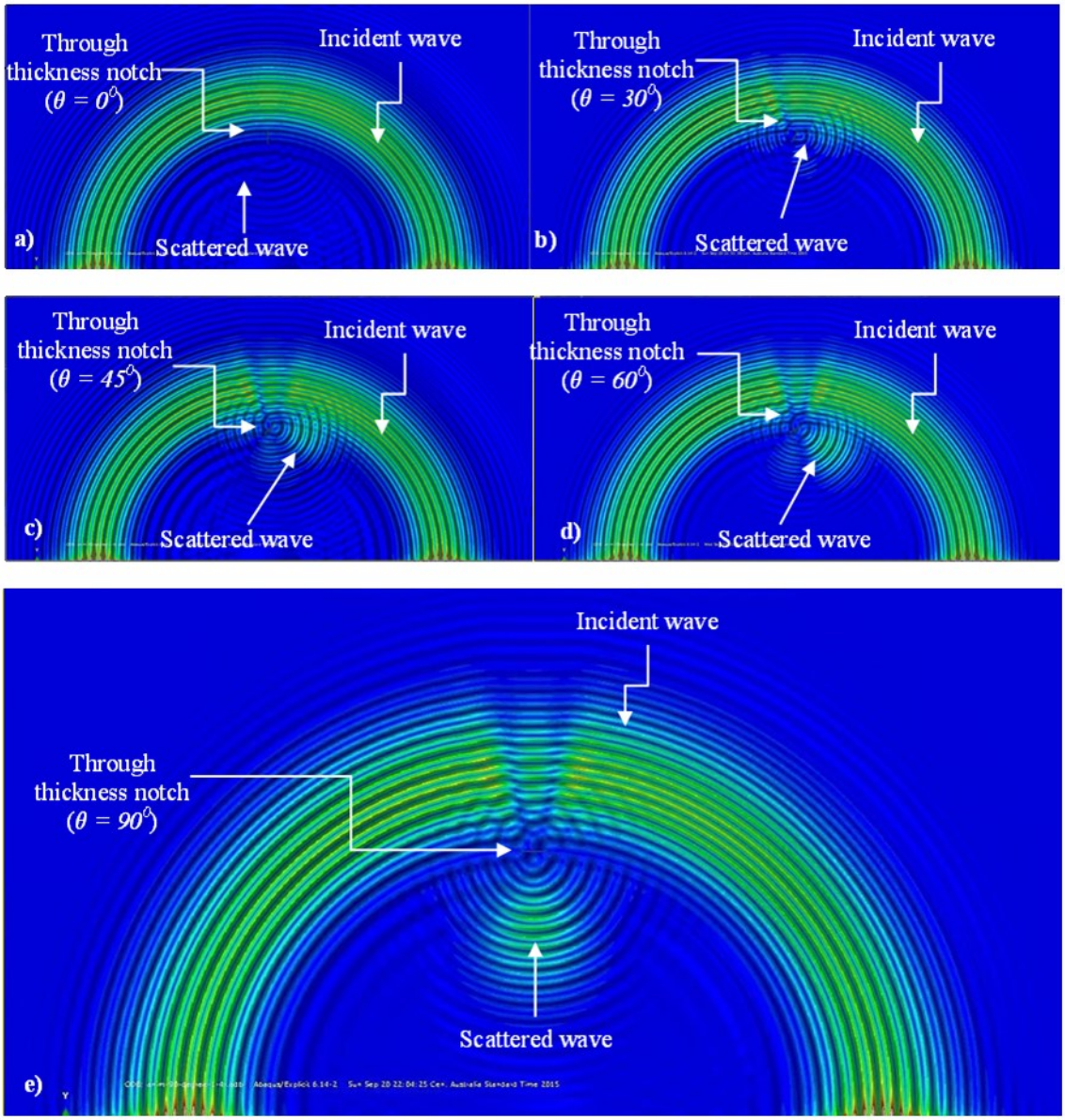

Figure 9. Typical contour plots of FE simulated out-of-plane displacement of the scattered A_0 Lamb wave at through-thickness notches with α=1.4 and notch orientations a) 0°, b) 30°, c) 45°, d) 60° and e) 90°, and t= 52 µs

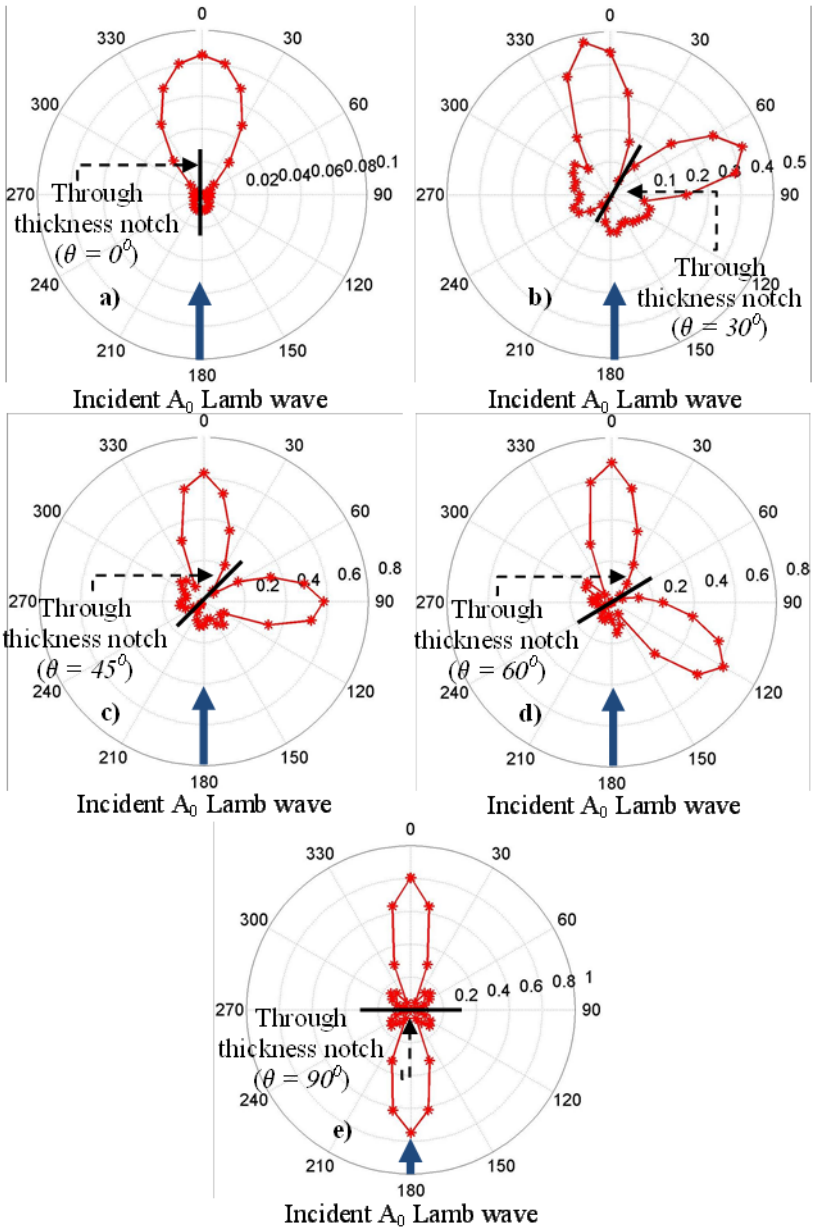

Figure 10. SDPs of the scattered A_0 Lamb wave from through-thickness notches with α =2.0 (Damage Case 10) and different orientations a) 0° b) 30° c) 45° d) 60° and e) 90°

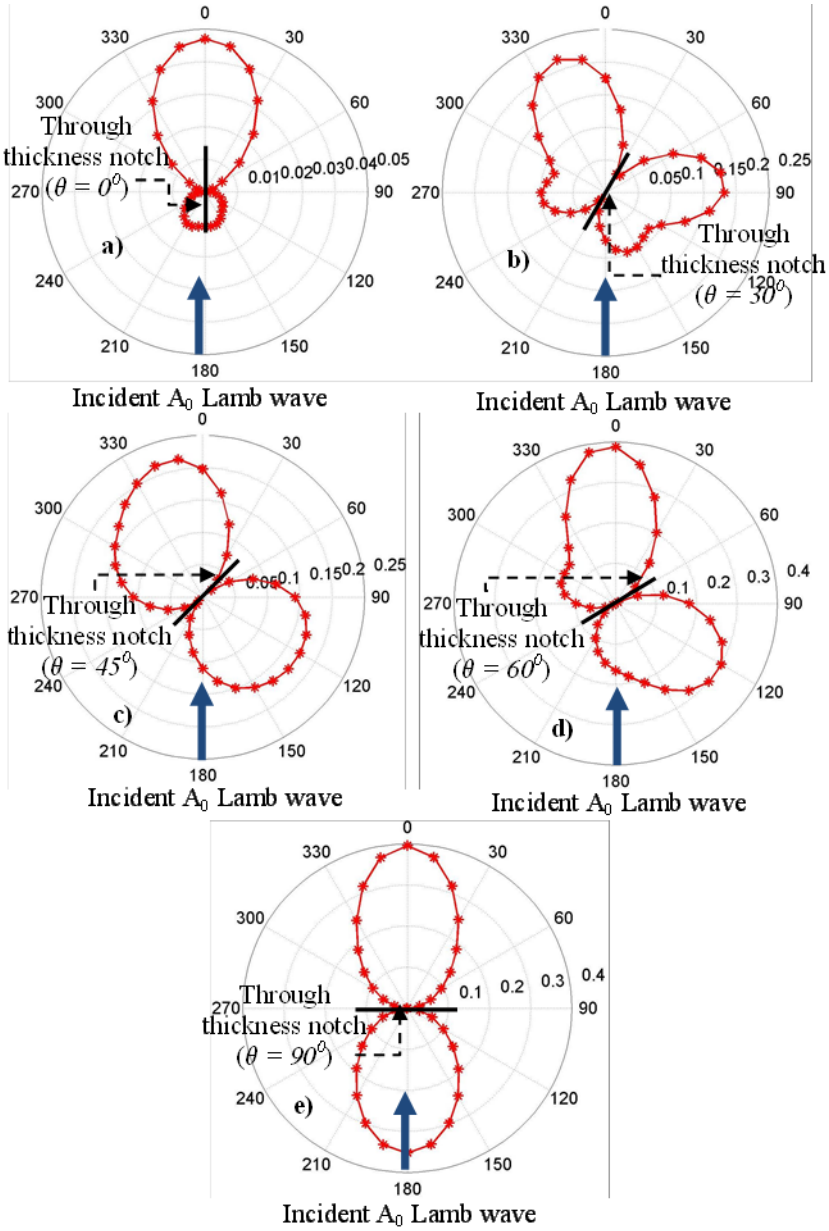

Figure 11. SDPs of the scattered A_0 Lamb wave from through-thickness notch α =1.0 (Damage Case 5) and different orientations a) 0° b) 30° c) 45° d) 60° and e) 90°

Figs. 11a - 11e show the SDPs of the scattered A_0 Lamb wave from through-thickness notches with α *=1.0* (Damage Case 5) and different orientations. The figures show that the SDP of notch orientation at *0°* and *90°* are symmetric with respect to 0° direction but SDP of other cases are not symmetric as the notch orientation suppresses the models symmetry. Therefore, the characteristics of the scattered A_0 Lamb wave become complicated when notch orientation is not symmetric. The results show that forward and backward scattering amplitudes have almost the same order for notch orientation at *90°* and they vary with the notch orientations.

However, the amplitude of forward scattering signals is larger than the amplitude of backward scattering signals in all cases shown in Fig. 11.

The results also show that the amplitude of the scattered A_0 Lamb wave from the notch has its largest magnitude when the notch is at orientation $90°$ (perpendicular to incident wave propagation direction) but it has the smallest magnitude for the notch at orientation $0°$ (parallel to incident wave propagation direction). Therefore, for damage detection purposes, the best results are obtained when the propagation direction is perpendicular to the notch orientation. The results of this study indicate that it is most challenging for the notch to be detected if the incident wave propagation direction is parallel to the notch orientation. The results of this section indicate that the amplitude of forward scattering waves have a larger magnitude than backward scattering waves for all considered notch orientations, and the amplitudes of the scattered waves are sensitive to the orientation.

4.4. Scattering characteristics of the scattered A_0 Lamb wave from through-thickness notches

In this section, the influence of notch length to wavelength ratio, notch orientation and the scattered A_0 Lamb wave at different directions from the through-thickness notches are investigated. The scattered A_0 Lamb wave amplitudes of a number of measurement points located at $r=40mm$ and $0 \leq \theta \leq 360$ with $30°$ intervals from the centre of notches are shown in Figs. 12 and 13. The results of forward and backward scattered wave are shown in Figs. 12 and 13, respectively. The scattered wave was extracted and the amplitude was normalised according to the method explained in Sec. 4.3. The normalised amplitudes of a number of monitoring points are presented against the notch length to wavelength ratio. It should be noted that the results of $\theta = 90°$ and $\theta = 270°$ have been included in both Figs 12 and 13. Figs.12a-12e and 13a-13e show the normalised amplitude of forward and backward scattered waves

against notch length to wavelength ratio for all damage cases with different notch orientations, respectively.

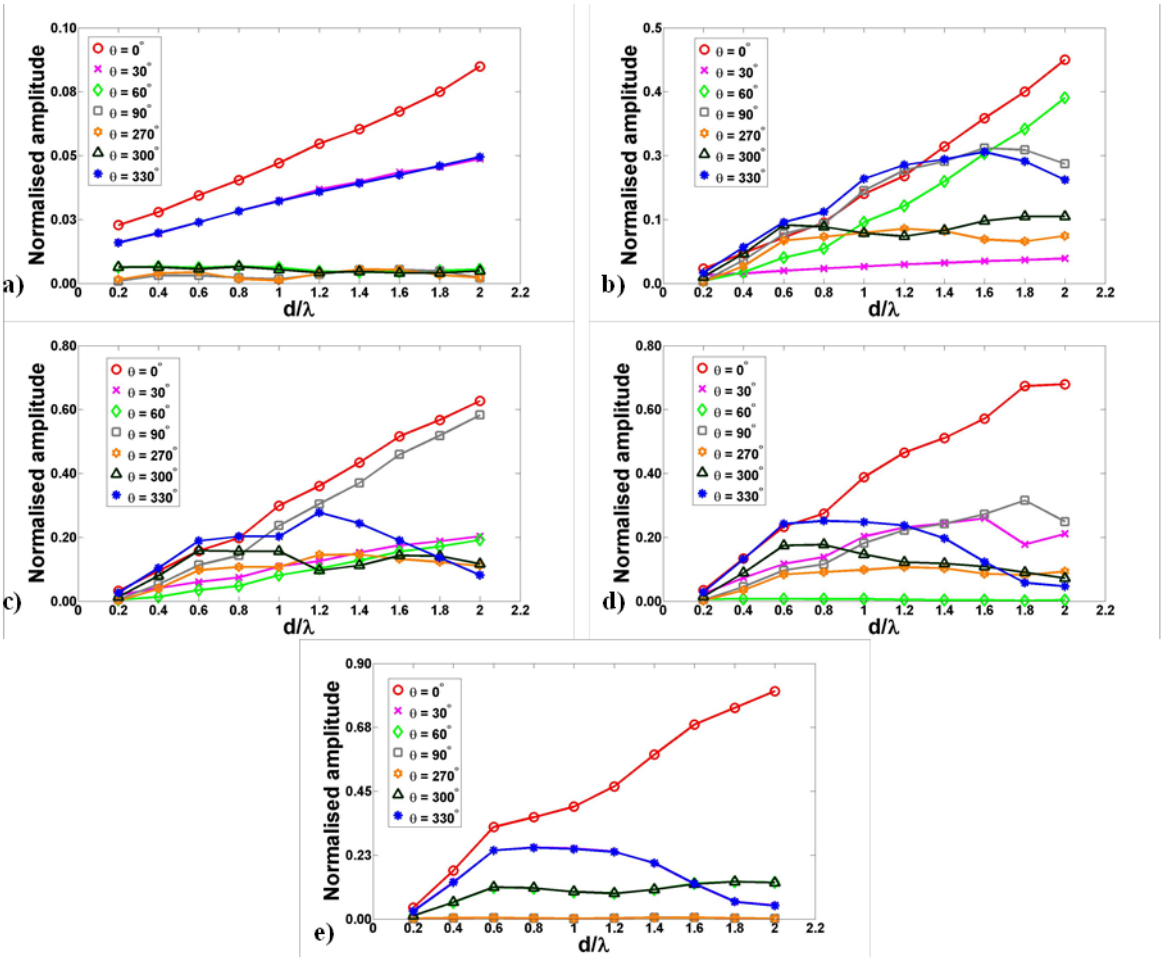

Figure 12. Normalised amplitude of the forward scattered A_0 Lamb wave against the notch length to wavelength ratio for all damage cases with notch orientations a) 0° b) 30° c) 45° d) 60° and e) 90°

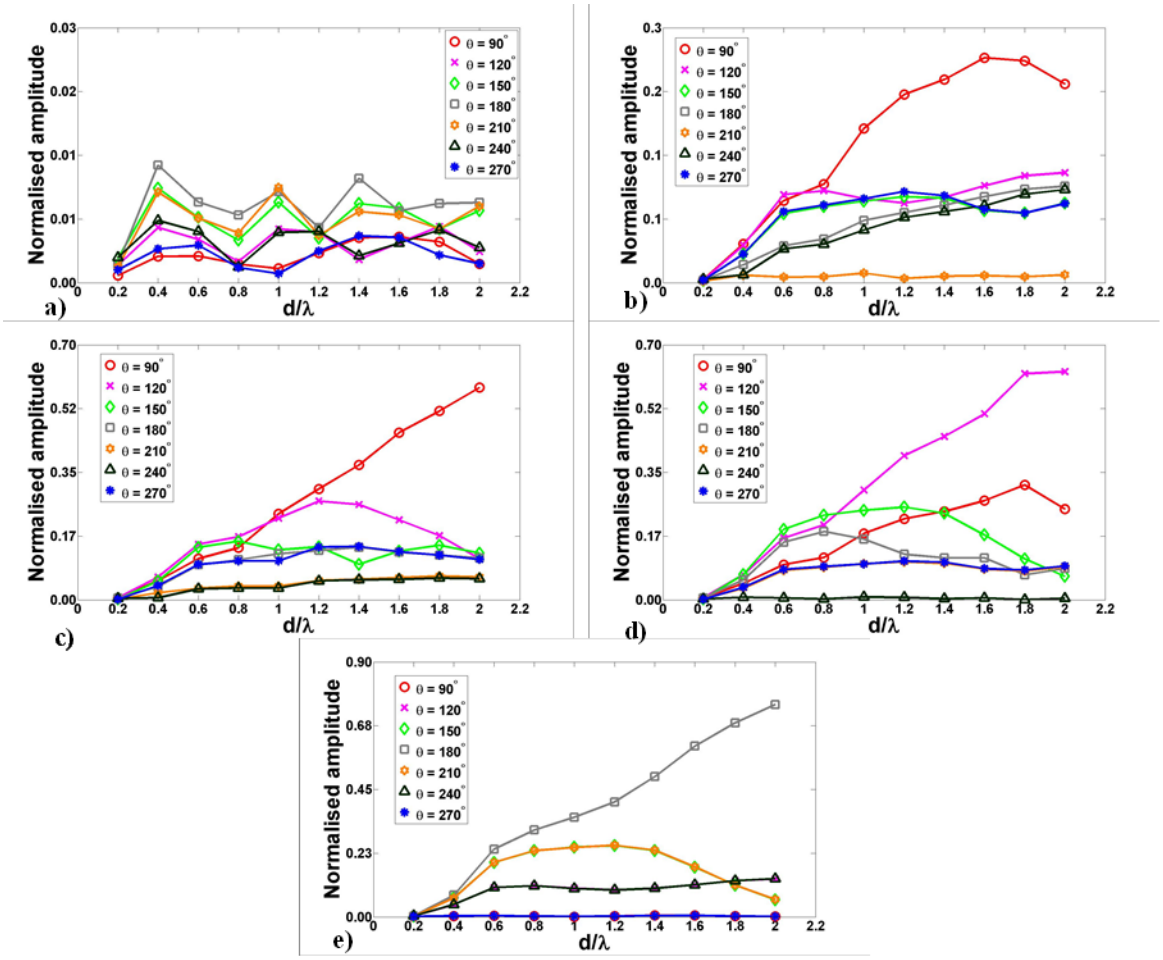

Figure 13. Normalised amplitude of the backward scattered A_0 Lamb waves against notch length to wavelength ratio for all damage cases with notch orientations a) 0° b) 30° c) 45° d) 60° and e) 90°

As shown in Figs. 12a-12e and 13a-13e, the amplitude of scattered waves increase with the notch length to the wavelength ratio and this is a major trend in most of the cases. However, this trend does not apply to all cases. The amplitude of scattered wave increases constantly with the increase of α for *0°* notch orientation and measurement point direction at θ = *330°* (Fig. 12a) but the trend of the scattered wave amplitude changes for the cases when the notch orientations are *30°, 45°*, *60°* and *90°*. In this case the amplitudes of scattered waves at this measurement point increases are first increase with α and then the amplitudes drop for larger value of α as shown in Figs.12b – 12e. However, the results show that there is a steady increase in the amplitude of forward scattering wave at θ=*0°*. Moreover, the amplitude of a scattered wave has the largest value at this measurement direction when the value of α is large for all cases. Therefore, it is expected that the amplitude of forward scattered wave can be a sensitive

tool for detecting notch length, especially for the measurement point at $\theta = 0°$. Figs. 13a-13e indicate that none of measurement point data show a steady increase in amplitude of backward scattered wave when α increases for all notch orientations. However some show this trend for particular notch orientations. For instance, the data captured at $\theta=120°$ show a steady increase with α for notch orientation of $60°$ (Fig. 13d). For other backward scattering cases, the amplitude of the A_0 Lamb wave increases at first and then decrease is the dominant trend. This shows that selecting an appropriate propagation and measurement direction studies is critical in damage detection of notches in Aluminium plates. The results of this section also indicate that small amplitudes of scattered waves are observed if the incident wave propagation direction is parallel to the notch orientation. This can be observed in Figs. 12a and 13a that have the smallest forward and backward scattered wave amplitudes in all considered cases.

5. Conclusion

This paper studied the A_0 Lamb wave scattering characteristics in an aluminium plate with different notch sizes and orientations. The A_0 Lamb wave propagation and scattering characteristics at through-thickness notches in aluminium plate has been studied using 3D explicit FE simulations. The paper investigated the effects of incident wave propagation and measurement direction on the scattered A_0 Lamb wave. A number of FE simulations have been carried out for different notch lengths and orientations. The results show that the SPD of the scattered A_0 Lamb wave is asymmetric in the plate when the notch orientation is not perpendicular or parallel to the incident wave propagation direction.

The study showed that the amplitude of the scattered A_0 Lamb wave is very sensitive to the incident wave propagation and measurement direction. The amplitude of the forward scattered wave is small when the incident wave propagation direction is parallel to the notch orientation. However, the amplitude of the scattered wave increases significantly when the incident wave propagation direction is perpendicular to the notch orientation. The results of the scattered A_0 Lamb wave from different notch length to wavelength ratios show that the amplitude of the

scattered A_0 Lamb wave increases with the notch length. However, the amplitude of forward scattered wave shows a steady increase with notch length when the propagation direction and monitoring point are perpendicular to the notch orientation. In other cases, the amplitude of the scattered wave has a major trend of increase with α and then decreases for larger notch length. The scattered the A_0 Lamb wave with largest amplitude is obtained when incident wave and monitoring point angels are perpendicular to the notch orientation. The results also show that a very small amplitude of scattered wave is obtained when the notch orientation is parallel to the incident wave direction. This can be considered as the worst case in damage detection.

The main outcomes of this paper which can be used for damage detection are listed as below;

- A_0 Lamb wave is sensitive to small notches and can detect the notches with a size of as small as a few millimetres.
- The FE simulation can be used for prediction of propagation of A_0 Lamb wave in Aluminium plates with notches.
- The study shows that the amplitude of A_0 Lamb wave in aluminium plates is sensitive to the notch orientation. Therefore, the findings of this study such as SPD patterns can be used for predicting the notch orientation.
- The findings of this study show that a successful damage detection may not be obtained when the incident wave propagation direction is perpendicular to the notch orientation. Therefore, to avoid this situation, a series of transducer may be needed for damage detection.

The results of this study provided improved physical insight into the characteristics of the A_0 Lamb wave scattering at a through-thickness notch in isotropic plates. The findings of this study help to further advance the use of the A_0 Lamb wave for detecting and identifying notches, which are important to further developments of damage detection techniques using the A_0 Lamb wave.

6. Acknowledgements

This work was supported by the Australian Research Council under Grant Number DE130100261. The supports are greatly appreciated.

7. References

1. Cawley P, Alleyne D (1996) The use of Lamb waves for the long range inspection of large structures, Ultrasonics 34:287-290
2. Rose JL (2002) A baseline and vision of ultrasonic guided wave inspection potential. J Press Vessel Tech 124(3):273-282
3. Raghavan A, Cesnik CES (2007) Review of guided-wave structural health monitoring. Sock Vib Digest 39(2):91-114
4. Giurgiutiu V (2008) Structural health monitoring with piezoelectric wafer active sensor, Elsevier Academic Press
5. Giurgiutiu V, Bao JJ (2004) Embedded-ultrasonics structural radar for in situ structural health monitoring of thin-wall structures, Struct Health Monitor 3(121):121-140
6. Sohn H, Par G, Wait JR, Limback NP and Farra CR (2004) Wavelet-based active sensing for delamination detection in composite structures, Smart Materials and Struct 13:153-160
7. Flynn EB, Todd MD, Wilcox, Drinkwater BW, Croxford AJ (2011) Maximum-likelihood estimation of damage location in guided-wave structural health monitoring, Proceed R Soc A 467:2575-2596
8. Ng CT (2014) Bayesian model updating approach for experimental identification of damage in beams using guided waves, Struct Health Monitor 13(4):359-373
9. Ng CT (2014) On the selection of advanced signal processing techniques for guided wave damage identification using a statistical approach, Eng Struct 67:50-60
10. Ng CT (2015) A two-stage approach for quantitative damage imaging in metallic plates using Lamb waves Earthquakes Struct 8(4):821-841

11. Ratassepp M, Lowe MJS, Cawley P, Kauson A (2008) Scattering of the fundamental shear horizontal mode in a plate when incident at a through notches aligned in the propagation direction of the mode, J Acoust Soc Am 124:2873-2882
12. Fromme P, Sayir MB (2002) Detection of cracks at rivet holes using guided wave, Ultrasonics 40:199-203
13. Moreau L, Velichko A, Wilcox PD (2012) Accurate finite element modelling of guided wave scattering from irregular defects, NDT&E Int 45:46-54.
14. Ng CT, Veidt M (2011) Scattering of the fundamental anti-symmetric Lamb wave at delaminations in composite laminates, J Acoust Soc Am 129:1288-1296
15. Ng CT, Veidt M (2012) Scattering characteristics of Lamb waves from debondings at structural features in composite laminates, J Acoust Soc Am 132:115-123
16. WANG Y, ZHU X, HAO H and OU J (2009) Guided wave propagation and spectral element method for debonding damage assessment in RC structures. Journal of Sound and Vibration 324(3-5): 751-772.
17. Ostachowicz W, Kudela P, Krawczuk M and Żak A (2011) Guided Waves in Structures for SHM. The Time–domain Spectral Element Method, John Wiley & Sons Ltd.
18. Norris AN, Vemula C (1995) Scattering of flexural wages on thin plates, J Sound Vib 181:115-125
19. Grahn T (2003) Lamb wave scattering from a circular partly through-thickness hole in a plate, Wave Motion 37:63-80
20. Auld B (1990) Acoustic fields and waves in solids Vol 2, Krieger, Malabar.
21. Crane LJ, Gilchrist MD, Miller JJH (1997) Analysis of Rayleigh-Lamb wave scattering by a crack in an elastic plate, Computational Mech, 19:533-537
22. Veidt M, Ng CT (2011) Influence of stacking sequence on scattering characteristics of the fundamental anti-symmetric Lamb wave at through holes in composite laminates, J Acoust Soc Am 129:1280-1287

23. Ramadas C, Balasubramaniam K, Joshi M, Krishnamurthy CV (2009) Interaction of the primary anti-symmetric Lamb wave (A_0) with symmetric delaminations: numerical and experimental studies, Smart Mater Struct 18(085011):1-7
24. Ostachowicz W, Kudela P, Krawczuk M, Zak A (2012) Guided waves in structures for SHM: the time-domain spectral element method, John Wiley & Sons
25. Schubert F (2004) Numerical time-domain modelling of linear and nonlinear ultrasonic wave propagation using finite integration techniques – theory and applications, Ultrasonics 42:221-229
26. Obenchain MB, Cesnik CES (2014) Guided wave interaction with hole damage using the local interaction simulation approach, Smart Mater Struct 23(125010):1-14
27. Wang L, Shen J (1997) Scattering of elastic waves by a crack in isotropic plate, Ultrasonics 35:451-457
28. Lowe MJS, Cawley P, Kao JY, Dillgent O (2002) The low frequency reflection characteristics of the fundamental antisymmetric Lamb wave a_0 from a rectangular notch in a plate, J Acoust Soc Am, 112:2612-2622
29. Lowe MJS, Diligent O (2002) Low-frequency reflection characteristics of the s_0 Lamb wave from a rectangular notch in a plate, J Acoust Soc Am 111:64-74
30. Lu Y, Ye L, Su Z, Yang C (2008) Quantitative assessment of through-thickness crack size based on Lamb wave scattering in aluminium plates, NDT&E Inter 41:59-68
31. Quek S. T, Tua P. S and Wang Q. (2003) Detecting Anomalies in Beams and Plate Based on the Hilbert–Huang Transform of Real Signals, Smart Materials and Structures, 12(3): 447–460.
32. Salvino L., Purekar A., and Pines D. (2005) Health Monitoring of 2-D Plates Using EMD and Hilbert Phase, Proceedings of the 4th International Workshop on Structural Health Monitoring, Stanford University, CA.

33. Sun, Z., Mao, Y., Jiang, W., and Zhang, D. (2000). Investigation on Interaction of Lamb Waves and Circumferential Notch in Pipe by Means of Wavelet Transform, Proceedings of the IEEE Ultrasonics Symposium, Vol. 1, San Juan, Puerto Rico, 827–830.
34. Fromme P, Rouge C (2001) Directivity of guided ultrasonic wave scattering at notches and cracks, J Phys Conf Series 269(012018):1-11
35. Kovic B, Lowe M (2003) DISPERSE User's Manual Version 2.0.16B Imperial College, University of London, Non-Destructive Testing Laboratory
36. Stewart JR, Gullerud, AS, Heinstein, MW (2006) Solution verification for explicit transient dynamics problems in the presence of hourglass and contact forces, J Comp Methods Applied Mech Eng 195: 1499–1516
37. Bathe KJ (1982) Finite Element Procedures in Engineering Analysis, Prentice-Hall, Upper Saddle River, New Jersey, USA.
38. Castaings M, Hosten B (2001) Lamb and SH waves generated and detected by air-coupled ultrasonic transducers in composite material plates, NDT & E Inter 34:249–258.

Statement of Authorship of the Journal Paper 2

Title of Paper	Mode conversion and scattering analysis of guided waves at delaminations in laminated composite beams
Publication Status	☑ Published ☐ Accepted for Publication ☐ Submitted for Publication ☐ Unpublished and Unsubmitted work written in manuscript style
Publication Details	Structural Monitoring and Maintenance, Vol. 2, No. 3 (2015) 213-236

Principal Author

Name of Principal Author (Candidate)	Reza Soleimanpour		
Contribution to the Paper	Performed the study and wrote the manuscript		
Overall percentage (%)	60		
Certification:	This paper reports on original research I conducted during the period of my Higher Degree by Research candidature and is not subject to any obligations or contractual agreements with a third party that would constrain its inclusion in this thesis. I am the primary author of this paper.		
Signature		Date	12/09/2016

Co-Author Contributions

By signing the Statement of Authorship, each author certifies that:

iv. the candidate's stated contribution to the publication is accurate (as detailed above);

v. permission is granted for the candidate in include the publication in the thesis; and

vi. the sum of all co-author contributions is equal to 100% less the candidate's stated contribution.

Name of Co-Author	Ching-Tai Ng		
Contribution to the Paper	Supervised development of the work and manuscript evaluation		
Signature		Date	12/09/2016

Please cut and paste additional co-author panels here as required

Soleimanpour, R. & Ng, C.T. (2015). Mode conversion and scattering analysis of guided waves at delaminations in laminated composite beams.
Structural Monitoring and Maintenance, *2*(3), 213-236.

Statement of Authorship of the Journal Paper 3

Title of Paper	Higher harmonic generation of guided waves at delaminations in laminated composite beams
Publication Status	☑ Published ☐ Accepted for Publication ☐ Submitted for Publication ☐ Unpublished and Unsubmitted work written in manuscript style
Publication Details	Structural Health Monitoring An International Journal, DOI: 10.1177/1475921716673021

Principal Author

Name of Principal Author (Candidate)	Reza Soleimanpour		
Contribution to the Paper	Performed the study and wrote the manuscript		
Overall percentage (%)	60		
Certification:	This paper reports on original research I conducted during the period of my Higher Degree by Research candidature and is not subject to any obligations or contractual agreements with a third party that would constrain its inclusion in this thesis. I am the primary author of this paper.		
Signature		Date	12/09/2016

Co-Author Contributions

By signing the Statement of Authorship, each author certifies that:

i. the candidate's stated contribution to the publication is accurate (as detailed above);

ii. permission is granted for the candidate in include the publication in the thesis; and

iii. the sum of all co-author contributions is equal to 100% less the candidate's stated contribution.

Name of Co-Author	Ching-Tai Ng		
Contribution to the Paper	Supervised development of the work and manuscript evaluation		
Signature		Date	12/09/2016

Name of Co-Author	Chun Wang		
Contribution to the Paper	Supervised development of the manuscript evaluation		
Signature		Date	12/09/2016

Please cut and paste additional co-author panels here as required

Chapter 5: Higher harmonic generation of guided waves at delaminations in laminated composite beams

Abstract: Detection and characterization of delamination damage is of great importance to the assurance of structural safety. The present work investigates the potential of a baseline-free structural health monitoring technique based on higher harmonics resulting from the nonlinear interaction of guided wave and a delamination. The nonlinearity considered in this study arises from the clapping of the sub-laminates in the delaminated region, which generates contact acoustic nonlinearity (CAN). Both explicit finite element (FE) simulations and experimental tests are conducted on composite laminates containing a delamination of different sizes and at different through-thickness locations. The results show that the interaction between the fundamental asymmetric mode (A_0) of guided wave and a delamination generates CAN in the form of higher harmonics, which provides a good measure for identifying the existence of delaminations and determining their sizes in laminated composite beams. This new insight into the generation mechanisms of nonlinear higher order harmonics in composite laminates will enhance the detection and monitoring of damage in composite structures.

Keywords

Contact acoustic nonlinearity, delamination, fiber reinforced laminated composite beam, finite element, nonlinear guided waves, higher harmonic

1. Introduction

Damage detection is essential to structural integrity management of engineered structures on which human safety depends. Structural health monitoring techniques employing guided waves and distributed sensors have shown promises in complementing existing non-destructive

evaluation (NDE) techniques, such as radiography, electro-mechanical impedance based, eddy current technique, visual inspection, shearography, thermography and conventional ultrasonic [1]. Compared to conventional NDE techniques, guided waves techniques [2-4] offer several major advantages, such as the ability to inspect inaccessible locations and large areas autonomously, without interrupting operations [5-9]. However, majority of guided wave methods require the baseline data, which is obtained by comparing the wave data obtained from the un-damaged state of structures (baseline data) and the data obtained the structures with defects [10,11].

Recently nonlinear ultrasonic phenomenon is emerging as a new concept to alleviate the need for baseline data by exploiting side bands and higher harmonics that are generated only by the clapping and/or friction between the faces of a crack subjected to an incident wave. When a guided wave encounters a linear structural feature, such as a hole or a stiffener, the scattered waves is of the same frequency as the incident wave. However, additional frequencies can be generated by geometrically nonlinear structural features, such as breathing cracks whose surfaces come into contact [12], or material nonlinearity [13,14]. Examples of these nonlinear acoustical phenomena include (a) higher harmonic generation, (b) sub-harmonic generation, (c) nonlinear resonance and (d) mix frequency response. Among these, higher order harmonic generation and frequency mixing have been commonly used as indicators of acoustic nonlinearities.

Basically the non-linear acoustic phenomena involve classical and non-classic responses. The classical non-linear response is mostly concerned with material imperfections, such as intrinsic nonlinearities due to imperfections in atomic lattices leading to higher harmonic generation. Localized fatigue cracks, distributed micro-cracks or other material imperfections are some of the sources of classical non-linear response. Research work in this area also involves higher harmonic generation of Lamb waves used for the detection of material nonlinearity and damage.

Classical nonlinear effects in guided waves propagation have been investigated by many researchers and explored for damage detection. Deng [15,16] investigated the generation of second harmonic of shear horizontal waves and Lamb waves in metallic plates. Müller *et al*. [17] investigated the characteristics of second harmonic generation of Lamb wave in a plate with quadratic nonlinearity. Liu *et al*. [13] investigated the symmetry properties of second harmonic Lamb waves by examining anti-symmetric Lamb mode pairs. Zhang *et al*. [18] reported the observation of cumulative second harmonic generation of Lamb wave in long bones based on the modal expansion approach to waveguide excitation and the dispersion characteristics of Lamb waves in long bones. It was shown that the second harmonic generated by fundamental Lamb waves in long bones is observed clearly, and the effect is cumulative with propagation distance when the fundamental Lamb wave mode and its second harmonic wave mode have the same phase velocities. Xiang *et al*. [19] developed an analytical model for the effect of the interactions of dislocations with precipitate coherency strains on the generation of second harmonic of Lamb waves in metallic alloys. Lissenden *et al*. [20] studied generation of higher harmonics of guided waves in aluminum plates with plastic deformation. It was shown that plastic deformation has a significant effect on the harmonic amplitude ratio. Pruell *et al*. [21] studied the generation of nonlinear guided waves by fatigue crack in metallic plates. It was shown that the phase and group velocity matching is essential for practical generation of nonlinear guided waves. A technique was developed for quantitatively assessing fatigue damages in metallic plates based on nonlinear guided waves. Bermes *et al*. [22] developed a procedure to determine the second harmonic of the Lamb waves in metallic plates. Srivastava and Lanza di Scalea [23] theoretically studied the symmetry characteristics of Rayleigh–Lamb guided waves in nonlinear, isotropic plates. It was shown that antisymmetric motion is prohibited at all the higher order even harmonics whereas all the higher order odd harmonics allow both symmetric and antisymmetric motions.

In contrast to classical nonlinear response, the non-classical non-linear response mostly arises in contact-type defects in material. Crack-wave interactions that exhibit vibro-acoustic

modulations, sub-harmonic generation or stress-strain hysteresis are some of the sources of non-classical nonlinear responses. For a tight crack without any gap between its faces, its surfaces will close under compressive stress, thus allowing the compressive part of the wave to propagate through unimpeded. The tensile part of the wave, however, will open the crack, thus causing scattering, as shown in Fig. 1. Therefore, a tight crack effectively behaves like a half-wave rectifier. When the crack surfaces come into contact, the dynamic pressure between crack faces generates additional waves approximately twice the frequency of the original wave, or nonlinear waves in the form of higher harmonics. Since higher harmonics are induced only by contacting surfaces, such as cracks, their presence, which can be identified directly from the total wave field without the need for accurate baseline data, offer a new route for baseline free damage detection or structural health monitoring.

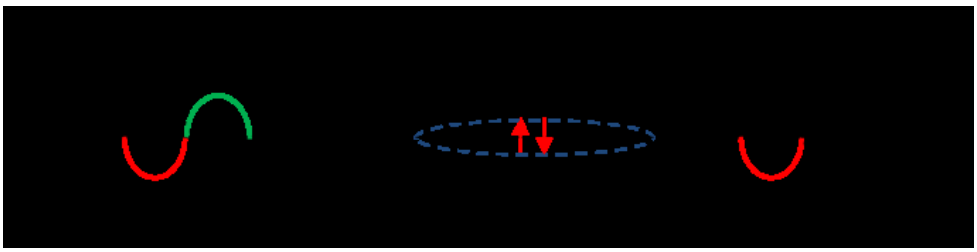

Figure 1. Interaction of an incident wave with a crack

There are two non-classical nonlinear mechanisms due to the interaction of crack surfaces with a propagating incident wave. The first one is referred to as clapping, which is generated due to asymmetry in stress-strain characteristics for damaged interfaces causing the stiffness of the materials to be higher in compression but lower in tension. This asymmetric variation in local stiffness will distort the wave pattern and results in wave nonlinearity in the form of higher even harmonics of the incident wave frequency. The friction between damage interfaces when they slip causes symmetric change in local stiffness, which results in the generation of higher odd harmonics. Awrejcewicz and Olejnic [24], Pecorari and Solodov [25], carried out comprehensive studies on the effect of this second type of mechanism for wave nonlinearity.

Nonlinear analysis methods focusing on non-classical nonlinear behavior of interfaces are referred to as local nonlinearities, which have attracted increasing interest in theoretical and applied research in the past few years [26,27]. Kim *et al*. [28] developed a nonlinear model for investigating the contact acoustic nonlinearity (CAN) of a closed crack in aluminum plate in order to analyze the nonlinear characteristics of the transmitted waves. These studies have found that the interfacial stiffness has a significant effect on the amplitude of the resultant second order harmonic. The experimental results showed that the amplitude of the second order harmonic correlates with the crack closure process, in agreement with numerical results. Recently, Hong *et al*. [29] investigated the phenomenon of CAN related to breathing fatigue cracks and material nonlinearity using a piezoelectric sensor network. It was shown that the relative acoustic nonlinearity parameter increases proportionally with the wave propagation distance due to the geometric and materials nonlinearities. Solodov *et al*. [30] investigated the acoustic wave interaction with non-bonded contact interfaces (crack) in solids through experiments and simulations. It was shown that changes in the interface stiffness characteristics are the major cause of CAN. The stiffness parametric modulation and instability of oscillations are due to the asymmetry in the contact restoring forces, which results in the generation of sub-harmonics. It was concluded that sub-harmonics and higher harmonics are good indicators for the existence of defects in metallic structures.

A recent study was reported by Kishiwada *et al*. [31] on using the fundamental antisymmetric mode (A_0) Lamb wave for detecting clapping actions between two thin aluminum plates under different pressures at the contact interface. The study showed that clapping between two aluminum plates generates higher harmonics especially odd harmonics of Lamb wave. Moreover, the applied pressure affects the dispersive behavior of asymmetric Lamb waves. It was concluded that the phenomena of generation of odd harmonics due to

clapping effect could be used for damage detection and imaging. More advanced non-classical nonlinear response techniques such as modulation methods were invented by Korotkov *et al*. [32] and Donskoy *et al*. [33] which involved both classical and non-classical nonlinear responses and exploited the effects of the nonlinear interaction between ultrasonic probing signal and a low frequency vibration for damage detection.

To date, most of the studies on non-classical responses of nonlinear ultrasonic have focused on isotropic materials. Very limited research has been reported on the generation of nonlinear guided waves by delaminations in composite laminates [34,35]. In this study we present an experimental and computational investigation of the interaction between narrow-band guided waves at the delaminations with a view of using of nonlinear guided waves for detecting delamination damage in fiber reinforced composites.

This paper is organized as follows. The first section describes the experimental method to characterise the propagation behaviour of guided waves, including group and phase velocity, attenuation constants and nonlinear wave measurement. The second section describes computational simulations using three-dimensional (3D) finite element (FE) method for both the propagation and generation of non-linear guided waves, taking into account of the effect of attenuation. Verification of the FE model is then provided in the third section, which consists of linear and nonlinear guided wave verification. The forth section presents a validation of the FE model by comparing the simulated results with experimental data. The effect of material damping is modeled using Rayleigh damping coefficients. In the sixth section a comprehensive study of the nonlinear guided wave at delamination in laminated composite beam is carried out using the FE model, especially for delamination of varying size relative to the wavelength of the incident wave and at different through-thickness locations in the laminate. In addition, the

effect of damping on the nonlinear guided wave is also discussed. Finally conclusions are presented together with opportunities for future research.

2. Experiment Details

The experiments described in this section were carried out to verify the 3D FE models that will be employed to simulate the propagation of both linear and nonlinear guided waves. The accuracy of using the 3D FE models to predict the linear guided waves was verified by comparing the phase and group velocity dispersion curves with experimental results. The accuracy in predicting the nonlinear guided waves was confirmed by comparing the numerical simulation nonlinear guided wave, i.e. higher harmonics, induced by CAN with the experimentally measured data.

2.1. Specimens

For experimental validation of the FE models, specimens were manufactured from eight plies of VTM264 unidirectional carbon/epoxy prepreg with a stacking sequence of $[0/90/0/90]_S$. This cured lamina has a fibre volume fraction of 0.55, with density and thickness being 1538 kg/m^3 and 0.2 mm, respectively. The elastic properties of the lamina are shown in Table 1.

Table 1. Elastic properties of the VTM264 prepreg lamina

E_{11} (GPa)	E_{22} (GPa)	E_{33} (GPa)	G_{11} (GPa)	G_{12} (GPa)	G_{13} (GPa)	v_{12}	v_{13}	v_{23}
120.20	7.47	7.47	3.94	3.94	2.31	0.32	0.32	0.33

The dimension of the composite beams is 285 mm × 12 mm × 1.6 mm. One specimen was intact, which is used to verify the performance of the 3D FE models in predicting the linear guided wave propagation. The other specimen had a 15 mm long delamination located between the third and fourth plies, as schematically shown in Fig 2. Two very short Teflon films were

first inserted between the third and fourth ply of the composite laminate during the manufacturing process. A three-point bending test was used to break the weak bonding between the laminae and Teflon films, and henc,e forming the delamination. The delamination was then grown to the desired length by increasing the applied load in the three-point bending test.

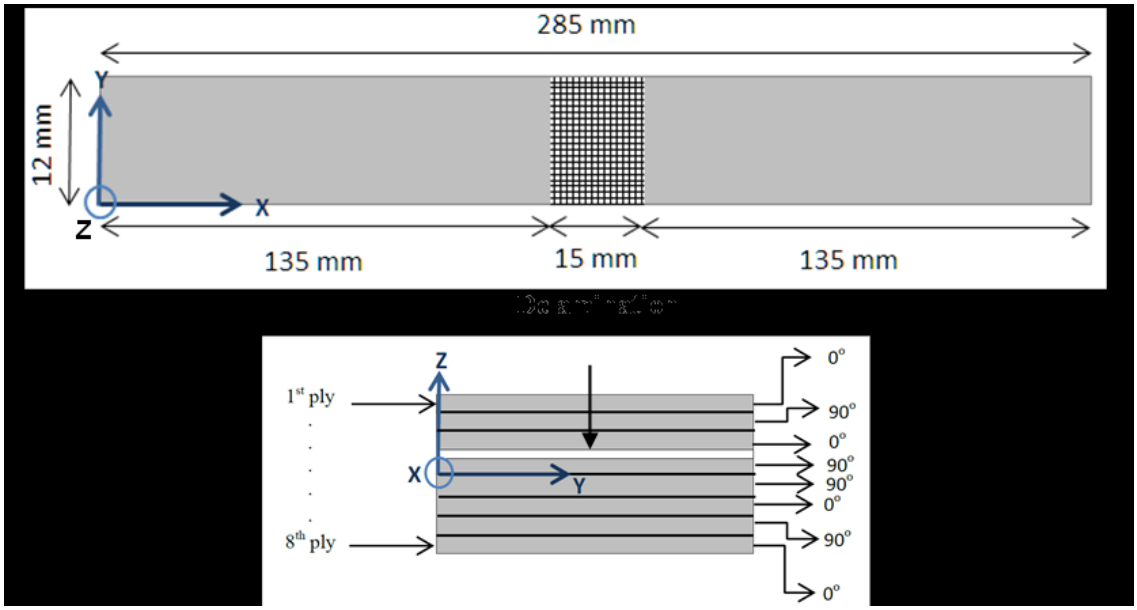

Figure 2. Schematic diagram of a composite beam specimen with delamination and its cross section

2.2. Experimental validation of linear guided waves

A 12 mm × 6 mm × 2 mm rectangular piezoceramic transducer was adhesively bonded to one end of the beam to excite the A_0 guided wave. A 3 mm thick brass backing mass was used to increase the excitability of the A_0 guided wave. The excitation pulse was generated by a computer controlled signal generator with a 10 V peak-to-peak output range, which was further amplified to 50 V peak-to-peak output voltages using an amplifier. The out-of-plane displacements were measured by using a scanning laser Doppler vibrometer (Polytec PSV-400-3D-M) and the data was sent to the laser controller and data acquisition system for post-processing. A band-pass filter was introduced to the system and the average of signals was calculated over 1000 repeats of acquisitions to improve the signal-to-noise ratio. Fig. 3 shows

the experiment setup used in this study. This study employed a 5-cycle sinusoidal tone burst pulse modulated by a Hanning window. The central frequency of the tone burst was swept from 20 kHz to 300 kHz at 20 kHz increments and the phase velocity and group velocity of the wave at each excitation frequency was calculated [11,36,37]. The phase and group velocity dispersion curves obtained using numerical simulation and experimental data were compared accordingly.

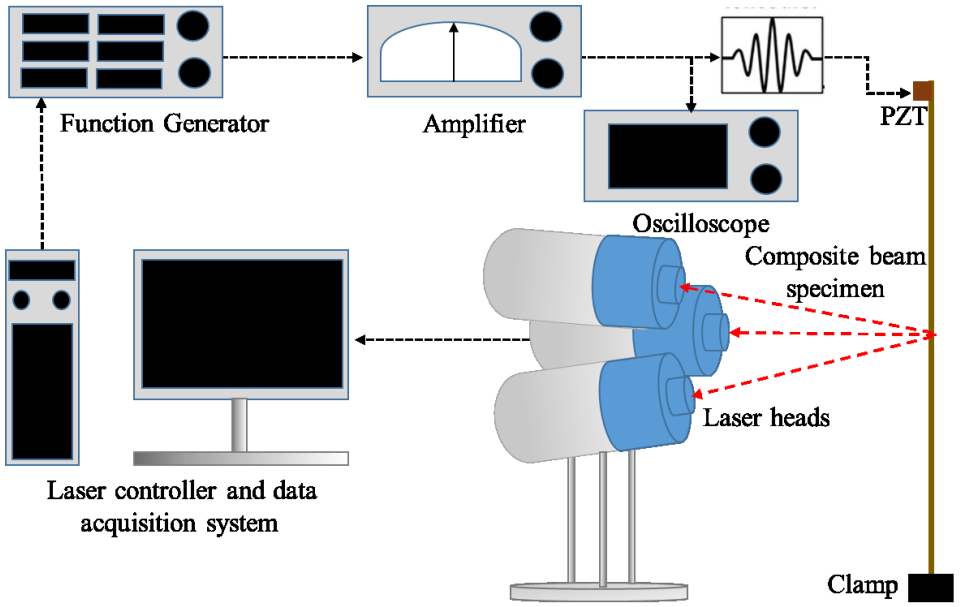

Figure 3. Schematic diagram of the experiment setup used for verification of FE models

2.3. Determination of material damping in laminated composite beams

To account for material damping on the propagation of guided wave, a 5-cycle sinusoidal tone burst pulse modulated by Hanning window with central frequency of 140 kHz was applied on the intact laminated composite beam. Although there are no certain criteria on the selection of the excitation frequency, an appropriate frequency is considered to be able to achieve good signal-to-noise ratio, smaller wave dispersion, less number of existing wave modes, and high sensitivity to damage. In this study, the optimum excitation frequency was obtained through experimental observation. A couple of frequencies within the range of 50 kHz to 200 kHz were examined. Since 140 kHz showed the best signal-to-noise ratio, this excitation frequency was used for the rest of study. The maximum magnitude of the out-of-plane displacement was

captured at 19 measurement points, at a spacing of 10 mm, located between 20 mm to 200 mm away from the actuator.

The attenuation coefficient (k_i) is determined by curve-fitting the following relationship with the attenuation data [38]:

$$\frac{\mathrm{A}(\Delta x)}{A_0} = \exp(k_i \Delta x) \tag{3}$$

where A_0 and $A(\Delta x)$ are the signal amplitudes at a reference point and at distance Δx away from the reference point, respectively. The attenuation curve was plotted by finding the best exponential fit to experimental results and is shown in Fig. 4. The value of k_i for the laminated composite beam employed in this study is 3.1 m^{-1}.

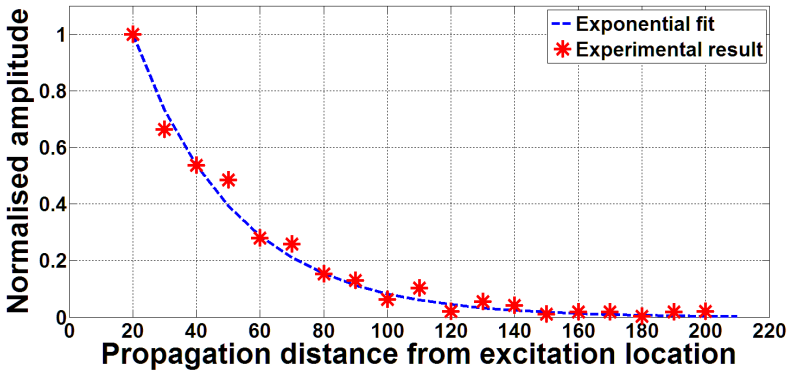

Figure 4. Attenuation of A_0 guided wave in composite structure at 140 kHz

Based on the attenuation coefficient, the Rayleigh mass proportional and stiffness proportional damping constants can be calculated from the following equations [38]:

$$\alpha_\omega = 2k_i C_g \tag{4}$$

$$\beta_\omega = \frac{2k_i C_g}{\omega^2} \tag{5}$$

where α_ω and β_ω are the mass proportional and stiffness proportional damping constants. C_g is the group velocity and ω is the angular central frequency of the tone burst wave. The estimated group velocity of the A_0 guided waves at 140 kHz is 1401 m/s. Therefore, the values of $\alpha_\omega$and

β_ω at frequency of 140 kHz are calculated as 8730 rad/s and 1.128×10^{-8} rad/s, respectively. These constants will be implemented in the FE models to account for the effect of material damping in the composite beams.

2.4. Experiment setup for validation of non-linear guided waves

Two rectangular piezoceramic actuators (12 mm × 6 mm × 2 mm) were adhesively attached to the beam with a delamination at 107.5 mm from the beam ends, respectively. The excitation signal was generated by a computer controlled arbitrary waveform generator (NI PXI-5412) with 10 V peak-to-peak output voltage and then amplified by an amplifier with peak-to-peak voltage of 50 V. The response of the receiver transducer was recorded by NI PXI-5105 digitizer for further post-processing. Fig. 5 shows the experiment setup used in this study.

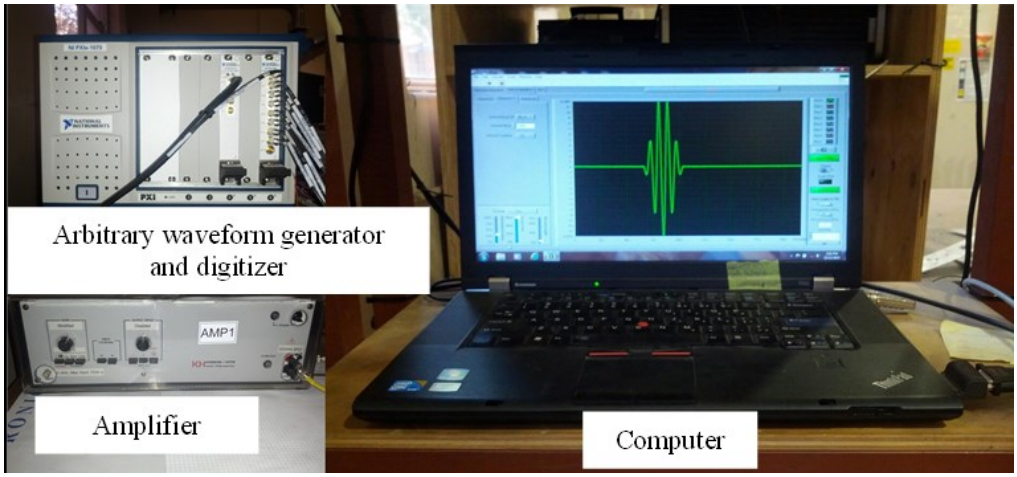

Figure 5. Schematic diagram of the experimental setup for investigating nonlinear guided wave

3. Numerical simulations of guided waves in composite laminate

In this study, a 3D explicit FE method [39] was used to simulate the propagation of guided wave in the cross-ply laminated composite beams. In the FE model, each lamina was modelled using a layer of eight-noded 3D fully integrated linear solid elements with incompatible modes (C3D8I) with hourglass control, and hence, there are eight layers of element across the thickness of the laminated composite beams. The incompatible modes have added internal degrees of freedom that improve the representation of bending in the interior of the element. Stewart *et al*.

[44] recommended limiting the hourglass energy to less than 2% of the total energy to ensure the accuracy of predicting the guided wave propagation in solids and this was implemented in all FE models throughout this study. Each node of the solid brick element has three translational degrees-of-freedom (DOFs). To ensure the numerical stability and to simulate the damping effect of composite materials, the FE models incorporate Rayleigh mass proportional and stiffness proportional damping discussed in the previous section [45].

The A_0 guided wave was excited by applying out-of-plane nodal displacements to surface nodes located at one end of the beam, which simulates a piston type excitation generated by a 12 mm × 6 mm rectangular transducer [46]. Linear solid elements with incompatible modes (C3D8I) and full integration, and having in-plane dimensions of 0.4×0.4 mm^2 and 0.2 mm thickness were used in the beam models. It has been shown that this type of elements with an aspect ratio of 2 is suitable for simulating the propagation of guided waves at delaminations in composite laminates [39]. Packo *et al*. [40] investigated the simulation of propagation of guided waves in isotropic and anisotropic plates. It was shown that, for simulation of propagation of fundamental and first-order modes of Lamb waves in anisotropic plates, a typical 4-8 number of elements per ply of material provides the perfect results. However, other studies [41-43] show that one element per ply can still predict the propagation of Lamb waves in composite beams and plates with good accuracy when the incident frequency is below the cut-off frequency. In this study, to reduce the computational cost, each lamina was modelled using one element per ply. The dynamic simulation was solved by the explicit FE code in ABAQUS v6.14, which uses the central difference integration [47]. In this scheme, the integration operator matrix is inverted and a set of nonlinear equilibrium equations is solved at each time increment. Since the central different integration scheme is conditionally stable, the increment time step has to be small enough to ensure the stability. In this study the increment time step is automatically calculated by ABAQUS.

In the FE model, CAN is simulated by applying frictionless surface-to-surface contact interaction (friction coefficient is set to be zero) to avoid interpenetration of the delamination surfaces during the wave propagation. Direct enforcement method was used to maintain the pressure-penetration relationship through Lagrange multiplier method. By applying the direct enforcement condition in variational formulation for a steady-state analysis [47], the contact virtual work contribution $\delta\prod^c$

$$\delta\prod^c = \delta ph + p\delta h \tag{6}$$

where p is the contact pressure and h is the overclosure. Hard contact was used in FE simulation, in which the contact pressure between two surfaces at a point is a function of the overclosure of the surfaces, i.e. the interpenetration of the surfaces. The hard contact model is described as

$p = 0$ for $h < 0$ surfaces are not in contact

$h = 0$ for $p > 0$ surfaces are contacting

Material damping was applied in FE simulation using experimentally obtained Rayleigh mass and stiffness proportional damping constants; the values are presented in the following section. The scattered wave $w_s(t)$ is determined by subtracting the baseline data $w_b(t)$ from the total wave $w_t(t)$. In terms of the Fourier transform, this can be expressed as

$$\widehat{w_s}(f_c) = \widehat{w_t}(f_c) - \widehat{w_b}(f_c) \tag{6}$$

By comparison, the second harmonics $\widehat{w_s}(2f_c)$ can be directly determined from the total field, because it is not present in the baseline,

$$\widehat{w_s}(2f_c) = \widehat{w_t}(2f_c) \tag{7}$$

The excitation signals in both the FE simulation and the experiment are a narrow-band tone burst in the form of an 8-cycle sinusoidal signal modulated by a Hanning window with a central frequency of 140 kHz. Fig. 6 shows a snapshot of the computational results of the interaction of A_0 guided wave with the delamination in the laminated composite beam.

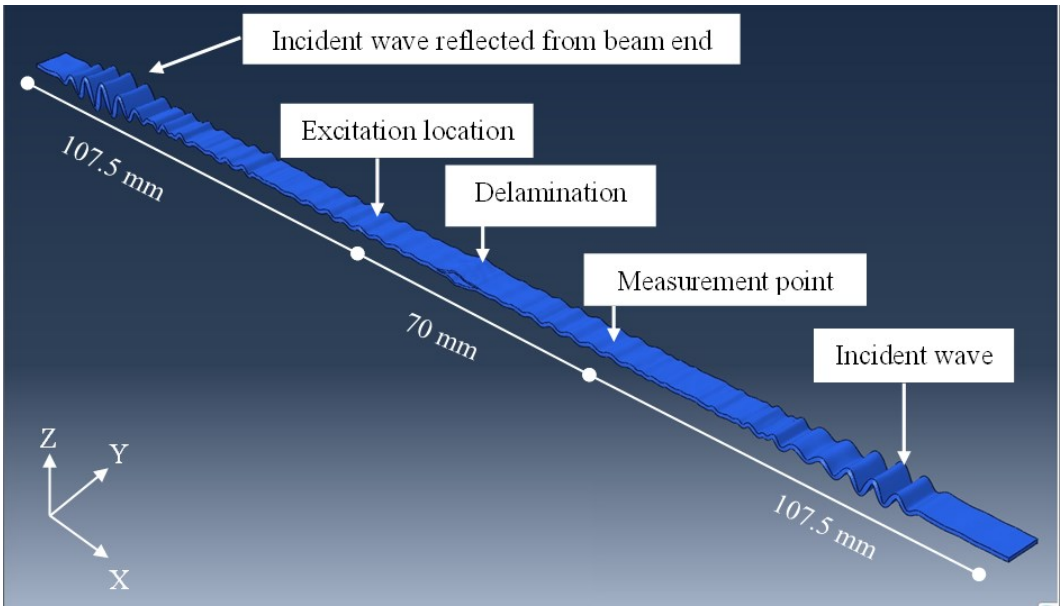

Figure 6. A typical contour snapshot of FE simulated out-of-plane displacement of guided wave in composite beam with a delamination (time = 128.9 μs. Scale factor = 250)

4. Results and discussions

4.1. Linear guided waves

In this section, an experimental verification of the FE simulations for linear wave propagation in fibre reinforced laminated composite beams is presented. The verification focuses on comparing the numerically calculated A_0 guided wave phase and group velocity dispersion curves with experimental results. In the FE simulations and experiments, the signal was extracted at four consecutive measurement points located 4 mm away from each other and the first measurement point was 100 mm from the excitation location. Since the first measurement location is away from the excitation more than four times of the wavelengths, the evanescent waves are negligible in the measurements. The captured data at four measurement points were used to calculate the phase and group velocity. The simulation results are compared with the experimental results to ensure the capability of the FE model in simulating the linear guided wave propagation in laminated composite beams. Fig. 7 shows the estimated phase and group velocity dispersion curves calculated from the FE simulated and experimentally measured data.

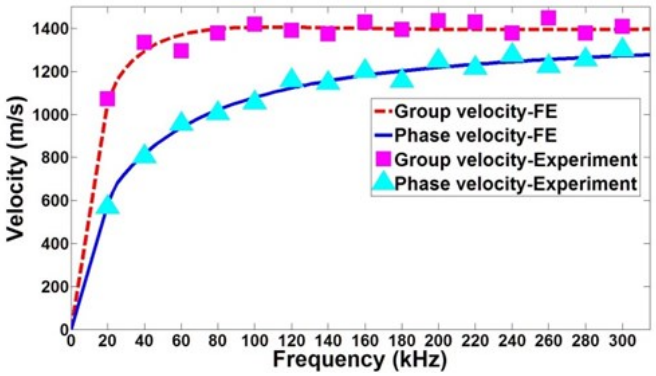

Figure 7. Phase and group velocity dispersion curves obtained by FE and experimental results

As shown in Fig.7, both the phase and group velocity dispersion curves obtained from FE simulations have a good agreement with the experimentally measured dispersion curves. This confirms that the FE model is able to accurately predict the phase and group velocities of the guided wave in fiber reinforced laminated composite beams.

4.2. Non-linear guided waves

To reveal the higher harmonic waves, the results from experiments and FE simulation are transformed to frequency domain using the Fast Fourier transform (FFT). Figs. 8a and 8b show the results measured at 70 mm from excitation point for both intact and delaminated specimens. As shown in Fig. 8b, both FE simulated and experimentally measured data contain higher frequency components at around 280 kHz (twice of the incident wave frequency). However, the data obtained from the intact laminated composite beam, as shown in Fig. 8a, does not have higher harmonic components. Therefore, CAN is the major source of nonlinear waves in the laminated composite beams with the delamination. As shown by the experimental data in Fig. 8b, the source of these humps can be due to surface roughness or friction at delamination interface [48]. Since friction was not considered in the FE model, these humps do not exist in FE model results. Overall these results confirm that the FE model is capable of predicting the generation of higher harmonic waves by delamination damage.

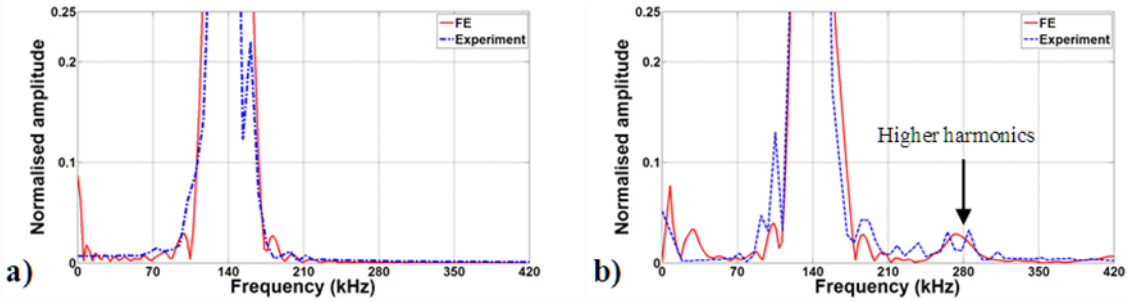

Figure 8. Normalized FFT of the signal obtained from the experiment and FE simulation, a) intact beam b) beam with the delamination located between 3rd and 4th ply. The response measured at 70 mm from excitation and 35 mm from centre of delamination.

To gain fundamental understanding on the effect of delamination size on the higher harmonics generation, a range of sizes and through-thickness positions of delaminations were modeled in the FE simulations. The incident wave wavelength was calculated using DISPERSE software [49]. Tables 2 and 3 summarize the delamination lengths through-thickness locations considered in this study. The excitation location was at the left end of the beam and measurement locations were at locations of 160 mm (measurement point A) and 240 mm (measurement point B) away from the left beam end, which provide backward and forward scattering wave packets data, respectively. The scattered waves from the delamination were obtained by monitoring the out-of-plane displacement at the mid-thickness of the beam model. This ensures only the A_0 guided wave is detected as the fundamental symmetric mode and shear horizontal mode of guided wave have zero out-of-plane displacement at this location.

Table 2. Summary of damage cases considered different delamination through-thickness locations

Damage case	1	2	3	4
Delamination through-thickness location	Between 1st & 2nd layers	Between 2nd & 3rd layers	Between 3rd & 4th layers	Between 4th & 5th layers

Table 3. Summary of the delamination size to wavelength ratios (d/λ) considered in each damage case shown in Table 2

d/λ	0.50	0.75	1.00	1.25	1.50	1.75	2.00
Delamination size (mm)	4	6	8	10	12	14	16

4.2.1 Nonlinear forward scattering signals

The time-domain out-of-plane displacement obtained from the FE models (with and without considering the surface contact effect) at measurement point B for Damage Case 3 with delamination size to wavelength ratio (d/λ) of 1.0 (delamination size = 8 mm, located between 3rd and 4th layers) is shown in Fig. 9. Wave distortion is observed in scattered wave signal when surface contact is modelled, while no discernible difference can be observed if surface contact is not considered. However, the wave distortion (the zoomed-in area in Fig. 9), which refers to nonlinear wave, is very small and hard to observe in the time-domain signal. The FE results show that there is only minor or no higher harmonic is observed when the delamination is located between 4th and 5th layer (Damage Case 4). This is because the delamination is located symmetrically in the through-thickness direction of the beam, which causes no contact interaction between the two sub-laminates within the delamination region when the incident pass through the delamination, and hence, no nonlinear guided wave is generated in this case.

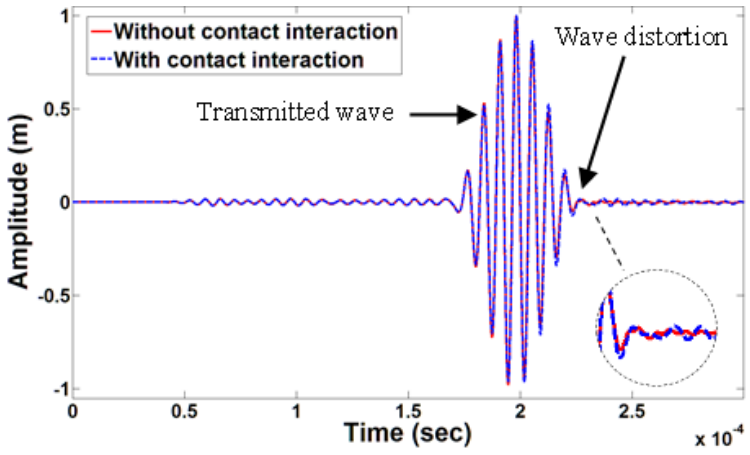

Figure 9. Transmitted wave response calculated by FE models with and without surface contact effect in Damage Case 3 (*d/λ*= 1)

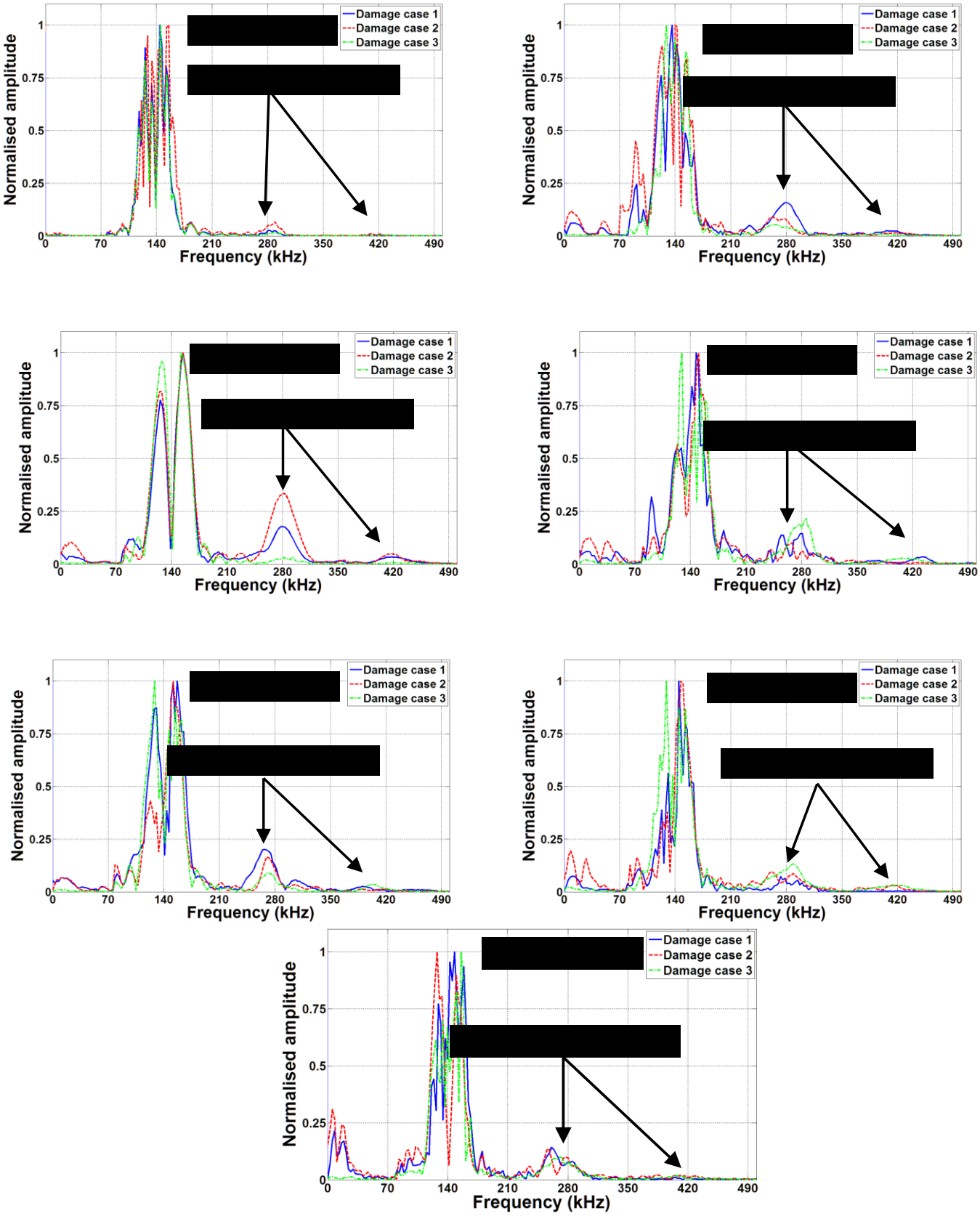

Figure 10. FFT of forward scattered wave by using baseline subtraction

To reveal the presence of higher harmonics, the time-domain signal was transformed to the frequency domain using FFT. Fig. 10 shows the normalised amplitudes of the forward scattering signals. To compare the amplitude of nonlinear higher harmonic wave with that of the linear wave, the scattered wave results were obtained by subtracting the responses from FE models with and without contact surface effect. After the baseline subtraction, the amplitudes of the components around 140 kHz and 280 kHz in frequency domain as shown in Fig. 10 are contributed by the linear scattered wave and the nonlinear guided wave due to the CAN at delamination, respectively. As shown in Fig. 10 several peaks are observed at higher frequencies in the model with contact interaction at the delamination region. In addition to the excitation frequency, second and third higher harmonics are visible in some cases.

The processed data in frequency domain only reveal the existence of higher harmonics. However, to ensure that the delamination is the only source of the existing humps at higher harmonic frequencies in FFT results, the time-of-flight of the nonlinear wave packets were calculated. In this study the Gabor wavelet transform was used to provide the time-frequency information of the guided wave signals. The results in the time-frequency domain are presented in Figs. 11a and 11b, respectively, which clearly shows higher harmonics. In some damage cases, the second higher harmonic wave at 280 kHz almost arrives at the same as the linear scattered wave. Nevertheless, for some other damage cases, such as the case in which the delamination is located between 3^{rd} and 4^{th} ply, the higher harmonic wave packets arrive after the linear scattered wave. The results show that the variation in the time-of-flight of the nonlinear wave packet is attributed to the time of initialization of clapping between sublaminate surfaces at the delamination region. This means that, for some damage cases, it takes a certain amount of time until the clapping initiated at the sublaminate surfaces of the delamination and thus nonlinear wave packets generation is delayed. As shown in Figs. 11a and 11b, higher harmonics are located between 200 μs to 225 μs. This matches the time domain results, which indicate the signal distortion occurring immediately after the arrival time of incident wave. As shown in the results, the nonlinear wave packets in scattered wave packets are hidden within

the incident wave and sometimes those wave packets cannot be separated in time-domain acquired data. Therefore, processing the data in the frequency domain and time-frequency can reveal more useful information regarding the delamination.

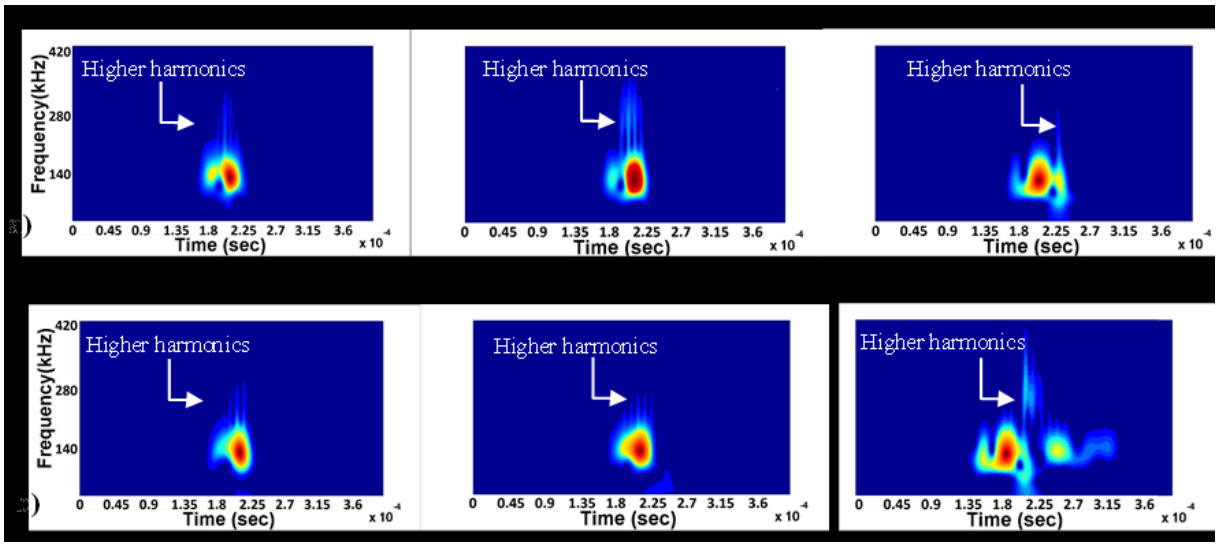

Figure 11. Time-frequency energy density spectrum of the forward scattered wave (after baseline subtraction) for Damage Cases 1-3 (left to right) and delamination size to wavelength ratio of a) 0.75 and b) 1.0.

4.2.2 Nonlinear backward scattering signals

Applying the same method used for studying the forward scattered wave, the FE simulation results are processed to extract the backward scattered waves. Similar to the forward scattering case, the Damage Case 4 (delamination located between 4th and 5th layers) did not generate any discernible nonlinear waves, while the other three cases produced nonlinear waves. The time-domain out-of-plane displacements of Damage Case 3 (d/λ = 1) obtained from FE models with and without considering contact are shown in Fig. 12. The data was captured at measurement point A. Similar to forward scattered signals, the distortion is visible in the total reflected wave. However, the wave distortion is very small and hardly visible in the time-domain data. In the case of measurement point being close to the excitation location, the backward scattered signal will mix with the incident wave and the distortion may not be visible, which makes the time domain data ineffective for damage detection.

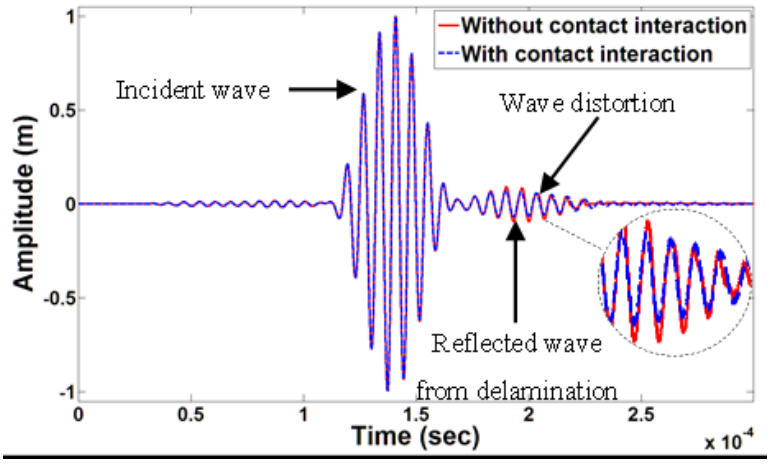

Figure 12. Reflected wave response calculated by FE models with and without surface contact effect in Damage Case 3 (d/λ = 1).

Fig. 13 shows the FFT of the extracted nonlinear backward scattered waves for all three damage cases. Several peaks are observed at higher frequencies. As shown in Figs. 14a and 14b, second harmonic at 280 kHz is visible in time-frequency energy density spectrums. Similar to time-frequency energy density spectrums of forward scattering waves, third harmonic is hardly visible in time-frequency energy density spectrums due to the small amplitude relative to the main reflected signal. It should be noted that the signal shown in the time-frequency energy density spectrums is obtained after the baseline subtraction, i.e. the incident wave information does not exist in the FFT and time-frequency energy density spectrums. The time-frequency energy density spectrums provide additional information about the frequency and the arrival time of each wave packet. According to the time domain data, the wave distortion is located between 180 μs to 225 μs, which agrees with time-frequency energy density spectrumsj, i.e. the arrival times of the higher harmonics. In addition the results also show that the amplitudes of the second harmonic varies with delamination sizes and through-thickness locations.

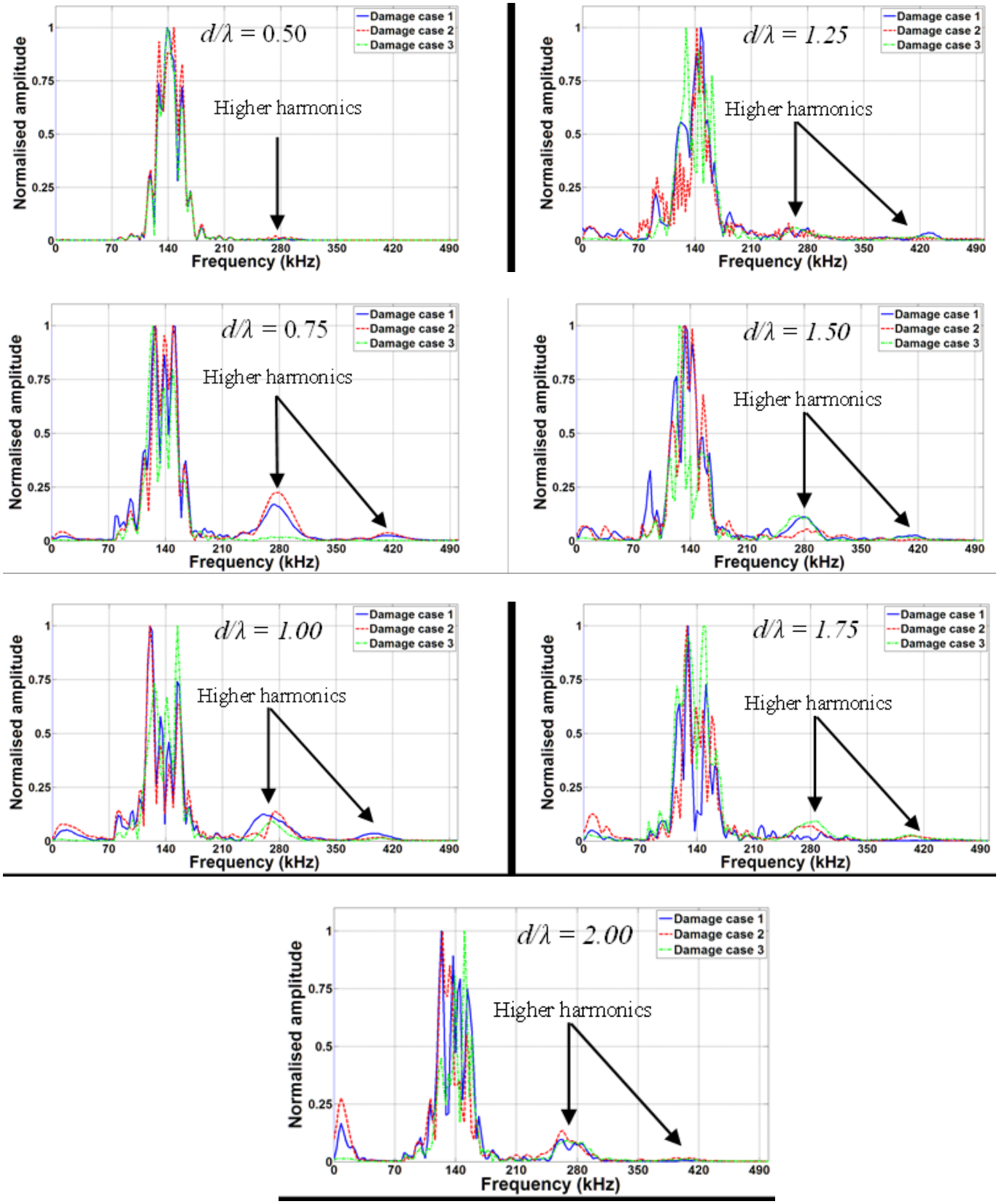

Figure 13. FFT of nonlinear backward scattering waves extracted using baseline subtraction

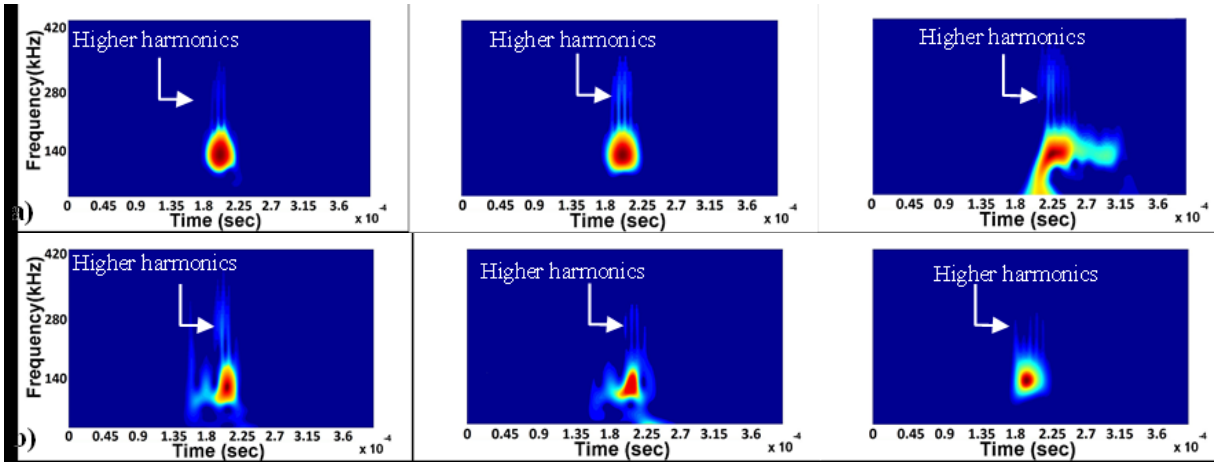

Figure 14. Time-frequency energy density spectrum of the backward scattered wave (after baseline subtraction) for Damage Cases 1-3 (left to right) and delamination size to wavelength ratio of a) 0.75 and b) 1

4.2.3 Comparison between the nonlinear forward and backward scattering waves

It has been found that the second harmonics induced due to the incident wave interaction at the delamination have larger magnitude in forward scattering direction than the backward scattering direction [10]. To examine the effect of damage size on the nonlinear scattered wave, a comparison of the normalized amplitude of the backward and forward higher harmonics are presented in Figs. 15a-15c. The captured data at each measurement point were normalized to the amplitude of incident wave at the same measurement points in intact model. As shown in Fig. 15b (Damage Case 2), the result for the delamination located between 2nd and 3rd layer has the maximum amplitude of second harmonic. Moreover, the amplitude of the second harmonic of the forward scattered waves is slightly greater than the backward scattered waves for all considered delamination size to wavelength ratio. For Damage Cases 1 and 2, the amplitude of the second harmonic is not necessarily increasing with delamination size to wavelength ratio. However, the amplitudes of the forward and the backward scattered waves increase with delamination size to wavelength ratio in Damage Case 3 as shown in Fig. 15c. Therefore, the results indicate that the amplitude of second harmonic may not necessarily increase with the delamination size and it also depends on the delamination through-thickness location. In general, larger amplitude of second harmonic is observed in forward scattering direction than

in backward scattered direction. This shows that reflected wave signals from the delamination provide more information about the delamination in the laminated composite beams than the forward transmitted wave signals.

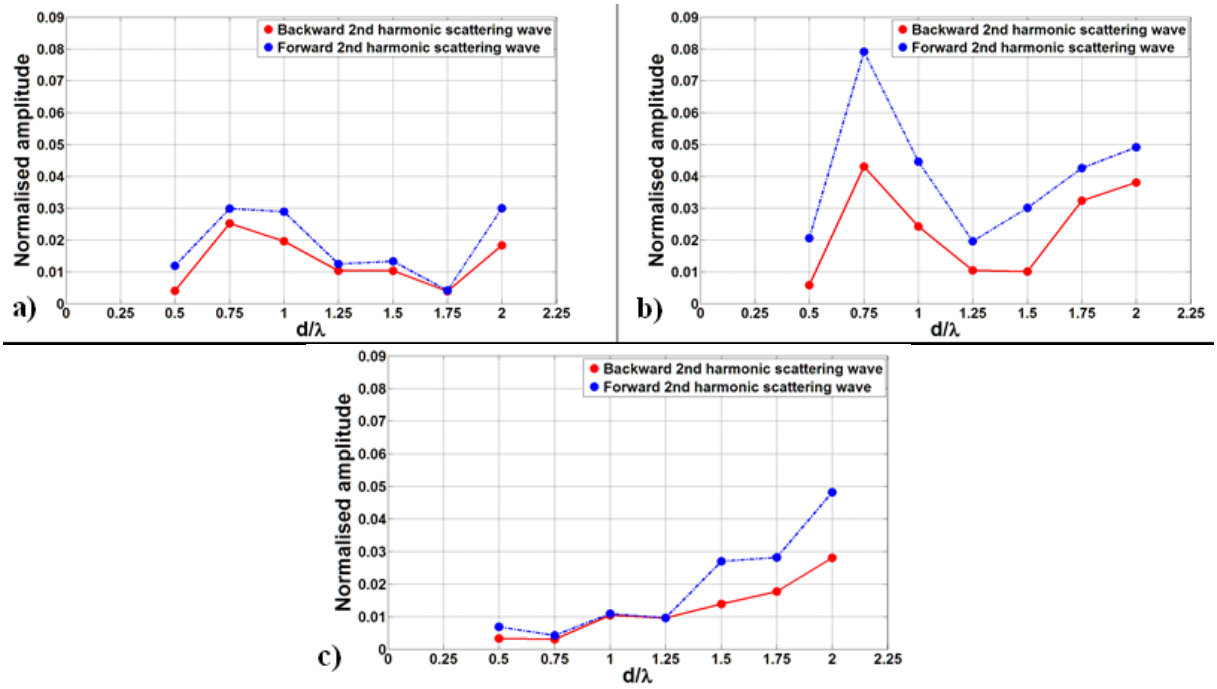

Figure 15. Normalized amplitude of second harmonic against delamination size to wavelength ratio for a) Damage Case 1 b) Damage Case 2 and c) Damage Case 3

4.3. Effect of damping and propagation distance

In this section the effect of damping on the interaction of A_0 guided wave with delamination due to CAN is studied. For this purpose, different Rayleigh damping values were considered in the FE models. The models were analysed using different Rayleigh damping values and the amplitude of second harmonic was captured and compared for all damage cases. The mass proportional Rayleigh damping coefficient α has a small effect when the excitation frequency is high. However, the frequency proportional Rayleigh damping coefficient β has a significant effect on the results. Therefore, α was considered constant in all models and β was varied from 1.128×10^{-15} to 1.128×10^{-6}. Fig. 16 shows the amplitude of the second harmonic for delamination with delamination size to wavelength ratio of d/λ = 1 in all three damage cases. The FE simulation results shown in Fig. 16 indicate that the amplitude of second harmonic decays with damping coefficient. The results indicate that amplitude of second

harmonic decreases rapidly with damping when the Rayleigh damping coefficient exceeds 1.128×10^{-8} rad/s. Considering that the Rayleigh damping coefficient for the present composite material is 1.128×10^{-8} rad/s at 140 kHz and the frequency proportional damping coefficient is inversely proportional to the square of frequency (Eq. 5), the excitation frequency has a significant influence on the amplitude of the nonlinear wave.

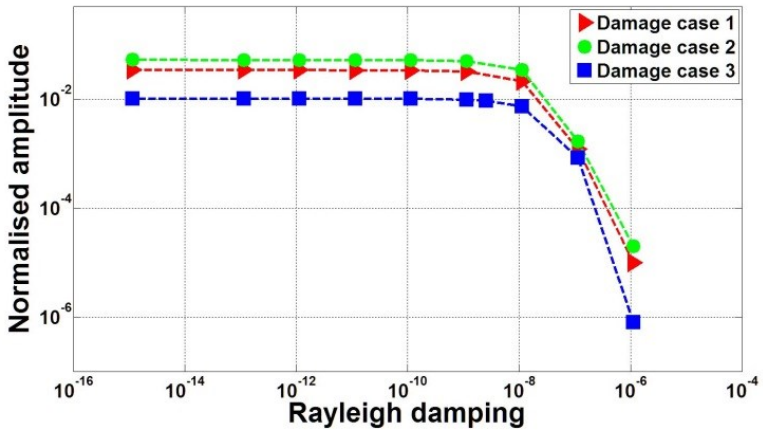

Figure 16. Normalized amplitude of second harmonic generated due to CAN as a function of Rayleigh damping value for delamination of d/ λ = 1 and incident wave at 140 kHz.

In addition to the effect of damping on the magnitude of second harmonic, the propagation distance also has a major effect on the magnitude of nonlinear waves. The data was captured at several measurement points in backward and forward scattering direction and presented in the frequency domain. Measurement points were located at 5λ ($\lambda = 8\ mm$) from the centre of the delamination and at a spacing of 10 mm (1.25 λ) between each measurement point. The captured data at each measurement point was normalized to the amplitude of incident wave at the same measurement points in intact model. The FE simulation results indicate that the amplitude of the second harmonic decreases with propagation distance in both forward and backward scattering directions. Figs. 17 shows the normalized amplitude of second harmonic against propagation distance for delamination of d/λ =1 and located at different through-thickness locations. The results show that the second harmonic wave decreases exponentially with the propagation distance in the forward and backward scattering directions. Moreover, the Fig. 17 shows that the magnitudes of higher harmonic for all damage cases decay with the same

slope. This means that larger amplitude of second harmonic may be obtained when measurement point is located closer to the delamination. Therefore, it is anticipated that better results are obtained when the measurement point is closer to the delamination.

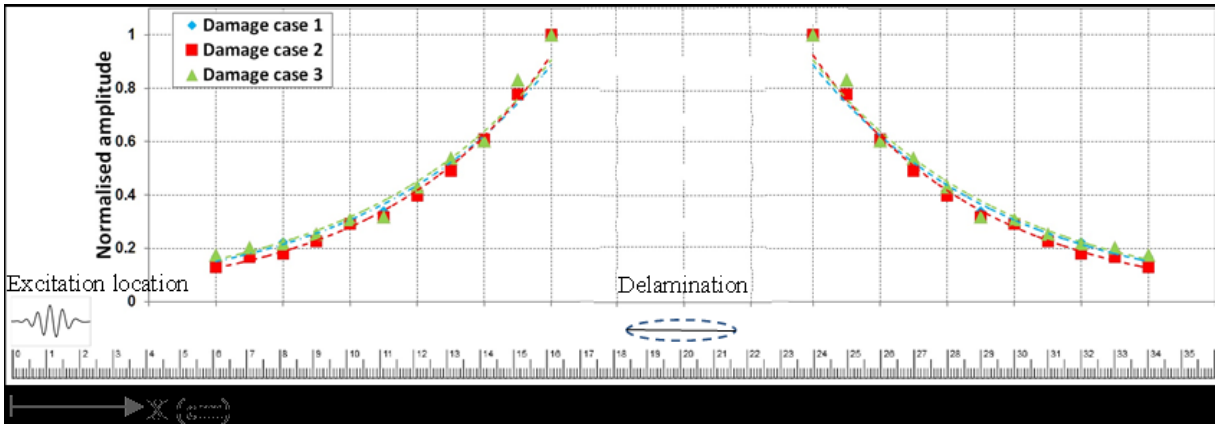

Figure 17. Normalized amplitude of second harmonic against propagation distance in forward and backward scattering directions for the delamination of d/λ = 1

4.4. Effect of incident wave amplitude and number of cycles

To investigate the effects of the amplitude and number of cycles of the incident wave on the second harmonic, FE simulations with different the peak amplitude and the number of cycles of the incident wave were carried out. The data was captured in both forward and backward scattering directions. To investigate the effect of incident wave amplitude and the number of cycles on the second harmonic wave packet amplitude, the data from all damage cases were normalized to the maximum amplitude of the whole data set. The FFT of the reflected wave signals at measurement points for Damage Case 3 and d/λ = 1 were calculated. The results are presented in Figs.18a and 18b. Figs. 19a and 19b show the same results for transmitted waves. The results show that the amplitude of the second harmonic increases with incident wave amplitude and the number of cycles for both forward and backward scattering directions wave. However, the ratio of second harmonic amplitude to incident wave amplitude remains constant for all damage cases. Since the proposed damage detection technique relies on the amplitude of

the higher harmonic wave packets, the results indicate that using larger incident wave amplitude and more number of cycles could provide better damage detection outcomes.

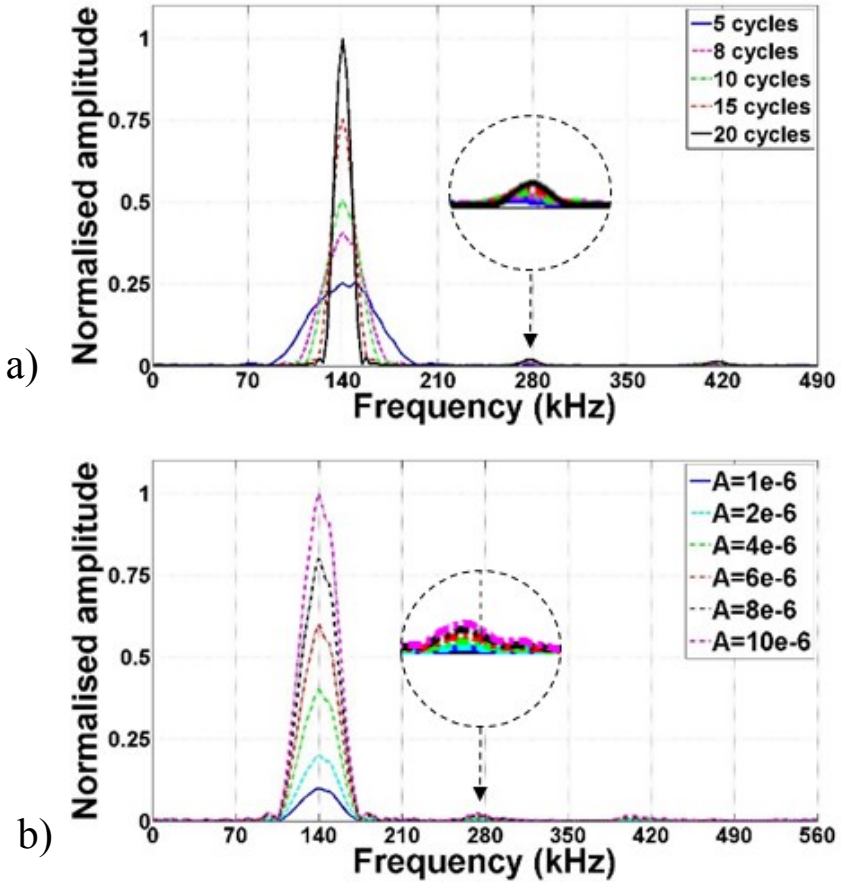

Figure 18. FFT of normalized reflected wave for various a) numbers of cycles and b) amplitude of incident wave in Damage Case 3 and d/λ = 1

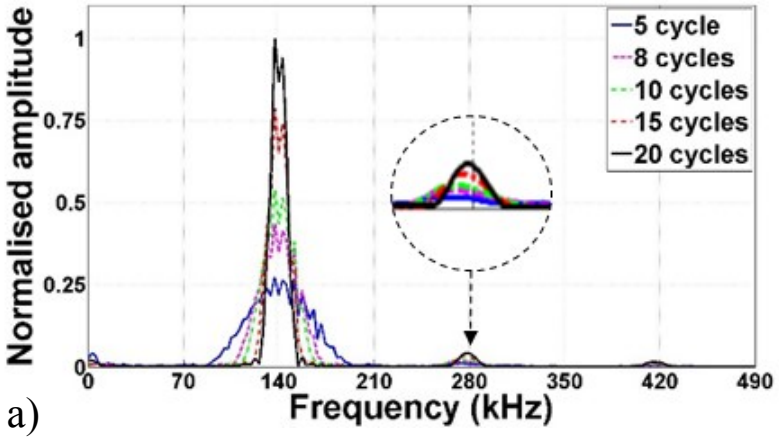

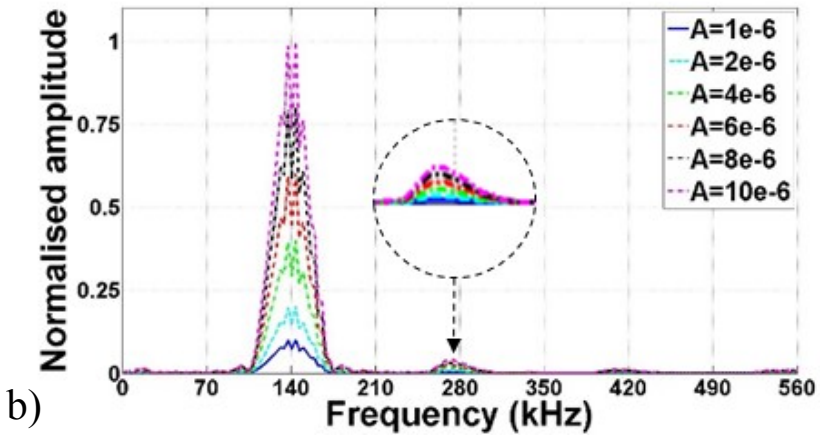

Figure 19. FFT of normalized transmitted wave for various a) numbers of cycles and b) amplitude of incident wave in Damage Case 3 and d/λ = 1

5. Conclusions

The generation and propagation of nonlinear wave by the interaction A_0 guided wave with the delamination in the fibre-reinforced laminated composite beams have been investigated using experimentally validated 3D FE simulations. The study has focused on the effects of size and through-thickness location of the delaminations on the higher harmonic generation. By accounting the surface contact and damping effect, the FE model is able to provide a reasonable prediction of the linear and nonlinear guided wave induced at the delaminations in the laminated composite beams. The higher harmonics induced by the interaction of the incident A_0 guided wave with the delamination have been extracted and analysed in frequency domain and time-frequency domain using FFT and continuous Gabor wavelet transform.

The results of the FE simulations of the laminated composite beams with delaminations show that second harmonic guided waves are generated due to the clapping effect of the sublaminate surfaces at the delamination region. The second harmonic guided waves have been observed in both forward and backward scattering directions. The magnitude of the second harmonic depends on the through-thickness location of the delamination. For the delaminations located at the mid-plane of the laminated composite beams, only minor or no higher harmonic

is observed in the guided wave signals. In general the existence of the second harmonics is a good indication for the delaminations in laminated composite beams. The second harmonic exhibits a larger magnitude in forward scattering direction than backward scattering direction. Therefore, it has an advantage in monitoring the higher harmonic waves at the forward scattering direction, i.e. the transmitted waves. Moreover, it has been shown that the generation of higher harmonics is influenced by the through-thickness location of the delaminations.

The studies on damping and propagation distance have shown that the amplitude of second harmonic decreases when damping and propagation distance increase. This is very important as longer propagation distance may result in smaller amplitude of second harmonic, which makes the damage detection more difficult and inefficient. It is also anticipated that damage detection becomes more complicated when the damping is high. The results of this study have shown an exponential decrease in second harmonic amplitude with damping coefficient. Therefore, the measurement location and damping are two important key factors for using second harmonic generated by CAN in damage detection.

The results of different incident wave amplitudes and numbers of cycles have shown that the amplitude of second harmonic wave packet increases with the incident wave amplitude and number of cycles. Therefore, the incident wave with larger amplitude and more number of cycles could provide better damage detection results. This study has also shown that processed data in frequency domain and time-frequency domain provide more information of the delaminations in laminated composite beams than the time domain data.

Overall this study has provided improved fundamental insights into the phenomenon of second harmonic generated by CAN at the delaminations in laminated composite beams. The characteristics of the nonlinear guided wave in forward and backward scattering directions have

been studied in detail. The findings of this study can be used to validate and improve the performance of damage detection methods using nonlinear guided waves.

6. Acknowledgements

This work was supported by the Australian Research Council under Grant Number DP160102233. Dr Eugene Chan from RMIT University contributed the manufacturing of the laminated composite beam specimens. The supports are greatly appreciated.

7. References

1. Achenbach JD. Quantitative non-destructive evaluation. *Int J Solids Struct* 2000; 37: 13-27.
2. Rose JL. A baseline and vision of ultrasonic guided wave inspection potential. *J Press Vess* 2002; 124: 273-282.
3. Raghavan A and Cesnik CES. Review of guided-wave structural health monitoring. *Shock Vib. Digest* 2007; 39: 91-114.
4. Veidt M, Ng CT, Hames S and Wattinger T. Imaging laminar damage in plates using Lamb wave beamforming. *Adv Mater Res* 2008; 47-50: 666-669.
5. An YK and Sohn H. Integrated impedance and guided wave based damage detection. *Mech Sys Sig Process* 2012; 28: 50-62.
6. Ng CT. Bayesian model updating approach for experimental identification of damage in beams using guided waves. *Struct Health Monitor* 2014; 13: 359-373.
7. Haynes C and Todd M. Enhanced damage localization for complex structures through statistical modelling and sensor fusion, *Mech Syst Sig Process* 2015; 54-55: 195-209.
8. Ng CT. A two-stage approach for quantitative damage imaging in metallic plates using Lamb waves. *Earthquake Struct* 2015; 8: 821-841.

9. Wandowski T, Malinowski PH. and Ostachowicz WM. Circular sensing networks for guided waves based structural health monitoring. *Mech Syst Sig Process* 2016; 66-67: 248-267.
10. Wang C.H. and Chang F.K. Scattering of plate waves by a cylindrical inhomogeneity. *Journal of Sound and Vibration 2005*: **282**: 429-451
11. Soleimanpour R and Ng CT. Mode conversion and scattering analysis of guided waves at delaminations in laminated composite beams. *Journal of Structural Monitoring and Maintenance 2015*:2:3: 213-236.
12. Klepka A, Staszewski WJ, Jenal RB, Szwedo M, Iwaniec J, and Uhl T. Nonlinear acoustics for fatigue crack detection – experimental investigations of vibro-acoustic wave modulations. *Structural Health Monitoring* 2011, 11:2: 197-211.
13. Liu Y, Kim, JY, Jacobs LJ, Qu J and Li Z. Experimental investigation of symmetry properties of second harmonic Lamb waves. *J. Appl. Phys* 2012; 111:053511-053511.
14. Kim J, Jacobs L and Qu J. Experimental characterization of fatigue damage in a nickel-base superalloy using nonlinear ultrasonic waves. *J Acoust Soc Am* 2006; 120: 1266-1273.
15. Deng M. Cumulative second-harmonic generation accompanying nonlinear shear horizontal mode propagation in a solid plate. *J Appl Phys* 1998; 84(7): 3500–3505.
16. Deng M. Cumulative second-harmonic generation of Lamb-mode propagation in a solid plate. *J Appl Phys* 1999; 85(6): 3051–3058.
17. Müller MF, Kim JY and Qu J, *et al*. Characteristics of second harmonic generation of Lamb waves in nonlinear elastic plates. *J Acoust Soc Am* 2010; 127(4): 2141–2152.
18. Zhang Z, Liu D, Deng M, Ta D and Wang W. Experimental observation of cumulative second-harmonic generation of Lamb waves propagating in long bones. *Ultrasound Med Bio* 2014; 40: 1660-1670.

19. Xiang Y, Deng M, Xuan FZ and Liu CJ. Effect of precipitate dislocation interactions on generation of nonlinear Lamb waves in creep damaged metallic alloys. *J Appl Phys* 2012; 111:104905.

20. Lissenden C. J, Liu Y, Choi G. W, Yao X. Effect of Localized Plastic Deformation on Higher Harmonic Guided Wave Mode Generation in Plate. *J Nondestruct Eval* 2014; 33:178–186

21. Pruell C, Kim JY, Qu J and Jacobs LJ. Evaluation of fatigue damage using nonlinear guided waves. *Smart Mater Struct* 2009; 18: 035003.

22. Bermes C, Kim J and Qu J. Experimental characterization of material nonlinearity using Lamb waves. *App Phys Let* 2007; 90(2):021901.

23. Srivastava A and Lanza di Scalea F. On the existence of antisymmetric or symmetric Lamb waves at nonlinear higher harmonics. *J Sound Vib* 2009: 323(3): 932–943.

24. Awrejcewicz J and Olejnik P. Friction Pair Modelling by a 2-DOF System; Numerical and Experimental Investigations. *Inter J. Bifurcation Chaos* 2005; 1931-1944.

25. Pecorari C and Solodov I. Non-classical Nonlinear Dynamics of Solid Interfaces in Partial Contact for NDE Applications. Springer Journals 2006; 307-324.

26. Nazarov VE and Sutin A. Nonlinear Elastic Contacts of Solids with Cracks. *J Acoust Soc Am* 1997; 102: 3349-3354.

27. Kishiwada S, Biwa S, Inserra C and Matsumoto E. Modelling of flexural wave propagation in a plate with contacting interface. *Proceed Asian Pacific Conf Mater Mech* 2009; 2368-2372.

28. Kim N, Lee TH, Jhang KY and Park IK. Nonlinear Behaviour of Ultrasonic Wave at Crack. *AIP Conf* 2010; 1211: 73.

29. Hong M, Su Z, Wang Q, Cheng L and Qing X. Modelling nonlinearities of ultrasonic waves for fatigue damage characterization. *Ultrasonics* 2014; 54: 770-778.

30. Solodov I. Wackerl J, Pfleiderer K and Busse G. Nonlinear self-modulation and subharmonic acoustic spectroscopy for damage detection and location. *Appl Phys Lett* 2004; 84(N26) 5386-5388.

31. Kishiwada S, Biwa S, Inserra I, Matsumoto E. Nonlinear Ultrasonic Characterization of Lamb Wave in a Plate with Contacting Interfaces. *Proceed ICCAS-SICE* 2009; *2368*: 1-6.

32. Korotkov AS, Slavinsky MM and Sutin AM. Variations of acoustic nonlinear parameters with the concentration of defects in steel. *J Acoust Phys* 1994; 40: 71-74

33. Donskoy A, Sutin A and Ekimov C. Nonlinear Acoustic Interaction on Contact Interfaces and its use for Nondestructive Testing. *NDT & E Int* 2001; 34: 231-238.

34. Li, W, Cho, Y, Achenbach J. D. Detection of thermal fatigue in composites by second harmonic Lamb waves. *Smart Mater Struct* 2012; 21:8: 085019.

35. Zhao, J, Chillara V. K, Ren B, Cho H, Qiu J, Lissenden, C. J. Second harmonic generation in composites: Theoretical and numerical analyses. *J App Phys* 2016; 119:6:064902.

36. Castaings M and Hosten B. Lamb and SH waves generated and detected by air-coupled ultrasonic transducers in composite material plates. *NDT & E Int* 2001; 34: 249-258.

37. Ng CT. On the selection of advanced signal processing techniques for guided wave identification using a statistical approach. *Eng Struct* 2014; 67: 50-60.

38. Ramadas C, Balasubramaniam K, Hood A, Joshi M and Krishnamurthy CV. Modelling of attenuation of Lamb waves using Rayleigh damping: Numerical and experimental studies. *Composite Struct* 2011; 93: 2020–2025.

39. Ng CT. On accuracy of analytical modelling of Lamb wave scattering at delaminations in multilayered isotropic plates. *Int J Struct Stab Dyn* 2015; 15(1540010): 1-12.

40. Packo P, Uhl T, Staszewski W.J. Generalized semi-analytical finite difference method for dispersion curves calculation and numerical dispersion analysis for Lamb waves. *J. Acoust. Soc. Am.* 2014;136 :3:993-1002.

41. Zhao J, Chillara VK, Ren B, Cho H, Qiu J and Lissenden, CJ. Second harmonic generation in composites: Theoretical and numerical analyses. *J App Phys* 2016;119(6): 064902.

42. Ng CT and Veidt M. A Lamb-wave-based technique for damage detection in composite laminates. *Smart Mater Struct* 2009;18: 1–12.

43. Maio L, Memmolo V, Ricci F, Boffa N.D, Monaco E, Pecora, R. Ultrasonic wave propagation in composite laminates by numerical simulation. *Comp Struct* 2015;121:64–74.

44. Stewart JR, Gullerud AS, Heinstein MW, Solution verification for explicit transient dynamics problems in the presence of hourglass and contact forces. *J Comp Methods App Mech Eng* 2006; 195: 1499–1516.

45. Ng CT, Veidt M and Rajic N. Integrated piezoceramic transducers for imaging damage in composite laminate. *Proceed SPIE* 2009; *7493*: 1-8.

46. He S and Ng CT. Analysis of mode conversion and scattering of guided waves at cracks in isotropic beams using a time-domain spectral finite element method. *Elect J Struct Eng* 2015; 14: 20-32.

47. ABAQUS Theory Manual Version 6.9, 2009, ABAQUS Inc.

48. Stepinski T, Uhl T, Staszewski W. Advanced Structural Damage Detection: From Theory to Engineering Applications, Wiley, 2003

49. Kovic B and Lowe M. DISPERSE User's Manual Version 2.0.16B. *Imperial College. University of London, Non-Destructive Testing Laboratory* 2003.

Statement of Authorship of the Journal Paper 4

Title of Paper	Locating delaminations in laminated composite beams using nonlinear guided waves
Publication Status	☐ Published ☑ Accepted for Publication ☐ Submitted for Publication ☐ Unpublished and Unsubmitted w ork w ritten in manuscript style
Publication Details	Journal of Engineering Structures

Principal Author

Name of Principal Author (Candidate)	Reza Soleimanpour		
Contribution to the Paper	Performed the study and wrote the manuscript		
Overall percentage (%)	60		
Certification:	This paper reports on original research I conducted during the period of my Higher Degree by Research candidature and is not subject to any obligations or contractual agreements with a third party that would constrain its inclusion in this thesis. I am the primary author of this paper.		
Signature		Date	12/09/2016

Co-Author Contributions

By signing the Statement of Authorship, each author certifies that:

i. the candidate's stated contribution to the publication is accurate (as detailed above);

ii. permission is granted for the candidate in include the publication in the thesis; and

iii. the sum of all co-author contributions is equal to 100% less the candidate's stated contribution.

Name of Co-Author	Ching-Tai Ng		
Contribution to the Paper	Supervised development of the work and manuscript evaluation		
Signature		Date	12/09/2016

Please cut and paste additional co-author panels here as required

Chapter 6: Locating delaminations in laminated composite beams using nonlinear guided waves

Abstract

This paper proposed a new method for detecting and locating delaminations in laminated composite beams using nonlinear guided wave. It is shown that when incident wave interacts at the delamination, the nonlinear effect of wave interaction with contact interfaces at the delamination can generate higher harmonic guided wave due to contact acoustic nonlinearity (CAN). The proposed method employs a transducer network to detect and locate the delaminations using the higher harmonic guided wave. A sequential scan is used to inspect the laminated composite beams by actuating A_0 guided wave at one of the transducers while the rest of the transducers are used for measuring the impinging waves. A series of numerical case studies are performed using three-dimensional explicit finite element simulations, which consider different delamination locations, lengths and through-thickness locations. In addition experimental case studies are carried out to further validate and demonstrate the proposed method. The results show that the proposed method is able to accurately detect and locate delamination in the laminated composite beams using the higher harmonic guided wave. One of the advantages of the proposed method is that it does not rely on baseline data to detect and locate the delaminations, and hence, it has less influence by varying operational and environmental conditions.

Keywords: nonlinear guided wave, contact acoustic nonlinearity, higher harmonic, delamination, laminated composite beam, baseline-free method, transducer network

1. Introduction

1.1. Overview

In last decade, fibre-reinforced composite materials have been widely used in different engineering structures due to its attractive characteristics, such as high specific stiffness, light-weight and corrosion resistance. Delamination is one of the common types of damage for this kind of material and it could lead to structural failure. It is a separation of adjacent subsurface laminae without any obvious visual evidence on the surface and is usually caused by fatigue loading, low velocity impacts and imperfections during manufacturing process. Many techniques have been developed for detecting the delamination. In last two decades low-frequency vibration damage detection approach has been extensively investigated in the literature [1-5]. However, this approach is generally not sensitive to local incipient defects, such as delamination.

In the recent years, the use of guided waves has attracted considerable attention for damage detection [6-9]. Many studies have been carried out and focused on different types of materials, such as isotropic [10-15] and composite materials [16-18]. In the literature, guided waves have gained prominence for damage detection due to their potential for online structural health monitoring and inspection at inaccessible locations. Moreover, guided waves have been proved to be sensitive to small and different types of defects and are able to propagate long distance for monitoring relatively large area of structures [6,7]. So far, most of the existing ultrasonic guided wave damage detection techniques rely on linear guided wave scattering phenomena, such as reflection, transmission and mode conversion information at the excitation frequency [19-23]. Majority of these techniques detect the damage by comparing the guided wave signals obtained from the current condition of a structure with signals obtained from its pristine condition. However, the changing environmental and operational conditions, e.g. temperature variation, can significantly affect the performance and accuracy of the damage detection techniques relied on baseline data [24,25] and could lead to misdetection of the damage and

false alarms. Therefore, it limits the practical applications of the damage detection techniques using linear guided wave.

1.1. Damage detection using nonlinear guided waves

The use of nonlinear guided waves has recently attracted considerable attention. Recent developments have shown that the sensitivity of nonlinear guided waves to small defects is much higher than conventional linear guided waves. Thus, there has been a growing interest in theoretical developments and applied research on using various classical and non-classical nonlinear phenomena for damage detection. The nonlinear guided wave techniques rely on higher harmonic generation due to material nonlinearity [26] or contact acoustic nonlinearity (CAN) [27-29]. The higher harmonic generation has been known to be an indication of defect existence in structures. Early developments on the use of the higher harmonics generated by CAN focused on determining the existence of the defects in the structures. In recent years, significant progress has been made towards using higher harmonic guided waves for damage detection, which demonstrated the feasibility of using them for detecting plastic strain, fatigue damage, micro-cracking and other types of material damages [30-35].

Li et al. [30] proposed to detect thermal fatigue damage in composite laminates using second harmonic Lamb waves. It was shown that there is a monotonic increase of acoustic nonlinearity with respect to thermal fatigue cycles. It was concluded that nonlinear Lamb waves can be used to assess thermal fatigue damage and the technique is better than conventional linear Lamb wave technique in terms of accuracy and efficiency. Soleimanpour and Ng [31] investigated the generation of second harmonic when guided waves interact at delamination in laminated composite beams. It was shown that the second harmonics generated due to CAN is sensitive to the existence of delaminations in laminated composite beams. Hong *et al*. [32] investigated the phenomenon of CAN related to breathing fatigue cracks and included material nonlinearity effect in their study. They showed that the relative acoustic nonlinearity parameter increases

proportionally with the wave propagation distance due to the geometric and materials nonlinearities. Zhao *et al*. [33] studied the second harmonic generation of Lamb waves in transversely isotropic plate and a symmetric composite laminate. They showed that for transversely isotropic plate, when waves propagate along material principal directions, the symmetric second harmonic Lamb-like waves modes can be generated whereas for propagation direction other than material principal direction only the symmetric second harmonic waves are generated. Moreover, for symmetric composite laminate, only the symmetric second harmonic waves can be generated provided that the power flux is non-zero.

Although extensive research works have been carried out on the use of higher harmonic for damage detection, there were very limited studies [34,35] focused on determining the location of the defects, especially for delamination in laminated composite materials using higher harmonic guided wave generated due to CAN. Kazakov *et al*. [34] proposed a method to determine the location of a crack using high-frequency tone bursts modulated by a continuous low-frequency wave. Experimental verification was carried out using a steel plate. Dziedziech *et al*. [35] proposed a damage detection method based on the synchronisation of the low-frequency vibration with the interrogating high-frequency guided wave. The method was employed to detect and locate fatigue crack in aluminium beam experimentally. Their results demonstrated the feasibility of using higher harmonic guided wave for baseline-free damage detection.

This paper presents a novel technique for determining the location of delaminations in laminated composite beams using higher harmonic guided wave generated by CAN. The proposed technique has the following advantages: 1) it does not rely on the baseline data for detecting and locating delaminations, and hence, it has less influence by varying environmental conditions; 2) the nonlinear damage feature is very sensitive to small incipient damages.

The paper is organized as follows. Section 2 describes the theoretical background of CAN in generating the higher harmonic guided wave. Section 3 presents the proposed damage detection

methodology, which describes the details of the proposed damage detection technique of determining the location of delamination in laminated composite beams. In Section 4 a series of numerical case studies are presented. In this section, the performance and capability of the proposed damage detection methodology are assessed and demonstrated through a number of numerical case studies. Delaminations with different locations, sizes and through-thickness locations are considered. In Section 5, experimental case studies are presented to verify the applicability of the proposed damage detection mehtod in practical situation. Finally, conclusions are drawn in Section 6.

2. Theoretical Background

Higher harmonic generation involves various classical and non-classical nonlinear phenomena in ultrasonic wave responses. Classical nonlinear phenomenon refers to higher harmonic generation due to material imperfections, in which the wave distortion occurs when incident wave interacts with nonlinear elastic response of the medium during the wave propagation. In the presence of micro-scale damages, e.g. distributed micro-cracks in the materials, the higher harmonic generation is significantly enhanced. The phenomenon of higher harmonic generation due to material nonlinearity was formulated by Hegedron [36], Lee and Choi [37] and Naugolnykhand and Ostrovsky [38]. It was shown that if a harmonic input with a central frequency of ω is imposed on a nonlinear system, the output of the system contains higher harmonics of 2ω and 3ω while the input signal only contains a single frequency component of ω. Therefore, the material nonlinearity can be a possible source of the wave nonlinearity.

In non-classical nonlinear phenomenon, higher harmonics can be generated due to CAN, which is a nonlinear effect of wave interaction with contact interfaces at material discontinuities, e.g. fatigue cracks and delaminations. CAN is related to the lack of stiffness symmetry for near-surface strain across the interfaces [28]. Since the compression is accompanied by weakening or rupture of the contact between the surfaces, the compression elasticity is higher than that of

a tensile stress. Therefore when the mechanical wave passes through the contact interfaces, a bi-modular area is created and can be simulated by a piece-wise stress–strain relation. This bi-modular surface causes clapping form of behaviour, which is generated due to asymmetry in stress-strain characteristics for damaged interfaces. The formulation of clapping between interfaces was proposed by Solodov *et al*. [28]. Consider a pair of interfaces, subjected to the clapping of the interfaces due to longitudinal or flexural wave. The clapping behaviour, which is caused by asymmetrical dynamics of the interface stiffness, can be approximated by a stress-strain relation as [28]

$$\sigma = E^{II}[1 - H(\varepsilon - \varepsilon^0)\left(\frac{\Delta \mathrm{E}}{E^{II}}\right)]\varepsilon \tag{3}$$

$$\Delta \mathrm{E} = [\mathrm{E}^{II} - \frac{\mathrm{d}\sigma}{d\varepsilon}] \text{ for } \varepsilon>0 \tag{4}$$

where ε is strain and σ is stress, $H(\varepsilon)$ is the Heaviside unit step function and E^{II} is the intact material second-order linear elasticity. ε^0 is the initial static contact strain.

A harmonic strain $\varepsilon(t) = \varepsilon_0 cos\omega t$ of period $T = 2\pi/\omega$, which passes through the bi-modular interface, it works like a mechanical diode causing variation in E^{II}. In this case the compressional part of the wave penetrates into the contact region while the tensile part does not. Thus, once the incident wave interacts with the interfaces, the waves shape becomes nearly half-wave rectification, which provides an unconventional nonlinear waveform distortion as shown in Fig. 1. As E^{II} is a periodic function of the frequency, at the damaged area the induced nonlinear part of spectrum σ^{NL} is

$$\sigma^{NL}(t) = \Delta E(t).\varepsilon(t) \tag{5}$$

which consists higher harmonics and the amplitude of the *n*-th harmonic A_n are modulated by the sinc-envelope function as follows [28]

$$A_n = \Delta \mathrm{E}\Delta\tau\varepsilon_0[sinc\big((n+1)\Delta\tau\big) - 2\cos(\pi\Delta\tau)\mathrm{sinc}(\mathrm{n}\Delta\tau) + \mathrm{sinc}((\mathrm{n}-1)\Delta\tau)] \tag{6}$$

$$\Delta\tau = \frac{\tau}{T}, \tau = \frac{T}{\pi}\text{Arc}\cos(\frac{\varepsilon^0}{\varepsilon_0}) \quad (7)$$

where $\Delta\tau$ is the normalized modulation pulse length. When the strain is larger than the threshold of clapping ε^0, i.e. $\varepsilon > \varepsilon^0$, the spectrum of nonlinear vibration contains both odd and even harmonics [28].

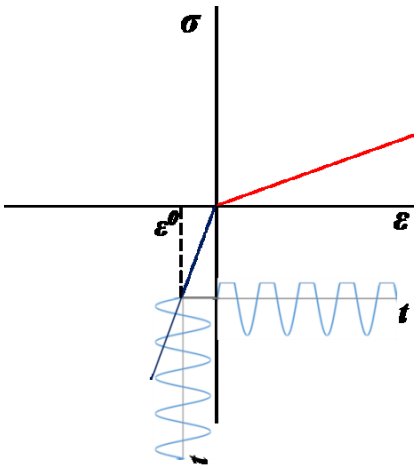

Figure 1. CAN strain-stress model and wave rectification

3. Damage Detection Methodology

The majority of existing damage detection techniques use baseline data for damage detection. It means that damage detection needs to be carried out by comparing the data obtained from the current state of the structure with the baseline data obtained from the pristine structure. However, the varying operational and environmental conditions of the structure can adversely influence the collected data and cause errors [2424,25]. To address this problem, this study proposes to use the second harmonic guided wave to detect and locate the delaminations in laminated composite beams, and hence, the damage detection does not rely on the baseline data.

It has been shown that the fundamental anti-symmetric mode (A_0) guided wave possesses a smaller wavelength compared to the fundamental symmetric mode (S_0) guided wave at the same frequency. In addition, the anti-symmetric mode guided waves have much larger out-of-plane displacement magnitude than that in in-plane direction. As the out-of-plane displacement is perpendicular to the subsurfaces of the laminae (contact surfaces in CAN) at the delamination,

it provides a better correlation in terms of higher harmonic guided wave generation at the delamination. Therefore, A_0 guided wave is used as the incident wave in this study.

3.1. Transducer arrangement for damage detection

Without loss of generality, a transducer network consists of at least three transducers is used to detect and locate the delamination in the laminated composite beams in this study. Each of the transducers can act as both actuator and receiver for excitation and measurement. The advantage of using the transducer network is that it provides a flexibility of inspecting a long length of one-dimensional (1D) waveguide (e.g. laminated composite beam), which addresses the wave attenuation issue due to material damping of laminated composite materials. In this section a transducer network consists of three transducers, labelled as Transducers 1, 2 and 3, is used to illustrate the concept of the proposed method for delamination detection and location. Fig. 2 shows a schematic diagram of the transducer arrangement. The laminated composite beam is divided into four zones. A sequential scan for inspecting the laminated composite beam can be performed by actuating the A_0 guided wave at one of the transducers while the rest of the transducers are used for measuring the impinging waves.

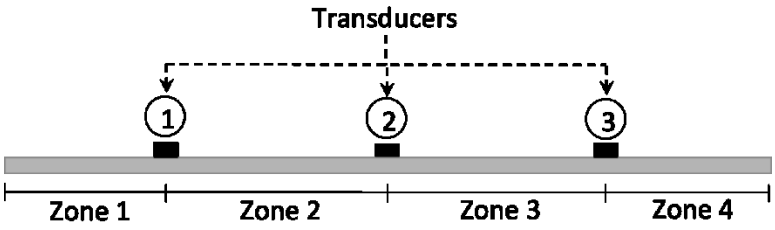

Figure 2. Schematic diagram of a transducer network for detecting and locating delaminations

In general there are two conditions, pulse-echo and pitch-catch, depending on the location of the delamination. Using the transducer network in Fig. 2, in which Transducers 1 and 2 are used as actuator and receiver, respectively, as an example, if the delamination is located in zone 3, it is the pulse-echo condition. Under this condition, Transducer 2 measures the reflected waves, i.e. reflected linear guided wave and higher harmonic guided wave, from

the delamination. If the delamination is located in zone 2, it is the pitch-catch condition. Transducer 2 measures the transmitted waves, i.e. scattered linear guided wave and higher harmonic guided wave induced at the delamination.

In this study a general approach, which considers both the pulse-echo and pitch-catch condition, is proposed to detect and locate the delamination in the laminated composite beams using the higher harmonic guided wave. Thus the proposed method is applicable to different actuation-sensing situations in the transducer network. Sections 3.2 and 3.3 describe the details of detecting and locating the delamination under the pulse-echo and pitch-catch conditions.

3.2. Pulse-echo condition

In the case of pulse-echo condition, the delamination is located at one side of both actuator and receiver as shown in Fig. 3c. The incident wave generated by the actuator passes through the receiver and then reaches the delamination. The receiver measures the reflected linear wave and second harmonic guided wave, which is induced due to the interaction of the incident wave with the delamination. The linear wave reflection is at the same frequency as the incident wave (f_c) while the second harmonic frequency is at frequency $2f_c$.

Figs. 3a and 3b show a schematic diagram of the incident wave and the second harmonic guided wave in time-domain and time-frequency domain, respectively. The incident wave and second harmonic guided wave package arrive the receiver at different times, i.e. t_{f_c} and t_{2f_c}. As shown in time-frequency energy density spectrum in Fig. 3b, there are three contours. Two contours are at the excitation frequency f_c and the other contour is at frequency $2f_c$. The two contours at f_c refer to the incident wave and reflected linear wave package from the delamination while the contour at frequency $2f_c$ refers to the second harmonic guided wave package generated due to CAN at the delamination.

The arrival time of the incident wave (t_{f_c}) is

$$t_{f_c} = \frac{d_{a-r}}{c_g(f_c)} \tag{14}$$

where d_{a-r} is the distance between the actuator and receiver as shown in Fig. 3c and $c_g(f_c)$ is the group velocity of the incident A_0 guided wave at the excitation frequency f_c. The arrival time of the second harmonic guided wave package (t_{2f_c}) is

$$t_{2f_c} = \frac{d_{a-r}}{c_g(f_c)} + \frac{d_{d-r}}{c_g(f_c)} + \frac{d_{d-r}}{c_g(2f_c)} \tag{15}$$

where $c_g(2f_c)$ is the group velocity of the second harmonic guided wave and d_{d-r} is the distance between the delamination and the receiver. Therefore, using Equations (14) and (15), the delamination location can be determined by

$$d_{d-r} = \frac{\Delta t.c_g(2f_c).c_g(f_c)}{c_g(2f_c)+c_g(f_c)} \text{ where } \Delta t = t_{2f_c} - t_{f_c} \tag{16}$$

where Δt is the time difference between the arrival time of the incident wave (t_{f_c}) and the second harmonic guided wave (t_{2f_c}). Once the value of Δt is determined from the measured guided wave data, the delamination location d_{d-r} can be obtained.

In the case of using linear scattered wave information to detect and locate the delamination, it usually requires the baseline data to extract the linear scattered wave information when the delamination is close to the receiver or the beam is relatively short as the linear scattered wave overlaps with the incident wave or wave reflected from boundaries. In contrast the determination of the delamination location d_{d-r} using the higher harmonic guided wave, it only relies on the information of t_{f_c} and t_{2f_c} , i.e. the arrival time of the incident wave and second harmonic guided wave, as shown in Equation (16). Thus the delamination can be detected and located without the baseline data.

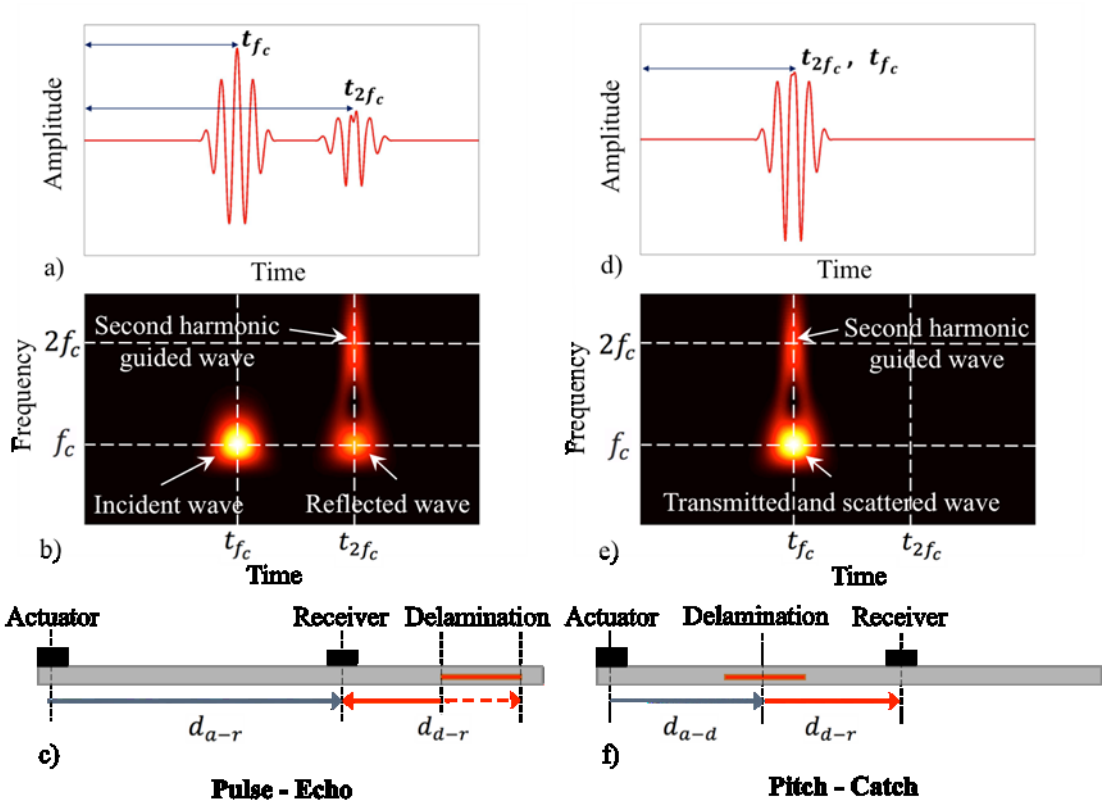

Figure 3. Typical signal in time domain, time-frequency domain and schematic diagram of the (a)-(c) pulse-echo and (d)-(f) pitch-catch condition

3.3. Pitch-catch condition

For the pitch-catch condition, the delamination is located between actuator and receiver as shown in Fig. 3f. Different to pulse-echo condition, the incident wave generated by the actuator first interacts with the delamination and then reaches the receiver. When the incident wave interacts with the delamination, it induces a linear scattered wave and a second harmonic guided wave due to CAN at the delamination. Figs. 3d and 3e show a schematic diagram of the incident wave and the second harmonic guided wave in time-domain and time-frequency domain, respectively. As shown in Fig. 3d the transmitted wave package contains the incident wave, linear scattered wave and second harmonic guided wave. The arrival time of the incident wave and higher harmonic guided wave are t_{f_c} and t_{2f_c}, and they can be obtained at frequency f_c and frequency $2f_c$ in the time-frequency domain, respectively.

The arrival time of the incident wave travel from the actuator to the delamination and then to the receiver (t_{f_c}) is

$$t_{f_c} = \frac{d_{a-d} + d_{d-r}}{c_g(f_c)} \tag{17}$$

where d_{a-d} is the distance between the actuator and delamination in the pitch-catch condition. The arrival time of the second harmonic guided wave is

$$t_{2f_c} = \frac{d_{a-d}}{c_g(f_c)} + \frac{d_{d-r}}{c_g(2f_c)} \tag{18}$$

Using Equations (17) and (18), the delamination location d_{r-d} can be determined by

$$d_{d-r} = \frac{\Delta t.c_g(2f_c).c_g(f_c)}{-c_g(2f_c)+c_g(f_c)} \text{ where } \Delta t = t_{2f_c} - t_{f_c} \tag{19}$$

Under the pitch-catch condition, if the excitation frequency is at the flat region of the A_0 group velocity dispersion curve, the group velocity of the higher harmonic guided wave $c_g(2f_c)$ is almost the same as the group velocity of the linear incident wave $c_g(f_c)$, and hence, $\Delta t \approx 0$. In this case, although information is not enough to determine the delamination location d_{d-r} in the pitch-catch approach, it can still indicate the existence of the delamination and also the delamination zone, based on the presence of higher harmonic guided wave measured by the actuator-receiver pair. If the excitation frequency is at the dispersive region of the A_0 group velocity dispersion curve, i.e. the low frequency non-flat region, the group velocity of the higher harmonic guided wave $c_g(2f_c)$ is higher than that of the incident wave $c_g(f_c)$. In this case, $\Delta t \neq 0$, and hence, the delamination location d_{d-r} be determined without the baseline data. In contrast, the pitch-catch approach using the linear guided wave does not provide enough information to determine the delamination location even the baseline data is available. Therefore, the use of the higher harmonic guided wave can provide additional information for the damage detection.

3.4. Determination of delamination zone and location

In this study, the excitation frequency is selected at the flat region of the A_0 group velocity dispersion curve, and hence, it can minimise the dispersion effect of the A_0 guided wave to maximize the wave propagation distance. Under this situation, the group velocity of the higher harmonic guided wave is almost the same as the linear incident wave, therefore, the pitch-catch condition is only used to determine the existence of the delamination and the delamination zone.

In practical situation, the existence and location of the delamination are unknown before the damage detection. A sequential scan is required to detect and locate the delamination using the transducer network as shown in Fig. 2, and hence, the actuator-receiver pair can be under pulse-echo or pitch-catch condition depending the location of the delamination. As discussed in Sections 3.2 and 3.3, if the difference of the arrival time between the incident wave and higher harmonic guided wave obtained from the measured data is $\Delta t \approx 0$, i.e. $d_{d-r} \approx 0$, this means it is the pitch-catch condition, and hence, the delamination is located between this actuator-receiver pair. Therefore, the delamination zone can be identified. The location of the delamination can be determined by using the other actuator-receiver pair under the pulse-echo condition. In this case Δt can be obtained from the measured data to determine the delamination location based on the Equation (16).

Table. 1 summarises all possible combinations in estimating the delamination location using a sequential scan of a transducer network with three transducers. The delamination location determined using the data measured by Transducer *i* is defined as d_{d-i} in Table 1. d_{d-i} is the distance of the delamination away from the Transducer *i*. Using Transducer 1 as the actuator, the rest of the transducers as receivers, and the delamination is located in zone 2 as an example, all actuator-receiver pairs are in pitch-catch condition, and hence, $d_{d-2} \approx 0$ and $d_{d-3} \approx 0$. It then needs to consider using Transducer 2 as the actuator. In this case, $d_{d-1} \approx 0$ and $d_{d-3} > 0$. Therefore the delamination is in zone 2 and the location is d_{d-3}. Similarly the delamination location can be obtained by using Transducer 3 as the actuator for the delamination located in zone 2, in which $d_{d-1} \approx 0$ but $d_{d-2} > 0$. This means the delamination is in zone 2 and the location is d_{d-2}. In general, damage zone can be identified using any actuator-receiver under the pitch-catch condition and at least an actuator-receiver pair needs to be under pulse-echo condition for determining the delamination location. Since the delamination location is calculated based on the information of the incident wave and second harmonic guided wave, it can be detected and located without using the baseline data.

Table 1. Possible combinations for estimating the delamination location using a sequential scan of a transducer network with three transducers for delamination located at different zones

Actuator	**Transducer 1**		**Transducer 2**		**Transducer 3**	
Receiver	Transducers 2 & 3		Transducers 1 & 3		Transducers 1 & 2	
Zone 1	$d_{d\text{-}2} \approx d_{d\text{-}3}$	$d_{d\text{-}2}$ $d_{d\text{-}3} > 0$	$d_{d\text{-}3} > d_{d\text{-}1}$	$d_{d\text{-}1}$ $d_{d\text{-}3} > 0$	$d_{d\text{-}2} > d_{d\text{-}1}$	$d_{d\text{-}1}$ $d_{d\text{-}2} > 0$
Zone 2	$d_{d\text{-}2} \approx 0$	$d_{d\text{-}3} \approx 0$	$d_{d\text{-}1} \approx 0$	$d_{d\text{-}3} > 0$	$d_{d\text{-}1} \approx 0$	$d_{d\text{-}2} > 0$
Zone 3	$d_{d\text{-}2} > 0$	$d_{d\text{-}3} \approx 0$	$d_{d\text{-}1} > 0$	$d_{d\text{-}3} \approx 0$	$d_{d\text{-}1} \approx 0$	$d_{d\text{-}2} \approx 0$
Zone 4	$d_{d\text{-}2} > d_{d\text{-}3}$	$d_{d\text{-}2}$ $d_{d\text{-}3} > 0$	$d_{d\text{-}1} > d_{d\text{-}3}$	$d_{d\text{-}1}$ $d_{d\text{-}3} > 0$	$d_{d\text{-}1} \approx d_{d\text{-}2}$	$d_{d\text{-}1}$ $d_{d\text{-}2} > 0$

3.5. Continuous Gabor wavelet transform

In this study the measured data is processed by the continuous Gabor wavelet transform, and hence, the time-frequency energy density spectrum can be obtained for accurately estimating the arrival time of the incident wave and the higher harmonic guided wave from the delamination. The continuous wavelet transform (CWT) displays the scale-dependent structure of a signal as it varies in time. This scale-dependent structure is essentially the frequency. Therefore, CWT provides a view of the frequency versus time behaviour of the signal [39]. The wavelet coefficient $WT(p,q)$ can be obtained by convolving the measured guided wave signal $u(t)$ with the translation p and dilation q as

$$WT(p,q) = \int_{-\infty}^{\infty} u(t)\chi_{p,q}^{*}(t)dt \tag{21}$$

where,

$$\chi_{p,q}(t) = \frac{1}{\sqrt{q}}\,\chi\left(\frac{t-p}{q}\right) \tag{22}$$

The asterisk donates the complex conjugate. $\chi(t)$ is the mother wavelet and Gabor wavelet is used in this study. The Gabor wavelet is defined as

$$\chi(t) = \frac{1}{\sqrt[4]{\pi}} \sqrt{\frac{\omega_0}{\eta}} \exp[-\frac{(\omega_0/\eta)^2}{2} t^2 + i\omega_0 t] \quad (23)$$

The time-frequency analysis resolution depends on the value of ω_0 and η. These values are usually considered as $\omega_0 = 2\pi$ and $\eta = \pi\sqrt{2/\ln 2} \approx 5.336$. The energy density spectrum is calculated by $|WT(p,q)|^2$, which indicates the energy distribution of the signal around $t = p$ and $\omega = \omega_0/q$. Thus, the energy density spectrum can be used to calculate the arrival time of the incident wave and higher harmonic guided wave at a specific frequency, and hence, the delamination location can be accurately identified.

4. Numerical Case Studies

An eight-ply $[(0/90)_2]_S$ laminated composite beam with a delamination was considered in this study. The dimensions of the beam is 166 mm × 12 mm × 1.6 mm. The elastic properties of the lamina are shown in Table. 2, and the thickness and density are 0.2 mm and 1538 kg/m^3, respectively. The delaminations considered in the numerical case studies have different delamination locations, sizes and through-thickness locations. In this study a three-dimensional (3D) explicit FE method [40] was used to simulate the propagation of linear and higher harmonic guided wave in the laminated composite beams. The model was created in ABAQUS®/CAE and the simulations were solved by the explicit finite element code in ABAQUS/Explicit, which uses the central-difference integration [40]. In this scheme, the integration operator matrix is inverted and a set of nonlinear equilibrium equations is solved at each time increment. The increment time step is automatically calculated by ABAQUS.

Table 2. Elastic properties of the lamina

E_{11} (GPa)	E_{22} (GPa)	E_{33} (GPa)	G_{11} (GPa)	G_{12} (GPa)	G_{13} (GPa)	ν_{12}	ν_{13}	ν_{23}
120.20	7.47	7.47	3.94	3.94	2.31	0.32	0.32	0.33

Each lamina was modelled using a layer of eight-noded 3D full integration linear solid elements (C3D8I) with incompatible mode and hourglass control. The incompatible mode elements have more internal degrees-of-freedom (DoFs) compared to reduced integration mode elements. Each node of the solid brick element has three translational DoFs. The hourglass energy was limited to less than 2% of the total energy to ensure the accuracy of the finite element simulations [41]. Damping effect of the composite materials was considered in the simulation. It was simulated using the Rayleigh mass proportional and stiffness proportional damping using experimentally obtained results from the sepcimens with the same material properties in the Section 5. The A_0 guided wave was used as the incident wave and it was simulated by applying out-of-plane nodal displacements to surface nodes of the beam, which simulates a piston type excitation generated by a 12 mm × 6 mm rectangular transducer. The in-plane dimensions of the elements were 0.4 mm × 0.4 mm and the thickness was 0.2 mm for all FE models. The delamination was modeled by duplicating the finite element nodes at the delamination region, which allows two sub-laminate interfaces located at the delamination region move independently. Contact-pair interaction with associated properties was assigned to the sub-laminate interfaces at the delamination to model the CAN effect described in Section 2.

In the numerical case studies the excitation signal was a 70 kHz narrow-band five-cycle sinusoidal tone burst modulated by a Hanning window. The wavelength of the A_0 guided wave at this excitation frequency and second harmonic frequency are 16 mm and 8 mm, respectively. The group velocity of the guided wave was calculated using the CWT described in Section 3.5 and compared with experimentally measured results. Fig. 4 shows the group velocity dispersion curve of the A_0 guided wave. There is a good agreement between the results of the numerical simulations and experimental data. The noise effect was considered in the numerical data, which was simulated by adding white noise to the time-domain guided wave response. The noise level considered in this study was approximately 1% of the maximum amplitude of each signal, which is similar to the noise level observed in the experimental data in] Section 5.

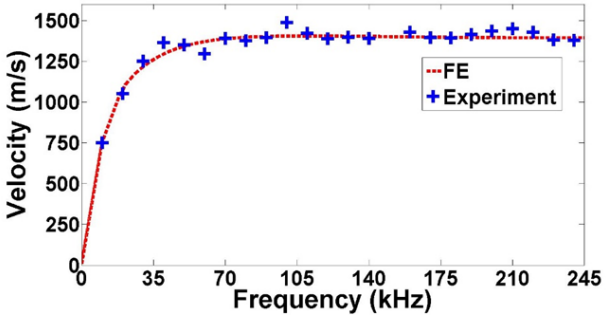

Figure 4. Group velocity dispersion curves of A_0 mode guided wave

Using the transducers network as shown in Fig. 2, two scenarios are considered in this study. Scenario 1 considers the delamination located in zone 3, i.e. between Transducers 2 and 3, while Scenario 2 considers the delamination located in zone 4, i.e. at the beam end. Each scenario was studied numerically in this section and also experimentally in Section 5. The distance between each transducer is 50 mm and the Transducers 1 and 3 are located at 33mm away from the left and right beam ends, respectively. Different delamination lengths from 4 mm to 16 mm in steps 4 mm were considered in the numerical study. Without loss of generality, the delamination lengths are presented in term as the delamination length to the wavelength of the incident linear A_0 guided wave ratio d/λ. Figs. 5a and 5b show the details of the Scenarios 1 and 2 with delamination length of 8 mm, i.e. $d/\lambda = 0.5$. For each delamination length, different delamination through-thickness locations were considered, i.e. the delaminations were located between the first and second, the second and third and third and fourth layers of the laminated composite beams. Table 3 shows a summary of damage cases considered in each scenario. In each scenario, 12 damage cases considering different lengths of delaminations located at different through-thickness locations were used to verify and demonstrate the performance of the proposed method in detecting and locating the delaminations. In total there were 24 damage cases considered in the numerical case studies.

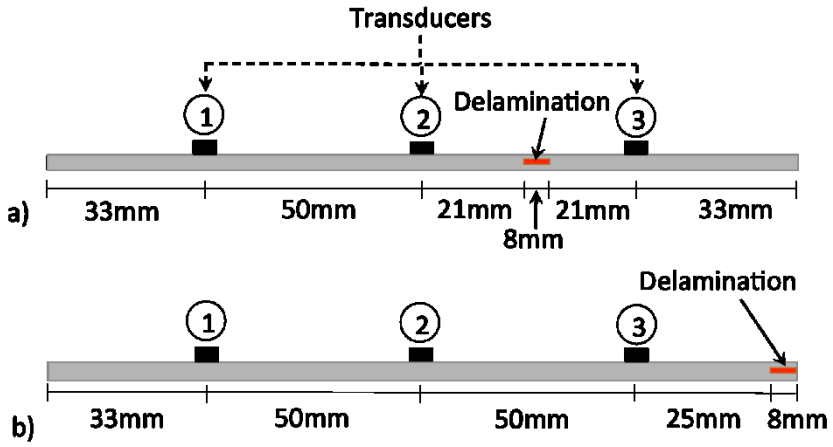

Figure 5. Schematic diagram of Scenarios a) 1 and b) 2 in numerical case studies

Table 3. Summary of delamination sizes and through-thickness locations of damage cases for each scenario in numerical studies

Delamination length to wavelength ratio (d/λ)	Delamination through-thickness location		
	1st and 2nd layer	2nd and 3rd layer	3rd and 4th layer
d/λ = 0.25	Case A_1	Case A_2	Case A_3
d/λ = 0.50	Case B_1	Case B_2	Case B_3
d/λ = 0.75	Case C_1	Case C_2	Case C_3
d/λ = 1.00	Case D_1	Case D_2	Case D_3

4.1. Scenario 1: Delamination is located between the actuator-receiver pair

Fig. 6 shows a snapshot of the finite element simulation results when the A_0 guided wave interacting with the delamination located at third and fourth layers in the laminated composite beam (Damage Case B_3), in which $d/\lambda = 0.5$. As shown in Fig. 6, the contact interaction applied to the subsurfaces of the laminae at the delamination, which prevents the interpenetration between the subsurfaces and simulates the CAN in delamination area.

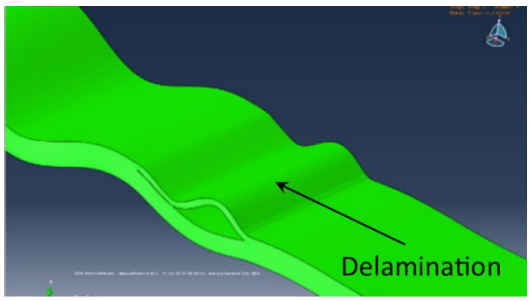

Figure 6. A snapshot of the A_0 guided wave interacting with the delamination in Damage Case B_3

The data calculated was the time-domain out-of-plane displacement responses at the location of the transducers. Figs. 7a-7c show the acquired data at the measurement locations in time-domain when the incident wave was excited at Transducer 1 and the data was measured at Transducer 2. In addition to the calculated time-domain data, the data proceed with Fast Fourier transform (FFT) is also shown in Fig. 7. According to the arrival time of the wave packages in Fig. 7, the first, second and third wave packages attribute to the incident wave, linear reflected wave from the delamination and wave reflection from the beam end, respectively. As the linear reflected wave is slightly overlapped with the incident wave package, it is difficult to accurately determine the arrival time of the linear reflected wave without the baseline data, especially for more complicated structures or delamination is close to the receivers. As shown by the frequency-domain data in Fig. 7, second harmonic was observed in all damage cases. To ensure the second harmonic was generated by the CAN at the delamination, an intact laminated composite beam was also created using the finite element method. It was confirmed that there is no higher harmonic in the intact laminated composite beam.

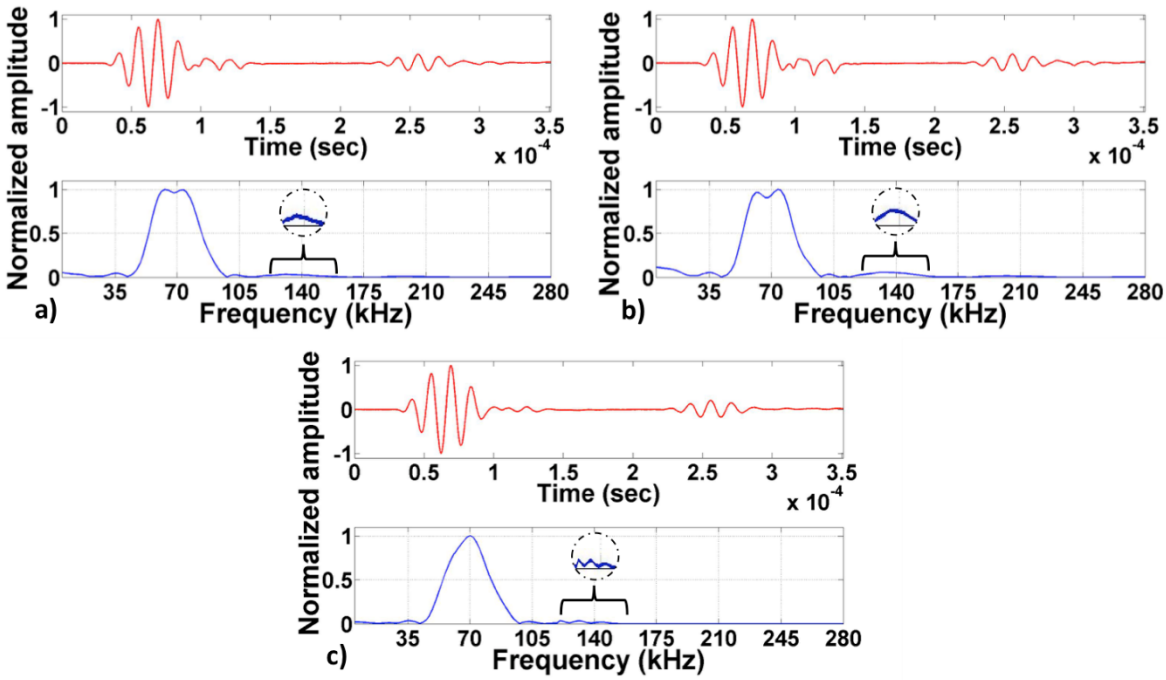

Figure 7. Calculated signal in time-domain and frequency-domain for Damage Cases a) B_1 b) B_2 and 3) B_3 in numerical case studies

Although the presence of higher harmonic components in frequency-domain can indicate the existence of damage in the laminated composite beams, more information is required, i.e. arrival time of the second harmonic guided wave, to locate the delamination. Therefore, the calculated data was transformed to time-frequency domain using CWT described in Section 3.5. Fig 8a, 8b, 8d, 8e, 8g, and 8h show the time-frequency energy density spectrum, which are zoomed-in at frequency ranges around the excitation and second harmonic frequency for Damage Cases B1 and B2 and B3. The information is useful for determining the location of the delaminations. As shown in the time-frequency energy density spectrum, the energy is concentrated at two frequencies, i.e. around the excitation frequency and second harmonic frequency at different times. Figs. 8c, 8f and 8i also show the corresponding normalized wavelet coefficients at the excitation and second harmonic frequency. The arrival times of the incident wave and second harmonic guided wave, which were determined based on the maximum magnitude of the normalized wavelet coefficients at the excitation frequency and second harmonic frequency, respectively, are indicated by vertical dash-dotted lines. The estimated Δt are also indicated in the figures.

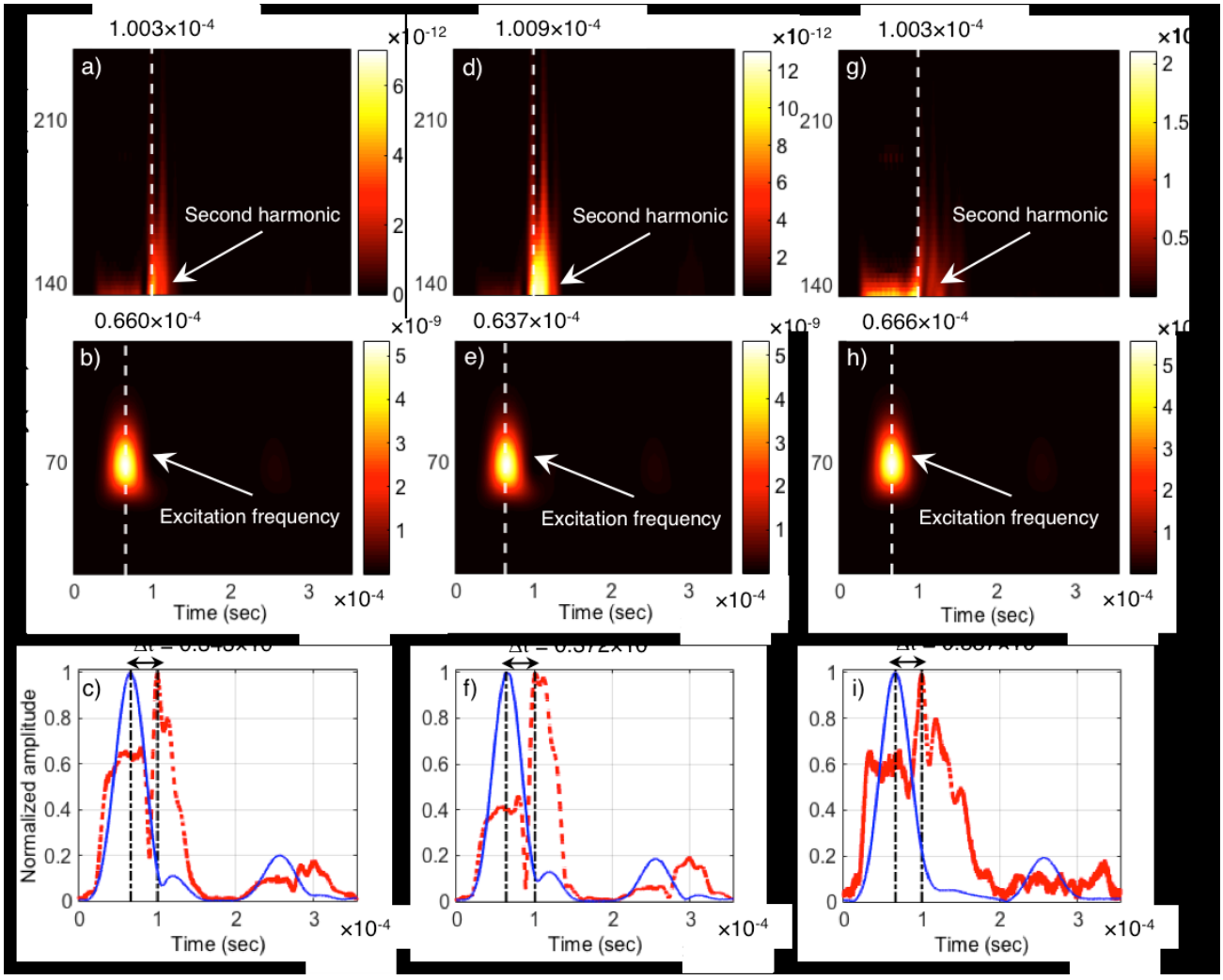

Figure 8. Time-frequency energy density spectrum, and corresponding normalised wavelet coefficient at excitation and second harmonic frequency for Damage Cases (a)-(c) B_1, (d)-(f) B_2 and (g)-(i) B_3

For Damage Case B1, the arrival time of the incident wave and second harmonic guided wave at the excitation frequency and second harmonic frequency are 66.0 µsec and 100.3 µsec, respectively. Hence, the estimated delamination location from the receiver using Equation (16) is d_{d-2} = 23.9 mm (from the Transducer 2 and between Transducers 2 and 3. Similarly, the estimated delamination location from the receiver for Damage Cases B2 and B3 are d_{d-2} = 25.9 mm and d_{d-2} = 23.5 mm, respectively. It should be noted that the true left and right end location of the delamination are at 21 mm and 29 mm from the receiver (Transducer 2), i.e. $\bar{d}_{d-2} = 21\ mm - 29\ mm$. Since the higher harmonic guided wave is contributed by the occurrence of CAN at different locations within the delamination region, i.e. 21 mm – 29 mm,

the identified delamination location within this range is considered to be reasonably accurate. The results of other damage cases are summarised in Table 4. In Scenario 1, the delamination is located in zone 3, the delamination distance from Transducer 2 (d_{d-2}) is useful for estimating the delamination location as the actuator-receiver pair (Transducer 1 – Transducer 2) is under the pulse-echo condition. Therefore, the results of d_{d-2} are included in the Table 4. The results confirm that the proposed technique can detect and locate the delaminations without using the baseline data. As shown in Table 4, the delamination locations are accurately estimated in all damage cases.

Table 4. Summary of all results for Scenario 1 in the numerical case studies

Damage case	Estimated arrival time		Estimated delamination location*	True delamination location*
	$t_{2f_c}(\mu sec)$	$t_{f_c}(\mu sec)$	$d_{d-2}\,(mm)$	$\bar{d}_{d-2}\,(mm)$
A1	98.4	65.1	23.2	23-27
A2	99.0	65.6	23.3	23-27
A3	96.8	64.8	23.3	23-27
B1	100.3	66.0	23.9	21-29
B2	100.9	63.7	25.9	21-29
B3	100.3	66.6	23.5	21-29
C1	100.3	66.1	23.8	19-31
C2	101.9	66.2	24.9	19-31
C3	103.7	67.1	25.5	19-31
D1	102.4	65.2	25.9	17-33
D2	100.0	65.6	24.0	17-33
D3	99.5	65.3	23.8	17-33

* Delamination location from Transducer 2 and between Transducers 2 and 3.

4.2. Scenario 2: Delamination is located at the beam end

Scenario 2 considers the delamination located at the beam end. The time-domain signal measured by Transducer 3 while the Transducer 2 is used as actuator shows that the signal is more complicated compared to the signal in Scenario 1. Fig. 9a shows the reflected wave from the delamination is hidden in incident wave reflected from the beam end boundary in Damage Case C_2. It is impossible to interpret the reflected linear wave from the delamination without the baseline data. However, the second harmonic can still be observed in the frequency-domain

as shown in Fig. 9b, which indicates the existence of the delamination. With the calculated signals from other actuator-receiver pairs, the delamination zone can be identified if the determined delamination location is close to zero. After that, the signal calculated by the actuator-receiver pair under the pulse-echo condition is used to estimate the delamination location. Table 5 summarises the estimated delamination locations for all cases and the results show that the delamination locations are accurately determined using the second harmonic guided wave without the baseline data.

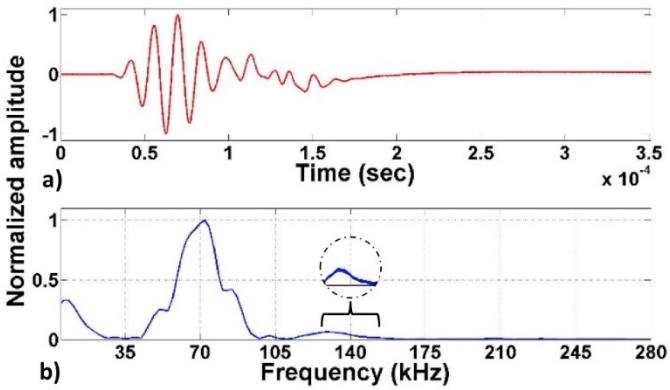

Figure 9. Calculated signal in time-domain and frequency-domain for Damage Case C_2 in numerical case studies

Table 5. Summary of all results for Scenario 2 in the numerical case studies

Damage case	Estimated arrival time		Estimated delamination location*	True delamination location*
	$t_{2f_c}(\mu sec)$	$t_{f_c}(\mu sec)$	$d_{d-3}\ (mm)$	$\bar{d}_{d-3}\ (mm)$
A1	110.5	66.6	30.8	29-33
A2	116.1	67.3	32.5	29-33
A3	113.1	67.4	31.8	29-33
B1	110.0	66.7	30.2	25-33
B2	109.6	66.3	30.3	25-33
B3	102.1	66.3	25.7	25-33
C1	98.7	66.4	22.5	21-33
C2	98.7	65.8	22.9	21-33
C3	950	64.8	21.3	21-33
D1	100.3	66.5	23.5	17-33
D2	104.2	67.0	25.9	17-33
D3	99.2	66.4	22.9	17-33

* Delamination location from Transducer 3 and between Transducer 3 and beam end.

5. Experimental Case Studies

In experimental case studies, two eight-ply $[(0/90)_2]_S$ laminated composite beams were manufactured. The specimens were made by unidirectional carbon/epoxy prepreg and the elastic properties of the lamina are E_{11} = 120.20 GPa, $E_{22} = E_{33}$ = 7.47 GPa, $G_{11} = G_{12}$ = 3.94 GPa, G_{13} = 2.31 GPa, ν_{12} = 0.32, $\nu_{23} = \nu_{13}$= 0.33 and ν_{13} = 0.32, which are the same as the material properties used in the finite element model as shown in Table 2. This lamina has a fibre volume fraction of 0.55, with density and thickness being 1538 kg/m^3 and 0.2 mm, respectively.

The dimensions of the laminated composite beams are 166 mm × 12 mm × 1.6 mm, which are the same as the numerical case studies. There was a 15 mm long delamination in each composite beam. In Damage Case 1, the delamination is located between the third and fourth ply. The true right and left end locations of the delamination are at 17.5 mm and 32.5 mm, respectively, i.e. $\bar{d}_{d-2}$ = 17.5 mm – 32.5 mm at the right hand side of the Transducer 2. In Damage Case 2, the delamination is located between the third and fourth ply and between the Transducer 3 and the right beam end. The true left and right end locations of the delamination are at 18 mm and 33 mm from the Transducer 3, i.e. ($\bar{d}_{d-3} = 18\,mm - 33\,mm$). The details of the specimens and the location of the transducers are shown in Fig 10. For creating the delaminations, two short Teflon films were first inserted at the required through-thickness location during the manufacturing process of each laminated composite beam. Three-point bending test was then employed to create the required delamination length by breaking the weak bonding between the plies and Teflon film.

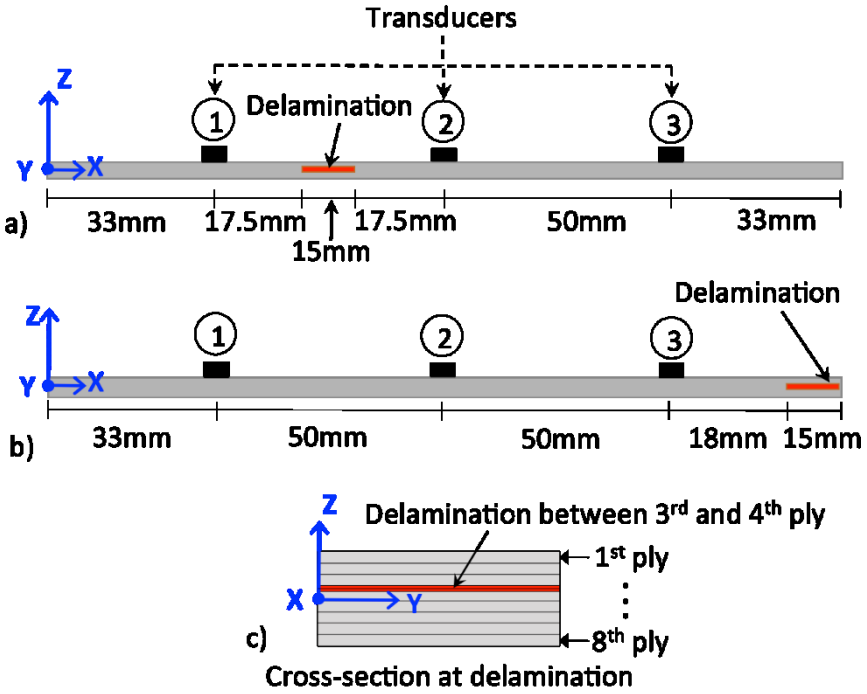

Figure 10. Schematic diagram of composite beam specimens with a delaminations for a) Damage Case 1 b), Damage Case 2 and c) cross-section at delamination location in experimental case studies

A computer controlled National Instrument PXIe-1073 chassis, which consists of a NI PXI-5412 arbitrary waveform generator and a NI PXI-5105 digitizer was used in the experimental study. Three rectangular piezoceramic transducers with dimension 12 mm × 6 mm × 2 mm were adhesively attached to the surface of the laminated composite beam specimens. The excitation signal was generated by the arbitrary waveform generator and then amplified by an amplifier with peak-to-peak voltage of 50 V. The responses of the receiver were recorded by digitizer and then sent to the computer. Fig. 11 shows the schematic diagram of the experiment setup. The excitation signal is the same as the numerical case studies in Section 4, i.e. a 70kHz narrow-band five-cycle sinusoidal tone burst modulated by a Hanning window.

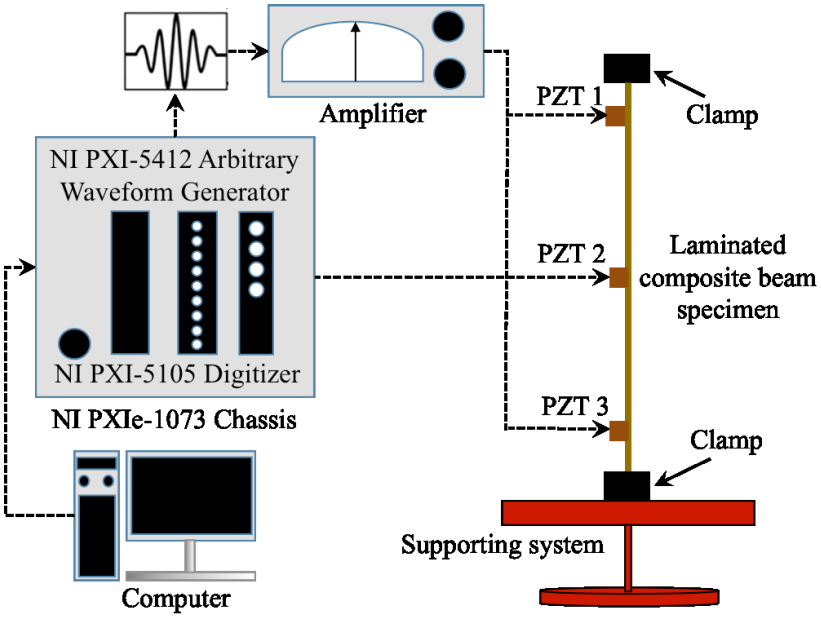

Figure 11. Experiment setup

The transducers were actuated sequentially, in which one of the transducers was used to generate the incident wave while the other two transducers were used for data acquisition. The delamination zone was first identified using Table 1. Figs. 12a and 12b show the measured results by one of the actuator-receiver pairs in the frequency-domain. Fig. 12a is the data measured by Transducer 2 while Transducer 3 was used as the actuator in Damage Case 1. In Fig. 12b, the data was measured using Transducer 3 while Transducer 2 was the actuator in Damage Case 2.

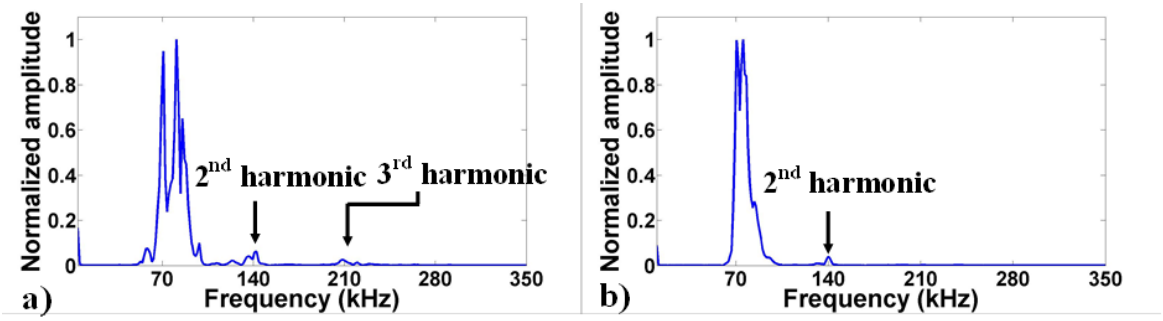

Figure 12. Measured signal in frequency-domain, a) Transducer 2 is the receiver while Transducer 3 is the actuator in Damage Case 1, b) Transducer 3 is the receiver while Transducer 2 is the actuator in Damage Case 2

To determine the delamination location, the measured data was transformed to time-frequency domain using CWT. Fig. 13a and 13b show the time-frequency energy density spectrum for Damage Cases 1 and 2, respectively. The normalized CWT coefficient at the incident wave frequency and second harmonic frequency are also shown in Figs. 13c and 13f. In Damage Case 1, the arrival time of the incident wave and second harmonic guided wave are 69.8 µsec and 116.4 µsec, respectively. The estimated delamination location is d_{d-2} = 32.5 mm from the receiver (Transducer 2), which is within the true delamination location range, i.e. $\bar{d}_{d-2}$ = 17.5 mm – 32.5mm. In Damage Case 2, the arrival time of the incident wave and second harmonic guided wave are 79.8 µsec and 107.9 µsec, respectively.

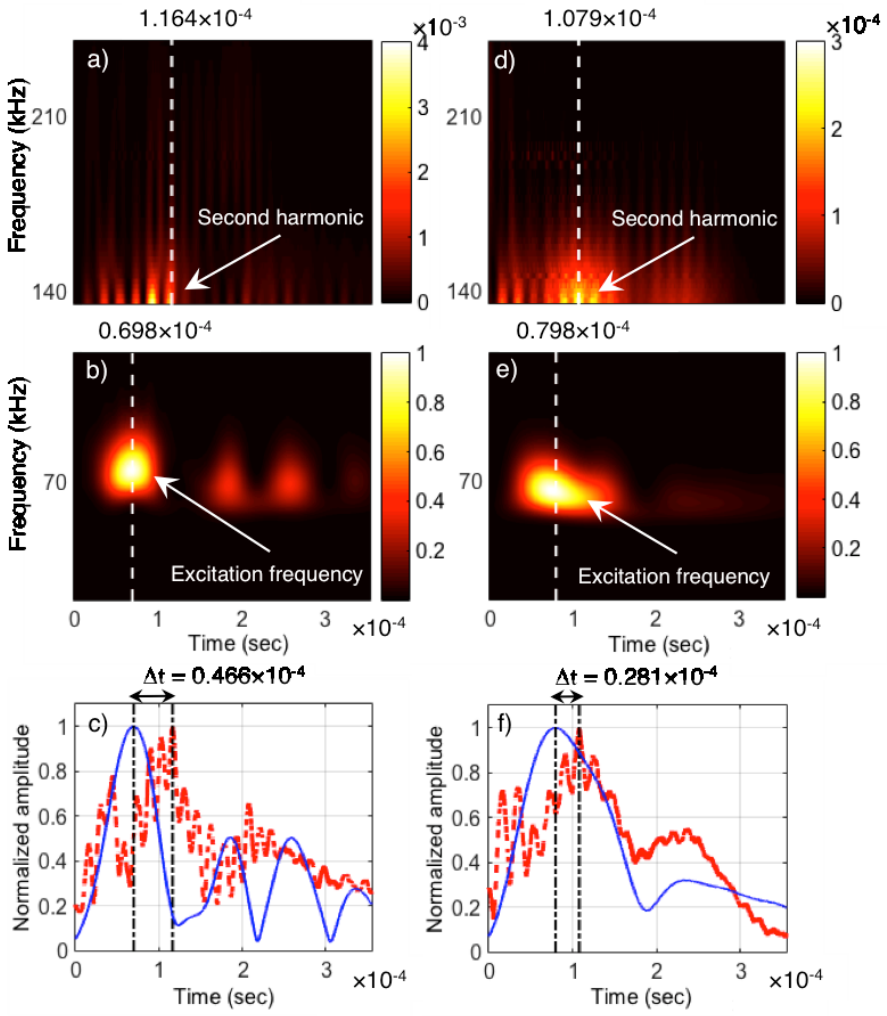

Figure 13. Time-frequency energy density spectrum zoom-in, and the corresponding normalised CWT coefficients at excitation and second harmonic frequency for a) Damage Case 1 and b) Damage Case 2.

Therefore the estimated delamination location is d_{d-3} 19.6 mm, which is again within the true delamination location range, i.e. $\bar{d}_{d-3}$= 18 mm – 33 mm. Overall the results show that the delamination location can be accurately determined without using the baseline data.

6. Conclusions

In this study, a baseline-free method has been proposed to detect and locate the delaminations in laminated composite beams using the higher harmonic generated guided wave due to CAN. To take into account the practical situation, the proposed method employs a transducer network consisting at least three transducers. A sequential scan for inspecting the laminated composite beam has been performed by actuating A_0 guided wave at one of the transducers while the rest of the transducers are used for measuring the impinging waves. The proposed method covers all possible conditions, i.e. pulse-echo and pitch-catch, in using the higher harmonic guided wave and the transducer network to detect and locate the delamination without baseline data. The continuous Gabor wavelet transform has been used to accurately extract the arrival time information of the higher harmonic guided wave. A series of numerical case studies have been carried out, which have considered 24 damage cases with different delamination locations, lengths and through-thickness locations. The experimental case studies have also been carried out to further validate and demonstrate the capability of the proposed method. Overall the results show that the proposed method is able to accurately detect and locate the delamination in the laminated composite beams without using the baseline data.

7. Acknowledgement

This work was supported by the Australian Research Council under Grant Number DP160102233.

8. References

1. Kim JT, Ryu YS, Cho HM, Stubbs N. Damage identification in beam-type structures: frequency-based method vs mode-shape-based method Eng Struct, 2003; 25: 57–67
2. Salawu OS. Detection of structural damage through changes in frequency: a review. Eng Struct 1997; 19(8): 718-723.
3. Kim JT, Ryu YS, Cho HM, Stubbs N. Damage identification in beam-type structures: Frequency-based method vs mode-shape-based method. Eng Struct 2003; 25:57-67.
4. Sahin M, Shenoi RA. Quantification and localisation of damage in beam-like structures by using artificial neural networks with experimental validation. Eng Struct 2003; 25:1785-1802.
5. Sohn H, Farrar CR, Hemez FM, Shunk DD, Stinemates DW, Nadler BR. A review of structural health monitoring literature from 1996–2001. Los Alamos National Laboratory, Los Alamos, NM, report no LA-13976-MS; 2004.
6. Cawley P, Alleyne D. The use of Lamb wave for the long range inspection of large structure. Ultrasonics 1996; 34: 287-290.
7. Rose JL. A baseline and vision of ultrasonic guided wave inspection potential. J Press Vessel Tech 2002; 124: 273-282.
8. Ng CT. On the selection of advanced signal processing techniques for guided wave damage identification using a statistical approach. Eng Struct 2014; 67: 50-60.
9. Mitra M, Gopalakrishnan S. Guided wave based structural health monitoring: A review. Smart Mater Struct 2016; 25: 053001.
10. Giurgiutiu V, Bao JJ. Embedded-utlrasonics structural radar for in situ structural health monitoring of thin-wall structures. Struct Health Monitor 2004; 3: 121-140.
11. Veidt M, Ng CT, Hames S, Wattinger T. Imaging laminar damage in plates using Lamb wave beamforming. Adv Mater Research, 47-50: Part 1: 666-669.
12. Ihn JB, Chang FK. Pitch-catch active sensing methods in structural health monitoring for aircraft structures. Struct Health Monitor 2008;7: 5-15.

13. Ng CT. A two-stage approach for quantitative damage imaging in metallic plates using Lamb wave. Earthquake Struct 2015; 8:f 821-841.
14. Haynes C, Todd M. Enhanced damage localization for complex structures through statistical modelling and sensor fusion. Mech Syst Sig Process 2015; 54-55: 195-209.
15. Soleimanpour R, Ng CT. Scattering of the fundamental anti-symmetric Lamb wave at through-thickness notches in isotropic plates. J Civil Struct Health Monitor 2016;,6: 1-13.
16. Sohn H, Park G, Wait JR, Limback NP, Farra CR. Wavelet-based active sensing for delamination detection in composite structures. Smart Mater Struct 2004; 13:153-160.
17. Ostachowicz W, Kudela P, Malinowski P, Wandowski T. Damage localisation in plate-like structures based on PZT sensors. Mec Syst Sig Process 2009; 23: 1805-1829.
18. Soleimanpour R, Ng CT. Mode conversion and scattering analysis of guided waves at delaminations in laminated composite beams. Struct Monitor Maintenance 2015; 2: 213-236.
19. Rajagopal P, Lowe, MJS. Scattering of the fundamental shear horizontal guided wave by a part-thickness crack in an isotropic plate. J Acoust Soc Am 2008, 124: 2895-2904.
20. Yeum CM, Sohn H, Lim HJ, Ihn JB. Reference-free delamination detection using Lamb waves. Struct Con Health Monitor 2013; 21: 675-684.
21. He S, Ng CT. Analysis of mode conversion and scattering of guided waves at cracks in isotropic beams using a time-domain spectral finite element method. Elec J Struct Eng 2015; 14: 20-32.
22. Ramdhas A, Pattanayak RK, Balasubramaniam K, Rajagopal P. Symmetric low-frequency feature-guided ultrasonic waves in thin plates with transverse bends. Ultrasonic 2015; 56: 232-242.
23. Ng CT. On accuracy of analytical modelling of Lamb wave scattering at delaminations in multilayered isotropic plates. Inter J Stuct Stab Dyn 2015, 15: 1540010.

24. Konstantinidis G, Drinkwater BW, and Wilcox PD. The temperature stability of guided wave structural health monitoring systems. Smart Mater. Struct 2006;. 15: 967–976.

25. Aryan P, Kotousov A, Ng CT and Wildy S. Reconstruction of baseline time-trace under changing environmental and operational conditions. Smart Mater Struct 2016; 25: 035018.

26. Bermes C, Kim JY, Qu J, Jacobs LJ. Nonlinear Lamb waves for the detection of material nonlinearity. Mech Sys Sig Process 2008; 22: 638-646.

27. Donskoy D, Sutin A, Ekimov A. Nonlinear acoustic interaction on contact interfaces and its use for non-destructive testing. NDT & E Inter 2001; 34: 231-238.

28. Solodv IY, Krohn N, Busse G. CAN: An example of nonclassical acoustic nonlinearity in solids. Ultrasonics 2002; 40: 621-625.

29. Klepka A, Staszewski W, Jenal RB, Szwedo M, Iwaniec J, Uhl T. Nonlinear acoustics for fatigue crack detection – experimental investigations of vibro-acoustic wave modulations. Struct Health Monitor 2012; 11: 197-211.

30. Li W, Cho, Y, Achenbach JD. Detection of thermal fatigue in composites by second harmonic Lamb waves. Smart Mater Struct 2012; 21: 085019.

31. Soleimanpour R, Ng CT. Numerical study of nonlinear guided waves in laminated composite beams with delaminations. 8th Australasian Congress on Applied Mechanics: ACAM8. Barton, ACT, Engineers Australia, 2014: 379-388.

32. Hong M, Su Z, Wang Q, Cheng L and Qing X. Modelling nonlinearities of ultrasonic waves for fatigue damage characterization. Ultrasonics 2014; 54: 770-778.

33. Zhao J, Chillara VK, Ren B, Cho H, Qiu J, Lissenden, CJ. Second harmonic generation in composites: Theoretical and numerical analyses. J Applied Phy 2016; 119: 064902.

34. Kazakov VV, Sutin A, Johnson PA. Sensitive imaging of an elastic nonlinear wave-scattering source in a solid. Applied Phy Letters 2002; 81: 646-648.

35. Dziedziech K, Pieczonka L, Kijanka P, Staszewski W. Enhanced nonlinear crack-wave interactions for structural damage detection based on guided ultrasonic waves. Struct Control Health Monitor 2016, 23: 1108-1120.
36. Hagedorn, P, Schramm, W. On the dynamics of large systems with localized nonlinearities. J Applied Mech, ASME 1988 55:946-951.
37. Lee LH, Choi IH, Jhang KY. The nonlinearity of guided wave in an elastic plate. Mod Phys Letter 2008; 22: 1135-1140.
38. Naugolnykh K, Ostrovsky L. Nonlinear Wave Processes in Acoustics. Cambridge University Press 1998.
39. Ng CT, Veidt M, Rajic N. Integrated piezoceramic transducers for imaging damage in composite lamiantes. Proc SPIE 2009; 7493: 1-8.
40. ABAQUS Theory Manual Version 6.9, 2009, ABAQUS Inc.
41. Stewart JR, Gullerud AS, Heinstein MW, Solution verification for explicit transient dynamics problems in the presence of hourglass and contact forces. J Comp Methods App Mech Eng 2006; 195: 1499–1516.

Chapter 7: Conclusions and Recommendations for Future Works

1. Conclusions

This thesis provided a study of linear and nonlinear guided waves in isotropic and anisotropic materials. This research commenced by studying the propagation of linear guided waves in isotropic material which has less complications compared to composite material. The linear parameters of guided waves interacting with defects was studied in the third chapter. The results of Chapter 3 showed that A_0 Lamb wave is sensitive to small defects and can detect the defects with a size of as small as a few millimetres. It was shown that the proposed FE simulation modelling techniques in this chapter could be used for prediction of propagation of A_0 Lamb wave in aluminium plates with notches. The results showed that the amplitude of A_0 Lamb wave in aluminium plates is sensitive to the notch orientation too. A couple of SPD patters were generated in this chapter which could be used for predicting the notch orientation. Moreover, the results showed that a successful damage detection may not be obtained when the incident wave propagation direction is perpendicular to the notch orientation. Therefore, to avoid this situation, it may needs a series of transducer for damage detection. The study was expanded to composite material in Chapter 4.

Propagation and scattering characteristics of linear A_0 guided wave in fibre reinforced composite beams was studied in Chapter 4. 3D finite element simulations were carried out and compared with experimental data. Good agreement was found between finite element calculated and experimentally measured phase and group velocity.

The results of intact composite beam showed that, in addition to, the incident wave, several wave packets are generated due to interaction of guided wave with the boundaries at the both sides of the beam cross-section. The interaction of incident wave with beam cross-section

boundaries incur some unique phenomena that do not exist in plates and should be considered carefully during the data analysis.

This chapter also investigated effect of several parameters, such as delamination size to the wavelength ratio and different delamination through-thickness locations, on scattering characteristics of A_0 guided wave. S_0 and A_0 guided waves were extracted using the arrival time of reflected wave packets from the delaminations and beam ends by using the measured nodal displacement at the top and bottom surfaces of the beam. The results showed that multiple mode conversions happen when S_0 and A_0 guided waves interact with delamination. The second and third interfaces delamination through thickness location cause largest wave reflections whereas larger wave transmission occurs when delamination is located between fourth and fifth layers. The findings of this chapter can be beneficial to damage detection in composite beams.

Chapter 5 investigated the non-classical nonlinear response of guided waves in composite beams. The FE simulation modelling technique and linear guided waves experimental method used in previous chapters were used for validation of preliminary results in this chapter. The results of the FE simulations showed that clapping effect of the sublaminate surfaces at the delamination region cause CAN in form of second harmonic guided waves in forward and backward scattering directions. It was shown that the existence of the second harmonics is a good indication for the delaminations in laminated composite beams.

The results showed that the magnitude of the second harmonic depends on the through-thickness location of the delamination. It has an advantage in monitoring the higher harmonic waves at the forward scattering direction as the magnitude of second harmonic is larger for forward scattering direction than backward scattering direction.

Some important parameters were considered in the study such as damping, propagation distance, incident wave amplitude and number of cycles. The studies on damping and propagation distance showed that the amplitude of second harmonic decreases when damping and propagation distance increase. It was shown that damage detection using nonlinear guided

waves in material with high damping ratio is more complicated. The measurement location and material damping are two important parameters in using second harmonic generated by CAN in damage detection.

The results showed that the incident wave with larger amplitude and more number of cycles could provide better damage detection results as the amplitude of second harmonic wave packet increases with the incident wave amplitude and number of cycles. This chapter concluded that without using a baseline data, processed data in time domain provide little information regarding delamination whereas the frequency domain and time-frequency domain provide more information of the delaminations in laminated composite beams.

In summary, Chapter 5 provided improved fundamental insights into the phenomenon of second harmonic generated by CAN at the delaminations in laminated composite beams and the findings of this chapter can improve the performance of damage detection methods using nonlinear guided waves.

In Chapter 6, a baseline-free damage detection and localisation method, which covers pulse-echo and pitch-catch conditions, was proposed for detecting delamination in laminated composite beams using CAN. A network of three transducers was employed for damage detection and damage localisation in the laminated composite beam by actuating one of the transducers and using the rest of the transducers as receivers for measuring the impinging waves. This chapter, takes the advantages of the validated methods presented in previous chapters such as FE simulation modelling technique, calculation of time of arrival of the wave packets, generation of higher harmonics due to CAN, experimental approach for detecting CAN and data processing in time-frequency domain. A series of numerical case studies were carried out, with taking important factors into consideration such as different delamination locations, lengths and through-thickness locations. The FE simulation results had a good agreement with experimental data which shows that proposed technique can successfully be used for damage detection and damage localisation in composite beams. This technique does not rely on baseline

data, which is its major advantage over conventional linear damage detection and damage localisation techniques.

2. Recommendations for future works

Similar to other research works, there are some limitations in the current research. Therefore, further researches are recommended as follows:

1. During 3D FE simulation, the A_0 guided wave was simulated by applying out-of-plane nodal displacements to surface nodes of the beam, which simulates a piston type excitation generated by a transducer. It is recommended that A_0 guided waves are generated by modelling the real piezoelectric elements in FE simulation, which may provide more realistic results.
2. 3D FE simulations were carried out assuming pure A_0 guided wave as the incident wave. However, generating pure asymmetric guided wave is practically impossible. Therefore, it is recommended that other possible modes such as symmetric mode are taken into consideration.
3. In Chapter 3, analytical approach was used for FE simulation validation. It is recommended that in addition to analytical approach, validation of results is carried out using experimental approach.
4. As explained in Chapter 5, the propagation distance of nonlinear guided waves is highly affected by the material damping. This could be an issue when this technique is used in composite laminate. Therefore, the proposed damage detection technique is open to further improvement as more study is carried out on possible methods for increasing the propagation distance of nonlinear guided waves in composite laminates.
5. Chapter 5 has investigated the phenomena of generation of nonlinear guided waves in composite beams. Similar study is recommended for composite plates.

6. In Chapters 5 and 6, 3D FE simulation of the models was carried out without taking friction coefficient into consideration. As explained, the friction may affect the generation of higher harmonics due to CAN. Therefore, further investigation is recommended regarding the effects of friction on generation of higher harmonics.
7. The proposed damage localisation technique in Chapter 6 is only applicable for beams, whereas more investigations is highly recommended for proposing a baseline free damage localisation for detecting defects in composite plates.
8. Chapters 5 and 6 study nonlinear guided waves due to CAN. However, previous studies show that material nonlinearity is also a major source of nonlinear response of guided waves. Therefore, it is recommended that further studies are required to take into account the two sources of nonlinear response (CAN and material nonlinearity).
9. The proposed technique in Chapter 6 is applicable for detecting and locating delamination in composite beams. However, further studies is recommenced for expanding the technique for damage quantification which is an important area in structural health monitoring.